Universitat Politècnica de Catalunya, Barcelona, 4-7 May 2004

Fluid-Structure Interaction in Fast Transient Dynamics

A Short Course by F. Casadei

(Auxiliary Course Notes)

Programme of the Course

1. Introduction
    a. Introductory example of a FSI problem
        i. Application spectrum and goals
    b. Modeling the structural domain
        i. Equilibrium equations
        ii. Explicit time integration scheme
    c. Treatment of essential boundary conditions
        i. The Lagrange multipliers method
        ii. Solving the linear system
2. ALE formulation
    a. Modeling the fluid domain
        i. Euler equations
        ii. Finite Element discretization
        iii. Finite Volume discretization
    b. Mesh rezoning algorithms
        i. Motivation
        ii. Mean-based algorithms
        iii. Giuliani's algorithm
    c. Free surface modeling
3. ALE Fluid-Structure Interaction
    a. Motivation
    b. Classification of FSI algorithms
    c. Equilibrium-based methods
        i. The Uniform Pressure (UP) method
        ii. Shortcomings
    d. Geometrical methods
        i. The FSA/FSR method
        ii. Shortcomings
    e. A combined method
        i. The FSCR method
4. Advanced topics and applications
    a. ALE description of structures
    b. Non-conforming FSI
    c. Lagrangian contact
        i. Classical methods
        ii. Pinballs
        iii. SPH
    d. Simple but detailed FSI example
    e. Industrial applications

The present document contains some notes and other auxiliary material related to the Course: Fluid-Structure Interaction in Fast Transient Dynamics, held by F. Casadei at the University of Barcelona (Universitat Politècnica de Catalunya), on 4-7 May 2004.

Prepared for the Course “Fluid-Structure Interaction in Fast Transient Dynamics”
Organised by UPC, Barcelona (E) 4-7 May 2004.

Course Notes

Part I

Introduction

Folco Casadei

Joint Research Centre - IPSC
European Laboratory for Structural Assessment, T.P. 480
21020 Ispra (Varese) - Italy
E-mail: folco.casadei@jrc.it
Web: http://europlexus.jrc.it

JOINT RESEARCH CENTRE

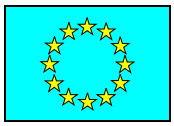

European Commission
Institute for the Protection and Security of the Citizen
European Laboratory for Structural Assessment

Introduction and application spectrum

We focus on the numerical simulation of ***fast transient dynamic interaction*** phenomena such as: explosions, crashes, impacts. Among the most typical applications are:

- ***Safety*** problems:
  - Safety vessels for nuclear or chemical plants.
  - Behaviour of pressurised components (pipelines, sub-assemblies, safety devices) under abnormal working conditions.
  - Vehicle crash.
  - Containers for the transportation of dangerous materials.
  - Effect of pressure waves on submerged structures (ships, submarines, offshore plants, tunnels).
  - etc.
- Technological ***processes***:
  - Forging, coining.
  - Extrusion.
  - etc.
- ***Support*** to experiments:
  - Pre-calculation and interpretation of experiments for the determination of the dynamic behaviour of materials used in mechanical or civil engineering.
  - Computational support to experiments aimed at verifying safety conditions in general.

Characteristics of the applications

The listed application problems often involve:

- Large displacements and rotations, large strains: i.e. ***geometric non-linearities***.
- Plasticity, viscoplasticity, damage or other complex material behaviour: ***material non-linearities***.
- Transient dynamic behaviour, involving a ***large spectrum of frequencies***.
- Simultaneous presence of fluids and structures: heterogeneity and ***interaction phenomena***.

In a word, these applications are typically quite ***complex***.

In order to find reliable solutions, simple and robust numerical methods are needed: ***direct time integration*** techniques seem best suited because they allow to exploit the very nature of the transient dynamic problem [1].

JOINT RESEARCH CENTRE

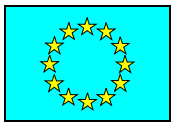

European Commission
Institute for the Protection and Security of the Citizen
European Laboratory for Structural Assessment

Computational framework

Following [1], the basic governing equation is the ***principle of virtual work***, which expresses the conservation of momentum (equilibrium, in a dynamic sense):

$$\int_V \rho \ddot{\underline{x}} \delta \underline{x} dV + \int_V \underline{\sigma} D(\delta \underline{x}) dV - \int_V \rho \underline{f} \delta \underline{x} dV - \int_{S_1} \underline{t} \delta \underline{x} dS = 0 \qquad (1)$$

- ρ is the mass density;
- V is the domain occupied by the ***current configuration***;
- S is the boundary ($S \equiv S_1 \cup S_2$) (1=natural, 2=essential);
- $\ddot{\underline{x}}$ are the accelerations ($\dot{}$ denotes time derivative);
- $\underline{\sigma}$ is the true stress (Cauchy stress tensor);
- D is a spatial derivative operator;
- $\underline{f}$ are volumetric forces per unit mass;
- $\underline{t}$ are boundary surface tractions.

Eq. (1) is to hold for all variations $\delta \underline{x}$ of displacements compatible with the essential boundary conditions on S_2, and ensures perfect equilibrium (equivalent to differential equilibrium equations).

This integral form lends itself to direct application of the Finite Element method. If a suitable spatial discretisation is introduced, (1) yields the following set of discrete differential equations in time:

$$\underline{M} \ddot{\underline{u}} = \underline{f}^{\text{ext}} - \sum_e \int_{V^e} \underline{B}^T \underline{\sigma} dV \qquad (2)$$

- $\underline{M}$ is a mass matrix (***decoupled*** by diagonalization (lumping));
- $\underline{u}$ is the nodal displacement vector;
- $\underline{B}$ is the matrix of shape function derivatives;
- V^e is the element (e) volume in the current configuration.

JOINT RESEARCH CENTRE

European Commission
Institute for the Protection and Security of the Citizen
European Laboratory for Structural Assessment

- The ***description*** is ***Lagrangian*** because it refers to material points (the observer follows the motion). In particular, the nodes and the Gauss points remain always associated to the same material point.

- The stress is the "***true***" one (***Cauchy*** stress) and is always expressed in the same Cartesian reference. The observer does not rotate along with the body but remains always oriented along the same reference (note, however, that for some special element types such as beams, plates and shells, for which out-of-plane deformations remain small it may be convenient to use a local reference that rotates with the element: ***co-rotational*** formulation).

- All terms on the right-hand side of (2) may be computed: the external loads $\underline{f}^{\text{ext}}$ are known and so are the finite-element related functions ($\underline{B}$), the stresses $\underline{\sigma}$ internal to the elements must be obtainable from the ***constitutive law*** of the material (see details below).

- Hence the acceleration $\underline{\ddot{u}}$ on the left-hand side of (2) may be obtained after inversion of the mass matrix. This operation becomes trivial if use is made of a ***diagonalised*** (lumped) mass matrix, e.g.:

$$\underline{M}^e = \int_{V^e} \underline{N} \rho \, dV \qquad (3)$$

  - $\underline{N}$ are the element shape functions.

- If a way can be found to integrate this acceleration in time by using only known quantities, it is possible to obtain a new configuration on which the semi-discrete equilibrium equation (2) may be applied again, and so on.

- Note that no use has been made so far of ***deformation*** and in particular of a ***reference configuration***, which is common in other approaches. We constantly work on the ***current configuration***.

Direct time integration

Time integration of (2) is achieved via a ***central difference*** scheme. This is usually written as:

$$\begin{aligned} \underline{\dot{u}}^{n+1} &= \underline{\dot{u}}^{n} + \frac{\Delta t}{2}(\underline{\ddot{u}}^{n} + \underline{\ddot{u}}^{n+1}) \\ \underline{u}^{n+1} &= \underline{u}^{n} + \Delta t\left(\underline{\dot{u}}^{n} + \frac{\Delta t}{2}\underline{\ddot{u}}^{n}\right) \end{aligned} \tag{4}$$

where n stays for t^n, $n+1$ for $t^{n+1} = t^n + \Delta t$, Δt being the time increment.

By introducing the notation:

$$\underline{v}^{n+1/2} = \underline{\dot{u}}^{n} + \frac{\Delta t}{2}\underline{\ddot{u}}^{n} \tag{5}$$

we see that the new configuration $n+1$ is obtained from configuration n by applying a linear motion with velocity $\underline{v}^{n+1/2}$. The final algorithm reads then:

$$\underline{u}^{n+1} = \underline{u}^{n} + \Delta t \underline{v}^{n+1/2}$$

$$\underline{\ddot{u}}^{n+1} = \underline{M}^{-1}\left(\underline{F}^{\mathrm{ext}(n+1)} - \sum_e \int_{V^{e(n+1)}} \underline{B}^T \underline{\sigma}^{e(n+1)} dV\right) \tag{6}$$

$$\underline{v}^{n+3/2} = \underline{v}^{n+1/2} + \Delta t \underline{\ddot{u}}^{n+1}$$

A new configuration is obtained first. On this known configuration equilibrium is enforced, and the new velocity is obtained only at the end of the time integration algorithm.

This time integration scheme is completely ***explicit***.

- The central difference scheme is ***second-order accurate***, and therefore comparable as far as accuracy is concerned with the implicit integrators often used in classical FE methods.

- However, it is stable only for time increments below a certain limit (***conditional stability***).

- For highly non-linear problems (which are of interest here) this is not a serious drawback because even unconditionally stable methods would need to use small time increments anyway for ***accuracy*** reasons.

Among the advantages of the chosen method are:

- The transient dynamic problem is reduced to the search of the state of stress inside the elements in a (new) configuration which is ***already known***, having at disposal not only the stress in the previous configuration but also, of course, the deformation process between these two configurations.

- This is very convenient compared with implicit methods where the new stress state is searched ***at the same time*** as the new configuration, sometimes by using complex iterative procedures governed by convergence criteria.

- The proposed method appears particularly ***simple*** for the treatment of complex non-linear problems. Hence, it is very ***robust***.

- Furthermore, direct application of the virtual work principle, together with a second-order accurate time integration scheme, guarantees a very ***high accuracy*** of the numerical results.

- Spectral analysis of the integration schemes reveals that frequencies resulting from the use of the central difference scheme are slightly higher than physical ones. The same effect is obtained by using a consistent mass matrix.

- On the other hand, use of a lumped (diagonal) mass matrix tends to reduce the frequency values. Consequently it is appropriate here for ***precision*** reasons to use a lumped mass matrix.

- This is an incredible gift of nature since, as we have seen, using a diagonalised mass matrix ***completely decouples*** the equilibrium equations: contrary to classical finite element methods, there is ***no need for system solvers***.

- The explicit character of this approach ***avoids the extra costs in terms of bandwidth***, which often raise very rapidly with the number of degrees of freedom in complex 3D problems treated by implicit methods.

JOINT RESEARCH CENTRE

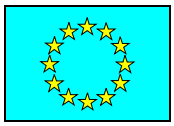

European Commission
Institute for the Protection and Security of the Citizen
European Laboratory for Structural Assessment

Essential Boundary Conditions

Conditions are imposed via a method of ***Lagrange multipliers*** [2].

- Assume that the imposed essential boundary conditions be expressed by a ***linear set of constraints*** on the velocities, of the form:

$$\underline{C}\underline{v} = \underline{b} \tag{7}$$

- Consider the subset of degrees of freedom for which essential boundary conditions are imposed. The equilibrium equations for this subset can be written, introducing ***unknown reactions*** $\underline{r}$:

$$\underline{m}\underline{a} = \underline{f}^{e} - \underline{f}^{i} + \underline{r} \tag{8}$$

- Without loss of generality, the unknown reactions can be expressed via a vector $\underline{\lambda}$ of Lagrange multipliers:

$$\underline{r} = \underline{C}^{T}\underline{\lambda} \tag{9}$$

- Substituting into (8), after some manipulation and by using the central difference integration scheme (5)-(6) in order to express the velocity $\underline{v}$ appearing in (7), $\underline{\lambda}$ can be symbolically obtained from:

$$\underline{B}^{*}\underline{\lambda} = \underline{W} \tag{10}$$

where $\underline{W}$ is a known vector and $\underline{B}^{*}$ a known, square symmetric matrix whose coefficients vary in general with time, e.g. due to large motions or large deformations.

Time integration scheme (structure)

1. Set initial conditions: $n = 0$, $\Delta t = 0$, $t^n = t^0$, $\underline{x}^n = \underline{x}^0$, $\underline{\sigma}^n = \underline{\sigma}^0$, $\dot{\underline{u}}^n = \dot{\underline{u}}^0$, $W^{\text{int}} = 0$, $W^{\text{ext}} = W^{\text{kin}}$;
   (W^{int}, W^{ext}, W^{kin} are internal energy, external work and kinetic en.);

2. `GO TO 5`;

3. (Note: $\underline{x}^n$, $\underline{\sigma}^n$, $\ddot{\underline{u}}^n$ and $\dot{\underline{u}}^n$ are known quantities);
   Update the mid-step velocity: $\underline{v}^{n+1/2} = \dot{\underline{u}}^n + (\Delta t^{\text{new}}/2)\ddot{\underline{u}}^n$;
   Set: $\boxed{n \leftarrow n+1}$, $\Delta t \leftarrow \Delta t^{\text{new}}$ and $t^n \leftarrow t^{n-1} + \Delta t$;

4. Update the configuration: $\underline{x}^n = \underline{x}^{n-1} + \Delta t \underline{v}^{n-1/2}$ (loop over nodes);

5. Compute the internal forces: $\underline{f}^{\text{int}} = \sum_e \int_{V^e} \underline{B}^T \underline{\sigma} dV$ (loop over elements);
   V^e and $\underline{B}^T$ are evaluated on the current configuration (n);
   If $n > 0$, then $\underline{\sigma}^n = \underline{\sigma}^{n-1} + \Delta\underline{\sigma}$;
   While computing element internal forces, evaluate Δt^{new} and add the internal energy increment to W^{int};

6. Assemble internal forces; evaluate and assemble external forces $\underline{f}^{\text{ext}}$; i.e:
   6.1 applied loads;
   6.2 reaction forces due to essential boundary conditions;
   Add external work increment to W^{ext};

7. Compute accelerations and update velocities (first half step):
   $\ddot{\underline{u}}^n = \underline{M}^{-1}(\underline{f}^{n,\text{ext}} - \underline{f}^{n,\text{int}})$ (loop over nodes);
   If $n > 0$, then $\dot{\underline{u}}^n = \underline{v}^{n-1/2} + (\Delta t/2)\ddot{\underline{u}}^n$ (loop over nodes);

8. If no output is required at this time, then `GO TO 3`;

9. Compute kinetic energy and check energy balance: $W^{\text{ext}} \approx W^{\text{int}} + W^{\text{kin}}$;
   Print requested output;

10. If final time not reached, then `GO TO 3`.

JOINT RESEARCH CENTRE

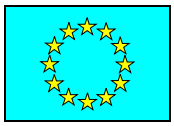

European Commission
Institute for the Protection and Security of the Citizen
European Laboratory for Structural Assessment

- The quality of the obtained solution may be checked globally by computing at each time step the ***energy balance***. In fact, the energy supplied to the system (work of external forces, initial kinetic energy etc.) must equal the sum of internal and kinetic energies.

- The balance error may e.g. be computed as:

$$\varepsilon = \frac{W^{ext} - W^{int} - W^{kin}}{W^{ext}} \qquad (11)$$

- This error indicator is used ***a posteriori*** in order to check the previously obtained solution and must not be confused with convergence parameters typical of iterative approaches.

- The main difficulties of the method, which is indeed quite compact, concentrate in the determination of the new stress or of the stress increment $\Delta\underline{\sigma}$ and in some cases also in the determination of 'external' forces (e.g. fluid-structure interaction problems).

- Note that the treatment of ***fluids*** requires some modifications to the above algorithm, that will be detailed below.

Treatment of geometric non-linearities

Kinematics

In the Lagrangian description, the reference is attached to ***material points***. For convenience, the ***material coordinates*** $\underline{X}$ are generally chosen corresponding with the initial configuration ($t = t_0$). Each particle then occupies at time t a position $\underline{x}$:

$$\underline{x} = \underline{x}(\underline{X}, t) \tag{12}$$

A measure of deformation may be obtained by applying to the material gradient of the configuration $\underline{F}$ ("***deformation gradient***"):

$$\underline{F} = \frac{\partial \underline{x}}{\partial \underline{X}} \tag{13}$$

the ***polar decomposition*** theorem:

$$\underline{F} = \underline{T}\underline{R} \tag{14}$$

where $\underline{R}$ is an orthogonal matrix that represents a ***rotation*** and $\underline{T}$ is a measure of deformation, known as the left stretching.

In practice, this means that a linear element $d\underline{X}$ in the reference configuration transforms into the element $d\underline{x}$ in the current configuration by undergoing a rotation $\underline{R}$, followed by a stretching $\underline{T}$.

From $\underline{R}$ one may derive a ***vorticity matrix*** $\underline{\Omega}$:

$$\underline{\Omega} = \dot{\underline{R}}\underline{R}^T \tag{15}$$

which represents a measure of the instantaneous rotation which may be used to update the stresses.

Measures of instantaneous deformation and rotation may also be derived from the ***spatial velocity gradient*** $\underline{L}$:

$$\underline{L} = \frac{\partial \dot{\underline{x}}}{\partial \underline{x}} \tag{16}$$

by means of the following ***additive decomposition***:

$$\underline{L} = \underline{D} + \underline{W} \tag{17}$$

- $\underline{D} = \frac{1}{2}(\underline{L} + \underline{L}^T)$ is the rate of deformation ("***stretching***");
- $\underline{W} = \frac{1}{2}(\underline{L} - \underline{L}^T)$ is the rate of rotation ("***spin***").

Finite Deformations

We have seen that the problem to be solved is to determine the ***increment of stress*** corresponding to the passage from the previous configuration of known stress state to the new configuration, which is already completely defined geometrically.

The above kinematic considerations indicate that the stretching process is generally accompanied by a material rotation which may be accounted for in various manners.

If deformations remain moderate, rotations may be considered uniform over each element. It is therefore possible to attach a local reference to each element and treat it as if it would be geometrically linear (co-rotational approach). It will be necessary to express the internal forces in the global system by means of an appropriate transformation matrix.

When deformations are very small, the rotation may even be considered uniform over the whole body (absence of geometric non-

linearity) and there are no difficulties because the rotation may be treated globally.

In non-linear problems the spatial integrations that lead to the internal forces are performed numerically and therefore they involve the knowledge of stress states only in some well-defined points of the elements. We call these ***Gauss points*** because very often a Gauss integration is adopted.

The idea is then to study the effect of large deformations separately and uniquely in the Gauss points.

In practice this means that for each Gauss points one must obtain the stretching and rotation corresponding to the time increment and from these compute the corresponding stress increment. The part resulting from the stretching through rheological effects (elasto-plasticity) will be detailed in a later section.

The state of stress of interest to us is Cauchy stress. Since this is referred to a fixed frame in space, it is obvious that its time derivative is not invariant with respect to rotation: $\dot{\underline{\sigma}}$ ***is not objective***.

An objective rate of stress may be obtained under the form:

$$\hat{\underline{\sigma}} = \dot{\underline{\sigma}} - \underline{A}\underline{\sigma} + \underline{\sigma}\underline{A} \qquad (18)$$

where $\underline{A}$ is an appropriate vorticity matrix.

For example, in the so-called ***Zaremba-Jaumann-Noll*** formulation:

$$\underline{A} = \underline{W} \qquad (19)$$

while in the so-called ***Green-Naghdi*** formulation it is:

$$\underline{A} = \underline{\Omega} \qquad (20)$$

Note, however, that the above considerations are valid only in the infinitesimal sense, while our problem requires the determination of a ***finite increment***.

We must therefore set up a numerical scheme for updating the Cauchy stress that is ***incrementally objective***. The 3D case presents technical difficulties but does not introduce further fundamental concepts and will therefore not be considered here.

From elementary geometric considerations it is possible to build up a scheme for two-dimensional problems that ensures objectivity in the presence of arbitrarily large time steps.

Let θ be the angle of rotation during a time interval Δt. From the transformation law of second-order tensors we know that the stress tensor transforms according to:

$$\underline{a}^T \underline{\sigma} \underline{a} \tag{21}$$

where:

$$\underline{a} = \begin{bmatrix} \cos\theta & \sin\theta \\ -\sin\theta & \cos\theta \end{bmatrix} \tag{22}$$

In the discrete process, it may be verified that the angle θ is related to the value of the vorticity A_{12} at half-step:

$$\tan\frac{\theta}{2} = \frac{1}{2}\Delta t A_{12} \tag{23}$$

In practice the update of stress may be performed by these three equations in conjunction with a ***constitutive law*** of the type:

$$\hat{\underline{\sigma}} = \dot{\underline{\sigma}} - \underline{A}\underline{\sigma} + \underline{\sigma}\underline{A} = \underline{C}(\underline{\sigma})\underline{D} \tag{24}$$

where $\underline{D}$ is the stretching.

Such a constitutive law, usually indicated as ***hypo-elastic***, will be used to describe the elasto-plastic behaviour.

Proposed algorithm

A very accurate algorithm is obtained by the following three-step procedure:

- We apply the ***first half*** of the rotation increment ($\theta/2$) to the state of stress $\underline{\sigma}^n$ (n corresponds here to the previous configuration), thus defining an intermediate stress state $\underline{\sigma}^*$:

$$\underline{\sigma}^* = \underline{p}\,\underline{\sigma}^n\,\underline{p}^T \tag{25}$$

with

$$\underline{p} = \begin{bmatrix} \cos\frac{\theta}{2} & \sin\frac{\theta}{2} \\ -\sin\frac{\theta}{2} & \cos\frac{\theta}{2} \end{bmatrix} \tag{26}$$

- Next, we apply the ***constitutive equation***, to account for the increment of deformation $\Delta t D^{n+1/2}$ that has been accumulated during the time interval Δt. We have therefore:

$$\underline{\sigma}^{n+1/2} = \underline{\sigma}^* + \Delta t \underline{C}\underline{D}^{n+1/2} \tag{27}$$

- Finally, we apply the ***second half*** of the rotation to $\underline{\sigma}^{n+1/2}$ in order to obtain the value at the end of the step:

$$\underline{\sigma}^{n+1} = \underline{p}\,\underline{\sigma}^{n+1/2}\,\underline{p}^T \tag{28}$$

The use of an intermediate configuration to apply the constitutive law causes an extra computational cost that has to be considered along with the desired precision level.

The central difference scheme offers a second-order accuracy in the time integration and the use of the stretching at half step ensures an optimal representation of the actual deformation velocity. In particular, one obtains an excellent approximation of the logarithmic strain (***natural strain***) when the increments are added to each other (this is only feasible in the absence of rotations, of course).

It should also be noted that the choice of a specific vorticity matrix ($\underline{W}$, $\underline{\Omega}$, others) is a matter subject to many discussions. In theory, this choice may not be separated from the choice of a constitutive law. In practice, however, it works quite well in many cases and yields excellent results in most engineering applications.

Modelling of elasto-plastic material

Theoretical aspects

The hypo-elastic constitutive law introduced above, Eq. (24), may be written for the case of elasto-plasticity:

$$\hat{\underline{\sigma}} = \underline{C}(\dot{\underline{\varepsilon}} - \dot{\underline{\varepsilon}}^{P}) = \underline{C}\dot{\underline{\varepsilon}}^{E} \qquad (29)$$

- $\dot{\underline{\varepsilon}}$ is the total strain rate ($\dot{\underline{\varepsilon}} \equiv \underline{D}$);
- $\dot{\underline{\varepsilon}}^{E}$ is the elastic strain rate;
- $\dot{\underline{\varepsilon}}^{P}$ is the plastic strain rate;
- $\underline{C}$ is Hooke's elasticity matrix.

In components form, $\underline{C}$ may be written:

$$C_{ijmn} = \mu(\delta_{im}\delta_{jn} + \delta_{in}\delta_{jm}) + \lambda\delta_{ij}\delta_{mn} \qquad (30)$$

where δ_{kl} is Kronecker's delta, λ and μ are Lame's constants:

$$\lambda = \frac{E\nu}{(1+\nu)(1-2\nu)} \quad , \quad \mu = \frac{E}{2(1+\nu)}$$

and E, ν are Young's modulus and Poisson's coefficient, respectively.

The material behaviour is elastic ($\dot{\underline{\varepsilon}}^{P} = 0$) until a ***limit state*** is reached characterised, for the ***Von Mises criterion***, by an ***equivalent stress*** $\bar{\sigma}$ equal to σ_S, the ***yield stress*** in a traction test:

$$\bar{\sigma} = \sqrt{\frac{3}{2}S_{ij}S_{ij}} = \sigma_S \qquad (31)$$

where S_{ij} are the components of the deviatoric part of the stress $\underline{\sigma}$:

$$S_{ij} = \sigma_{ij} - \frac{1}{3}\delta_{ij}\sigma_{kk}$$

JOINT RESEARCH CENTRE

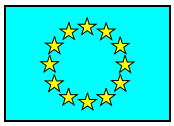

European Commission
Institute for the Protection and Security of the Citizen
European Laboratory for Structural Assessment

The plasticity criterion may be represented by an yield surface $f(\underline{\sigma})$:

$$f(\underline{\sigma}) = \frac{1}{2} S_{ij} S_{ij} = \frac{1}{3} \sigma_S^2 \qquad (32)$$

In the space of principal stresses this surface is a cylinder, oriented along the line that trisects the first octant and of radius R:

$$R = \sqrt{\frac{2}{3}} \sigma_S$$

The ***admissible stress states*** are those that lie either ***internally or upon*** the yield surface.

Once reached the yield surface, the plastic component of the strain rate may be derived, by using the ***normality principle***, from an ***associated flow rule***:

$$\dot{\underline{\varepsilon}}^P = \dot{\Lambda} \underline{N} \qquad \text{or } 0 \text{ (elastic case)} \qquad (33)$$

where $\underline{N}$ is the unit normal outgoing from the yield surface.

The amplitude $\dot{\Lambda}$ of plastic flow may be obtained from a ***consistency condition*** which ensures that ***the state of stress remains on the yield surface***.

For the Von Mises cylinder, it is evident that:

$$\underline{N} = \frac{\underline{\underline{S}}}{R} \qquad (34)$$

In fact, the normal cross-section of the yield surface is a circle.

In order to determine whether the deformation process remains elastic or not when the current stress state is on the yield surface and a strain rate $\dot{\underline{\varepsilon}}$ is applied, a ***trial stress rate*** $\dot{\underline{\sigma}}^{tr}$ is introduced:

$$\dot{\underline{\sigma}}^{tr} = \underline{C}\dot{\underline{\varepsilon}} \tag{35}$$

- if $\underline{N} \cdot \dot{\underline{\sigma}}^{tr} \leq 0$ the deformation process is purely ***elastic***, and the trial stress rate is the actual stress rate: $\dot{\underline{\sigma}} = \dot{\underline{\sigma}}^{tr}$
- else if $\underline{N} \cdot \dot{\underline{\sigma}}^{tr} > 0$ the process is ***elasto-plastic***.

Usually, materials subjected to plastic deformation exhibit some ***hardening***: the yield limit varies as the deformation proceeds.

By defining an equivalent plastic strain rate $\dot{\overline{\underline{\varepsilon}}}^{P}$:

$$\dot{\overline{\underline{\varepsilon}}}^{P} = \sqrt{\frac{2}{3}\dot{\varepsilon}_{ij}^{P}\dot{\varepsilon}_{ij}^{P}} \tag{36}$$

where $\dot{\varepsilon}_{ij}^{P}$ are the components of $\dot{\underline{\varepsilon}}^{P}$, the model for ***isotropic*** linear hardening may be written as:

$$\dot{\sigma}_S = E^P \dot{\overline{\underline{\varepsilon}}}^{P} \tag{37}$$

where E^P is the so-called plastic modulus.

Other hardening models may be defined: for example, the ***kinematic*** hardening model where the whole yield surface is translated in order to account for the Bauschinger effect.

Let us illustrate the effect in the case of a simple traction-compression test:

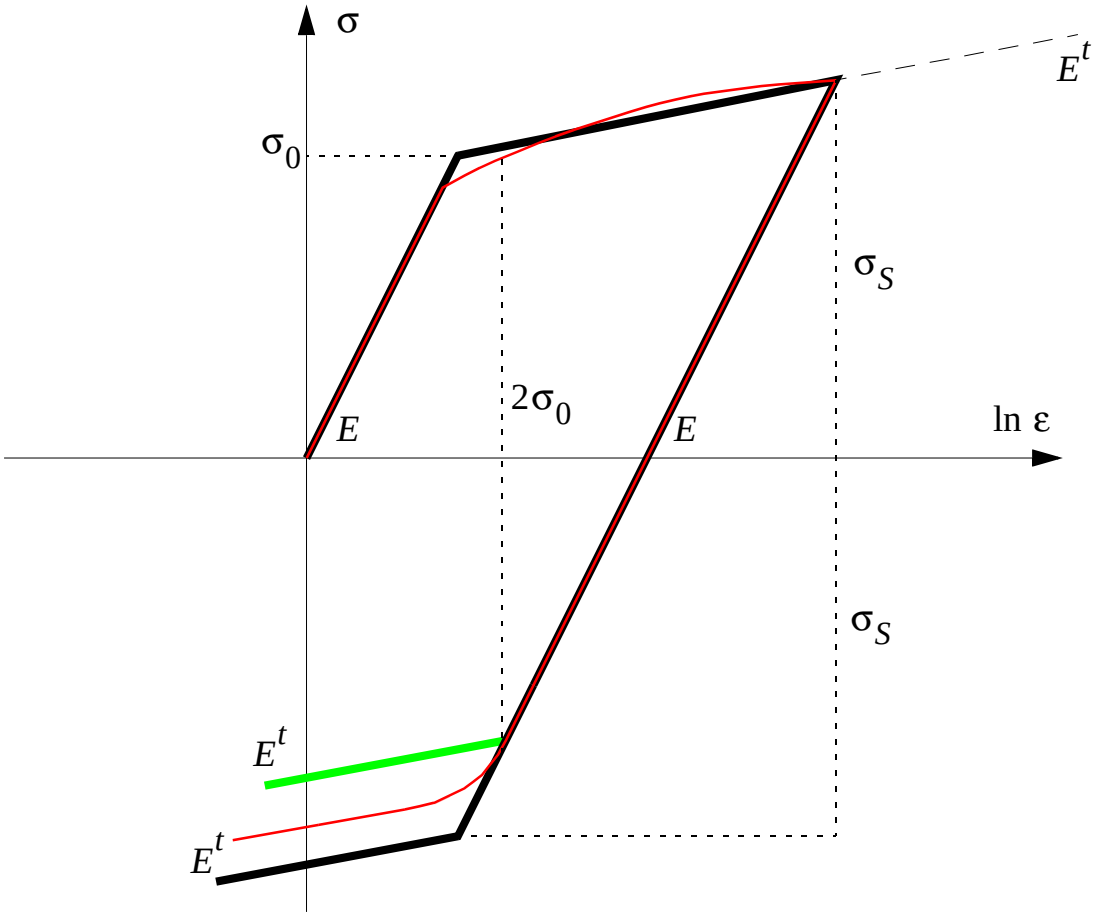

$$E^P = \frac{EE^t}{E - E^t}$$

experiment

isotropic hardening model

kinematic hardening model

$\sigma_0 \equiv \sigma_S$ of the virgin material

E^t is the tangent modulus $(E^t \ll E)$

Various hardening models may be set up on the basis of the theory presented above.

JOINT RESEARCH CENTRE

European Commission
Institute for the Protection and Security of the Citizen
European Laboratory for Structural Assessment

When performing studies on material behaviour, it is often interesting to have at disposal a model that somehow combines the isotropic and kinematic hardening. However, in many applications an isotropic model or even an elastic/perfectly plastic model ($E^t = 0$) is completely adequate.

In the following we will consider for simplicity an ***elastic/perfectly-plastic material***, for which the yield surface remains constant.

One must evaluate $\dot{\Lambda}$ in order to compute $\dot{\underline{\varepsilon}}^P$, the plastic part of the strain rate. Also in this case a simple drawing is of help:

$\sigma_1, \sigma_2, \sigma_3$ principal stresses

$\underline{C}$ is isotropic

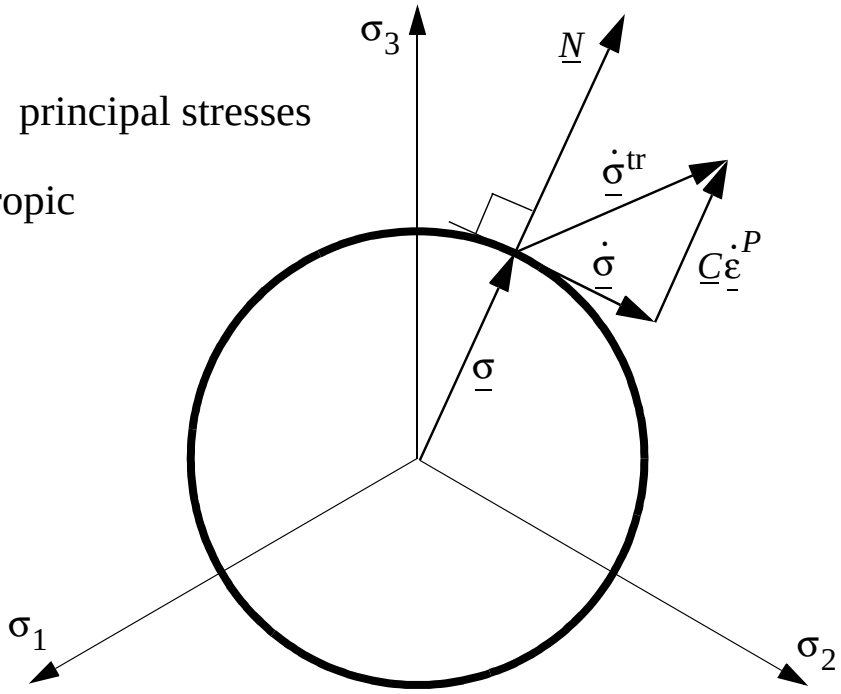

$$\dot{\underline{\sigma}} = \dot{\underline{\sigma}}^{tr} - \underline{C}\dot{\underline{\varepsilon}}^P = \underline{C}\dot{\underline{\varepsilon}} - \underline{C}\dot{\underline{\varepsilon}}^P$$

- $\underline{N}$ and hence also $\dot{\underline{\varepsilon}}^P$ lie in the deviatoric plane;
- $\dot{\underline{\sigma}}$ is the orthogonal projection of $\dot{\underline{\sigma}}^{tr}$ on the plane tangent to the yield surface.

JOINT RESEARCH CENTRE

European Commission
Institute for the Protection and Security of the Citizen
European Laboratory for Structural Assessment

The previous drawing stresses the fact that the use of Von Mises criterion transforms the ***orthogonality*** (deriving from the normality principle) ***into "radiality"***.

This characteristics of radiality opens the way to an ***efficient, accurate and at the same time simple*** treatment of elasto-plastic behaviour.

Finally, notice that the consistency condition for the elastic/perfectly-plastic case reduces to the following analytical expression:

$$\dot{\Lambda} = \underline{N} \cdot \dot{\underline{\varepsilon}} \qquad (38)$$

Résumé of the formulation for the elastic/perfectly-plastic case (Von Mises criterion)

- ***Constitutive equation***: $\hat{\underline{\sigma}} = \underline{C}(\dot{\underline{\varepsilon}} - \dot{\underline{\varepsilon}}^{P})$;
- ***Plastic flow rule***: $\dot{\underline{\varepsilon}}^{P} = \begin{cases} \underline{0} & \text{(Elastic)} \\ \dot{\Lambda}\underline{N} & \text{(Plastic)} \end{cases}$;
- ***Consistency condition***: $\dot{\Lambda} = \underline{N} \cdot \dot{\underline{\varepsilon}}$;
- ***Unit normal***: $\underline{N} = \underline{S}/R \quad , \quad R = \sqrt{2/3}\sigma_S$;
- ***Trial stress rate***: $\dot{\underline{\sigma}}^{\text{tr}} = \underline{C}\dot{\underline{\varepsilon}}$;
- ***Definition of an elastic process (E)***:

$$f(\underline{\sigma}) = \frac{1}{2}S_{ij}S_{ij} < \sigma_S^2 \quad \text{, or}$$

$$f(\underline{\sigma}) = \sigma_S^2 \quad \text{and} \quad \underline{N} \cdot \dot{\underline{\sigma}}^{\text{tr}} \leq 0$$

- ***Definition of a plastic process (P)***:

$$f(\underline{\sigma}) = \sigma_S^2 \quad \text{and} \quad \underline{N} \cdot \dot{\underline{\sigma}}^{\text{tr}} > 0$$

In case of hardening, the formulation is quite similar but of course includes also the equations describing the evolution of the yield surface. The consistency condition becomes slightly more complex, but the essence of the formulation remains the same.

This theory considers only ***infinitesimal*** aspects which are not automatically generalised to the case of ***finite increments***: it remains to define an ***algorithm***.

The radial return algorithm

The radial return method (due to Wilkins) consists in a discrete analog of the geometric concept used in the theory (see the previous figure). In fact, this method relies upon the normality principle.

Given a known state of stress $\underline{\sigma}_n$ and by applying an increment of deformation $\Delta\underline{\varepsilon}$, the method consists of ***two phases*** [3]:

- ***First***, an elastically induced trial stress state is evaluated:

$$\underline{\sigma}^{tr}_{n+1} = \underline{\sigma}_n + \underline{C}(\Delta\underline{\varepsilon}) \tag{39}$$

- ***Then***, this trial stress state is tested in order to check whether it lies within or outside the yield surface:
  - if $\underline{\sigma}^{tr}_{n+1}$ lies within (or onto) the yield surface, the process is elastic and one simply puts:

$$\underline{\sigma}_{n+1} = \underline{\sigma}^{tr}_{n+1} \tag{40}$$

  - else if $\underline{\sigma}^{tr}_{n+1}$ lies outside the yield surface the process is (elasto-)plastic and $\underline{\sigma}_{n+1}$ is defined by the intersection between the yield surface and the line which connects its centre with the trial stress state $\underline{\sigma}^{tr}_{n+1}$.

The method is used in the deviatoric plane as sketched below:

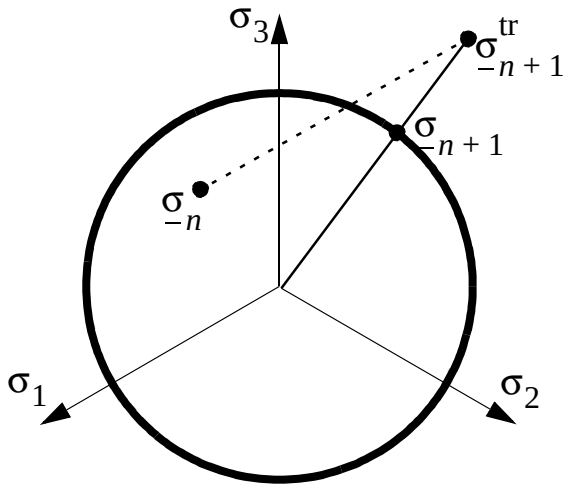

In spite of its extreme simplicity, this algorithm gives excellent results in practice. It may be shown that the algorithm is ***asymptotically exact*** both for very small increments and for increments tending to infinity.

Accuracy is always very good, even excellent if one takes into account the uncertainties which are anyway related to material behaviour.

Furthermore, it is easily extended to the case with hardening.

It should be noted that the practical efficiency of the algorithm stems in particular from the fact that the deformation increment is defined without ambiguity ***before*** starting the search of $\underline{\sigma}_{n+1}$, the new stress state.

In iterative methods, the nature of the numerical problem is different. Therefore, there is no *a priori* evidence that the radial return method is useful also in conjunction with implicit time integration schemes.

Résumé of the radial return algorithm

- ***Compute the trial stress state***:

$$\underline{\sigma}_{n+1}^{tr} = \underline{\sigma}_n + \underline{C}(\Delta\underline{\varepsilon})$$

- ***Compute the hydrostatic stress***:

$$\sigma_H = \frac{1}{3}(\sigma_{mm})_{n+1}^{tr}$$

- ***Compute the trial deviatoric stress state***:

$$\underline{S}^{tr} = \underline{\sigma}_{n+1}^{tr} - \sigma_H \underline{I} \qquad \text{(with } \underline{I} \text{ the identity matrix)}$$

- ***Compute a trial equivalent stress state (scalar)***:

$$A^{tr} = \underline{S}^{tr} \cdot \underline{S}^{tr}$$

- ***If*** $A^{tr} \leq R^2$ (with R the radius of the Von Mises cylinder)***, then***:

$$\underline{\sigma}_{n+1} = \underline{\sigma}_{n+1}^{tr}$$

- ***Else if*** $A^{tr} > R^2$***, then***:

$$\underline{\sigma}_{n+1} = \frac{R}{\sqrt{A^{tr}}}\underline{S}^{tr} + \sigma_H \underline{I}$$

This scheme [3] describes all numerical operations necessary to obtain $\underline{\sigma}_{n+1}$ from $\underline{\sigma}_n$ and $\Delta\underline{\varepsilon}$.

It is all the same in the presence of hardening, except the last point, because the new hardening surface must be determined in order to let the new stress $\underline{\sigma}_{n+1}$ lie on it.

Validation examples (structure)

To illustrate the methods proposed in the previous sections, a few validation examples are considered.

Longitudinal waves in a bar

Consider a long bar subjected to longitudinal loading:

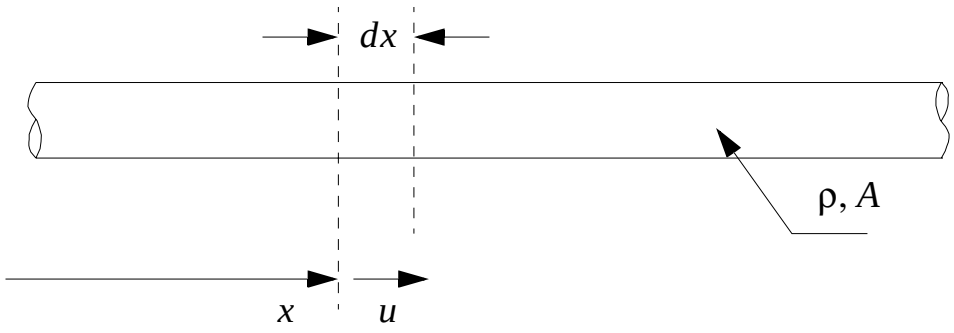

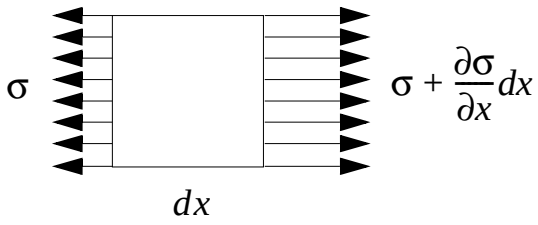

Assume that:

- The cross-section A is constant;
- The material, of density ρ, is homogeneous and isotropic;
- Plane, parallel cross sections remain plane and parallel;
- The stress σ is uniform in each cross section;
- We neglect the effect of ***lateral inertia***.

The (dynamic) equilibrium is expressed by the following equation (equation of motion):

$$-\sigma A + \left(\sigma + \frac{\partial \sigma}{\partial x} dx\right) A = \rho A dx \frac{\partial^2 u}{\partial t^2} \tag{41}$$

from which we obtain:

$$\frac{\partial \sigma}{\partial x} = \rho \frac{\partial^2 u}{\partial t^2} \tag{42}$$

For an elastic material we have $\sigma = E\varepsilon$, and since the longitudinal deformation is $\varepsilon = \frac{\partial u}{\partial x}$, we may re-write (42) as:

$$E \frac{\partial^2 u}{\partial x^2} = \rho \frac{\partial^2 u}{\partial t^2} \tag{43}$$

or, finally:

$$\frac{\partial^2 u}{\partial t^2} = c_0^2 \frac{\partial^2 u}{\partial x^2} \qquad \text{with} \qquad c_0 = \sqrt{\frac{E}{\rho}} \tag{44}$$

Equation (44) is known as ***wave equation*** and the constant c_0 is the sound speed in the elastic material.

The general solution (D'Alembert's solution) to (44) reads:

$$u(x, t) = f(x - c_0 t) + g(x + c_0 t) \tag{45}$$

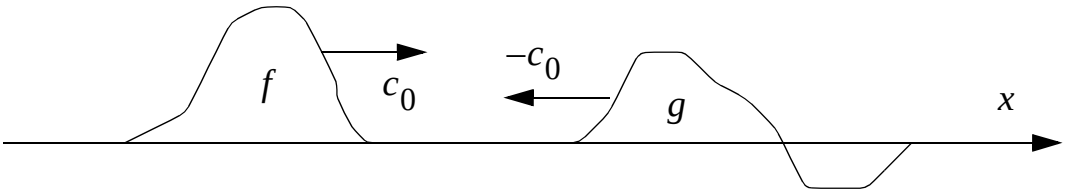

- The two "***waves***" f and g propagate ***without distortion***;
- The spatial form of f and g is determined by ***initial conditions*** and by ***boundary conditions***.

While the waves propagate at (constant) velocity c_0, the material particles move at velocity:

$$v(x,t) = \frac{\partial u}{\partial t} = -c_0 \frac{\partial f}{\partial t} = -c_0 f'(x - c_0 t) \tag{46}$$

But since:

$$\sigma(x,t) = E\varepsilon = E\frac{\partial u}{\partial x} = E f'(x - c_0 t) \tag{47}$$

we have:

$$v(x,t) = -\frac{c_0}{E}\sigma(x,t) \tag{48}$$

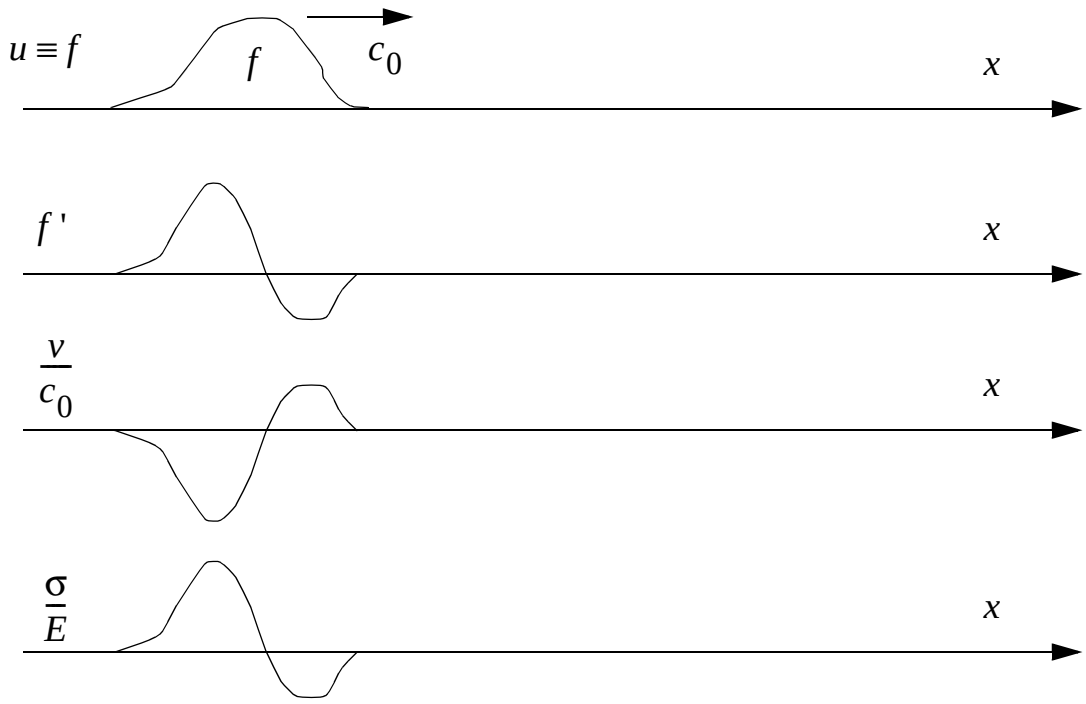

JOINT RESEARCH CENTRE
European Commission
Institute for the Protection and Security of the Citizen
European Laboratory for Structural Assessment

Method of Images

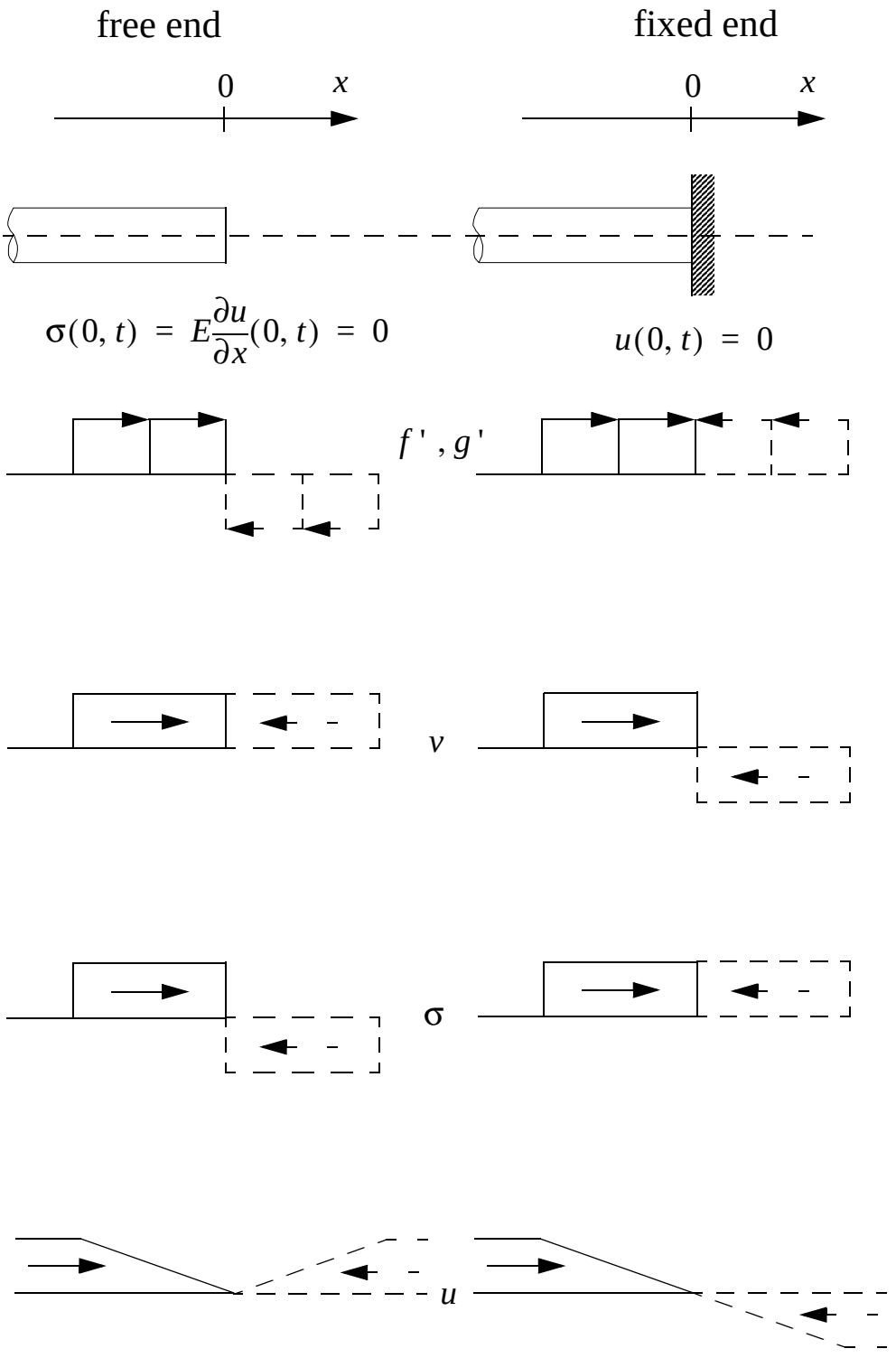

Symbols used in the examples [4]

E	Young's modulus	σ_y	First yield stress
ρ	Density	E_p	First plastic modulus
ν	Poisson's ratio	σ_{y2}	Second yield stress
		E_{p2}	Second plastic modulus

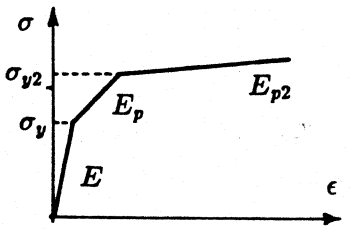

Wave propagation in a long bar (1D bar impact)

E	200 GPa
ρ	8000 kg/m^3
R_0	1 m
L_0	1 m
v_0	50 m/s

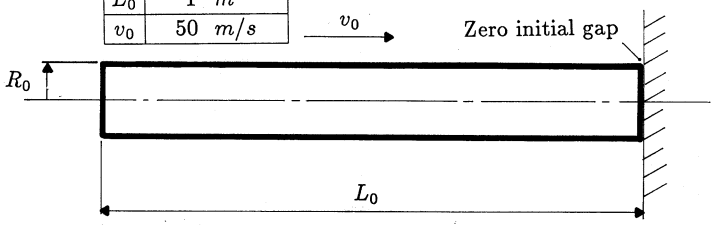

1D IMPACT

Problem definition

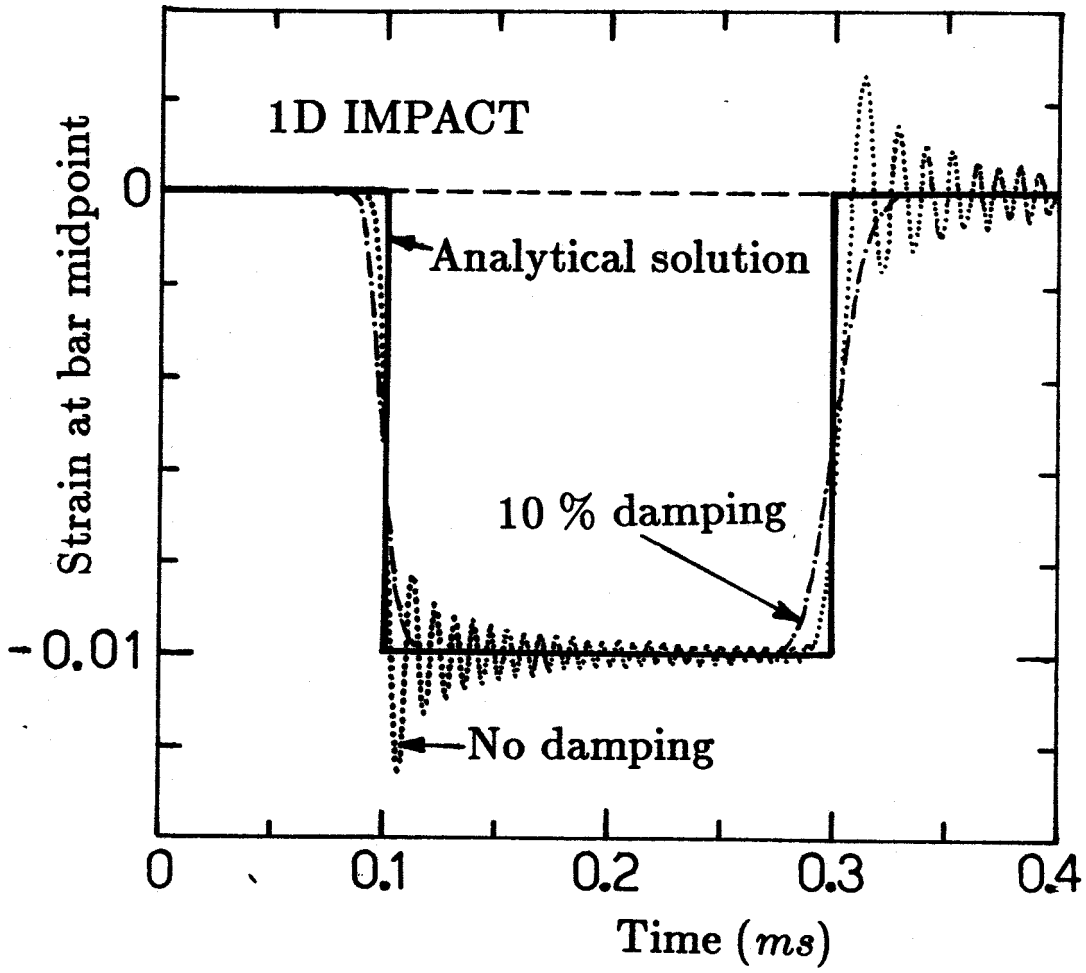

Solutions

JOINT RESEARCH CENTRE
European Commission
Institute for the Protection and Security of the Citizen
European Laboratory for Structural Assessment

Elasto-plastic wave propagation

1-D ELASTIC (-PLASTIC) WAVE PROPAGATION

Model: 2-D Plane Stress Analysis

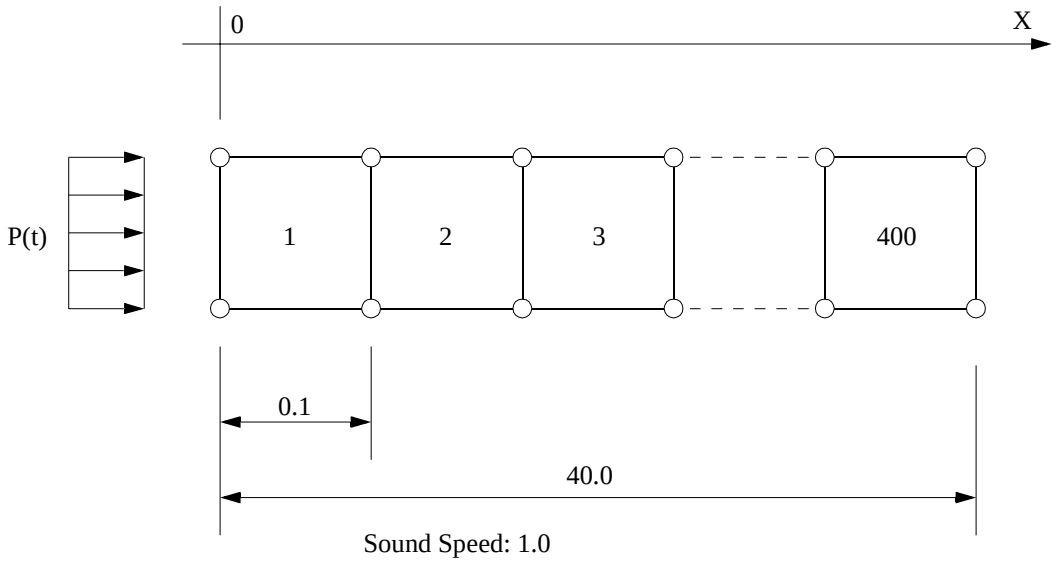

Sound Speed: 1.0
Particle Velocity: 0.01
Mesh Velocity (ALE cases): +-0.25 (starting at t=24)
Final Time: 32

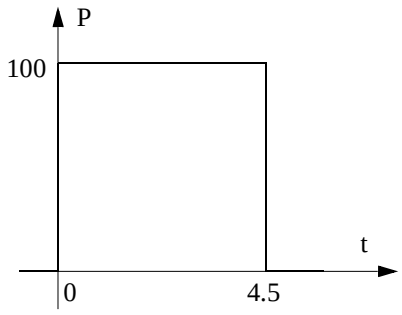

Wave Generation

Material Data	
Density	10000
Young’s Modulus	10000
Yield Stress	75
Plastic Modulus	3333.33
Poisson’s Ratio	0.0

Problem definition

JOINT RESEARCH CENTRE

European Commission
Institute for the Protection and Security of the Citizen
European Laboratory for Structural Assessment

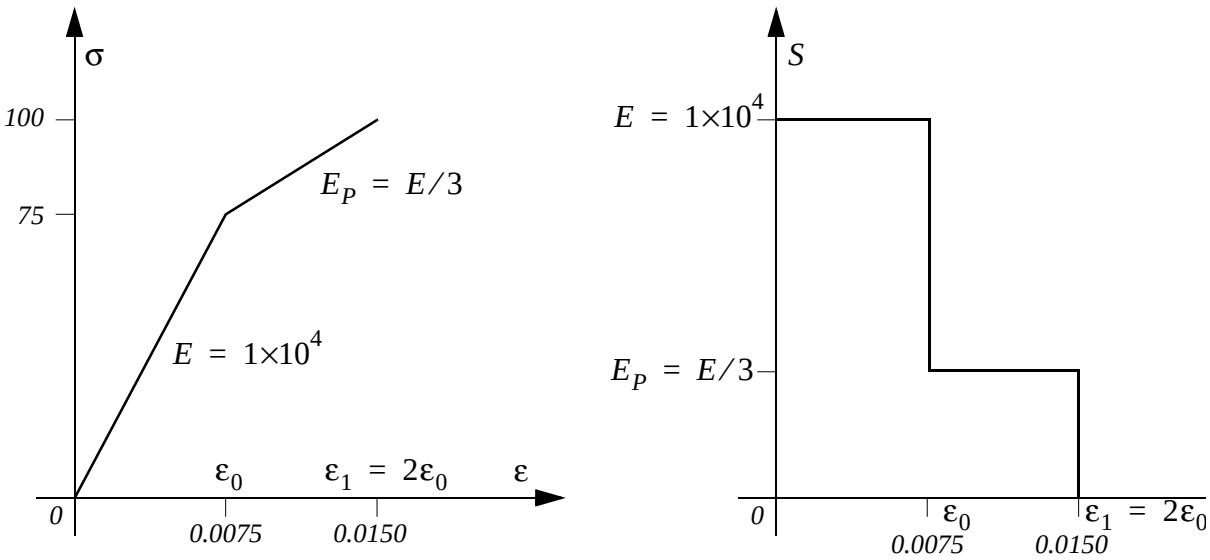

Material properties

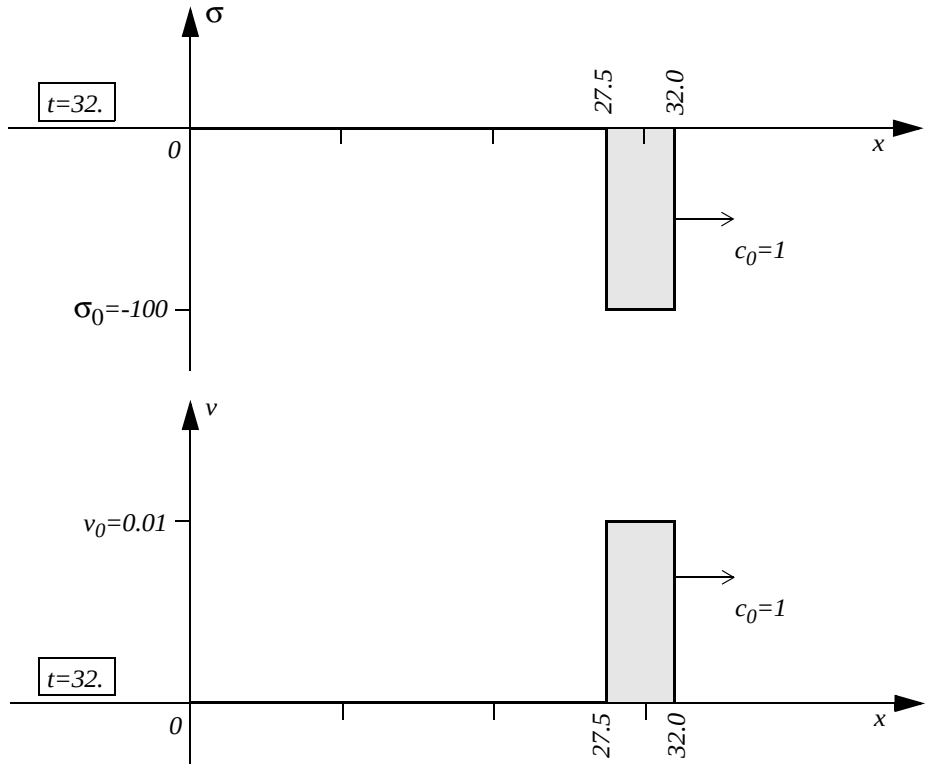

Elastic solution

JOINT RESEARCH CENTRE

European Commission
Institute for the Protection and Security of the Citizen
European Laboratory for Structural Assessment

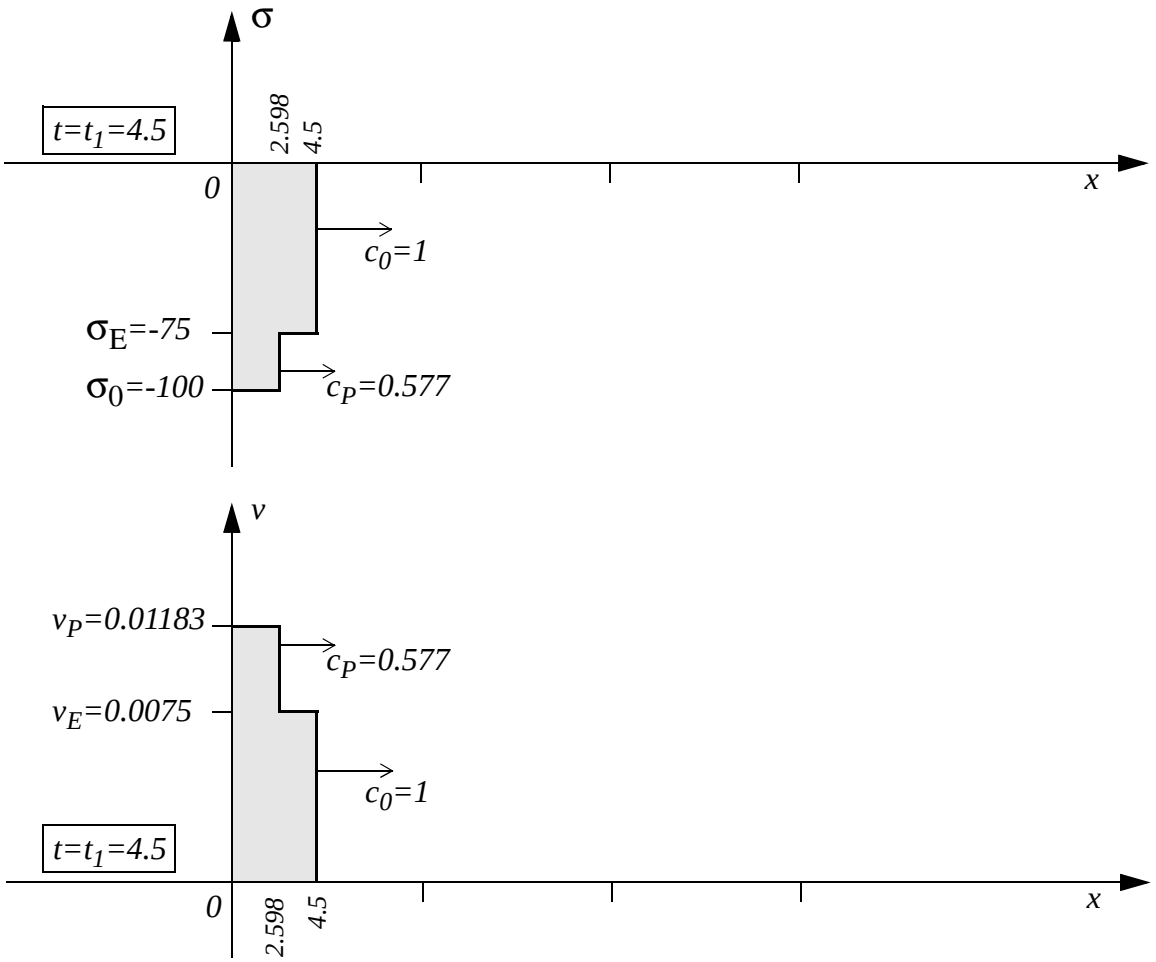

(a)

Elasto-plastic solution at t = 4.5

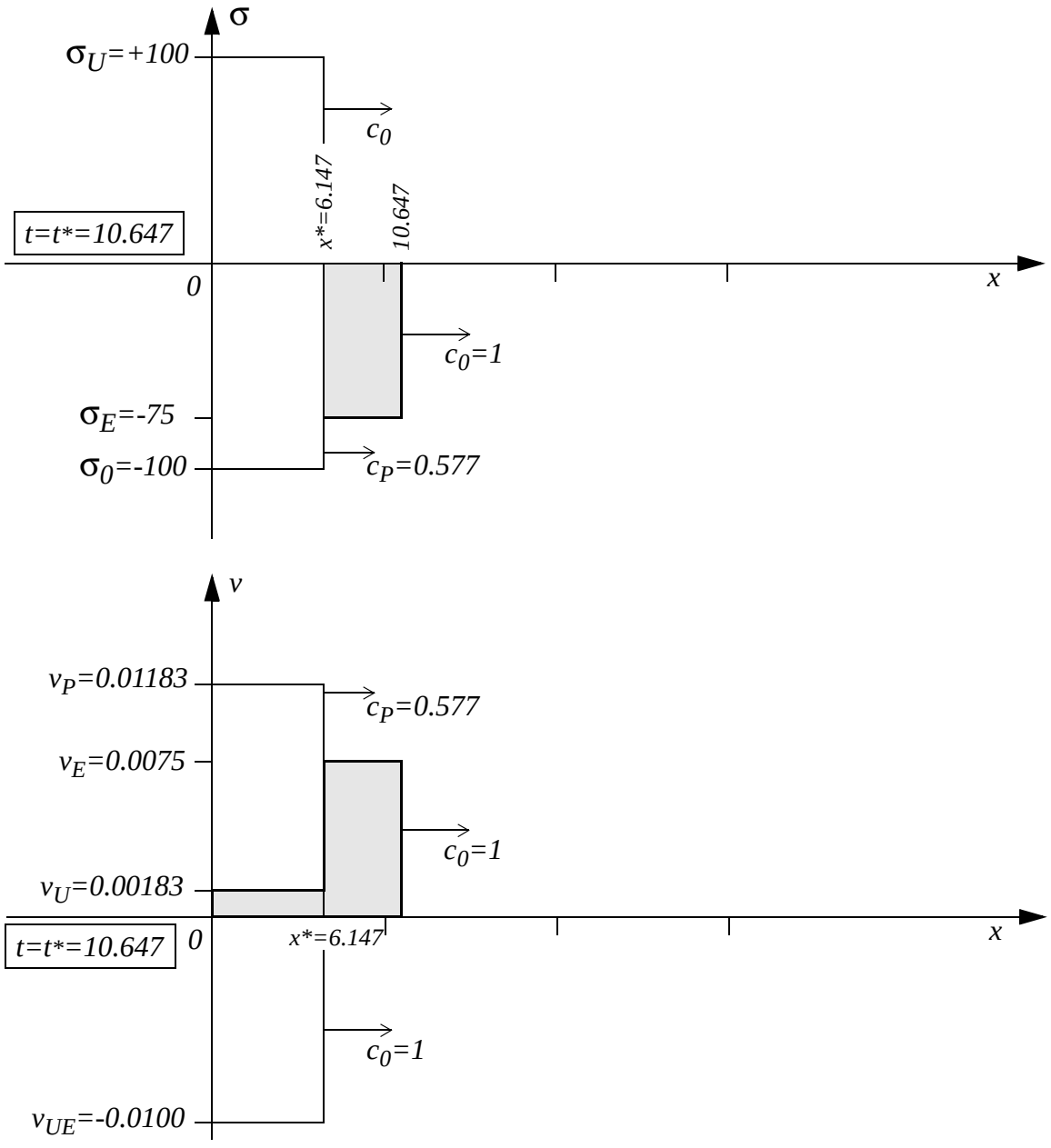

(b)

Elasto-plastic solution at t = 10.647

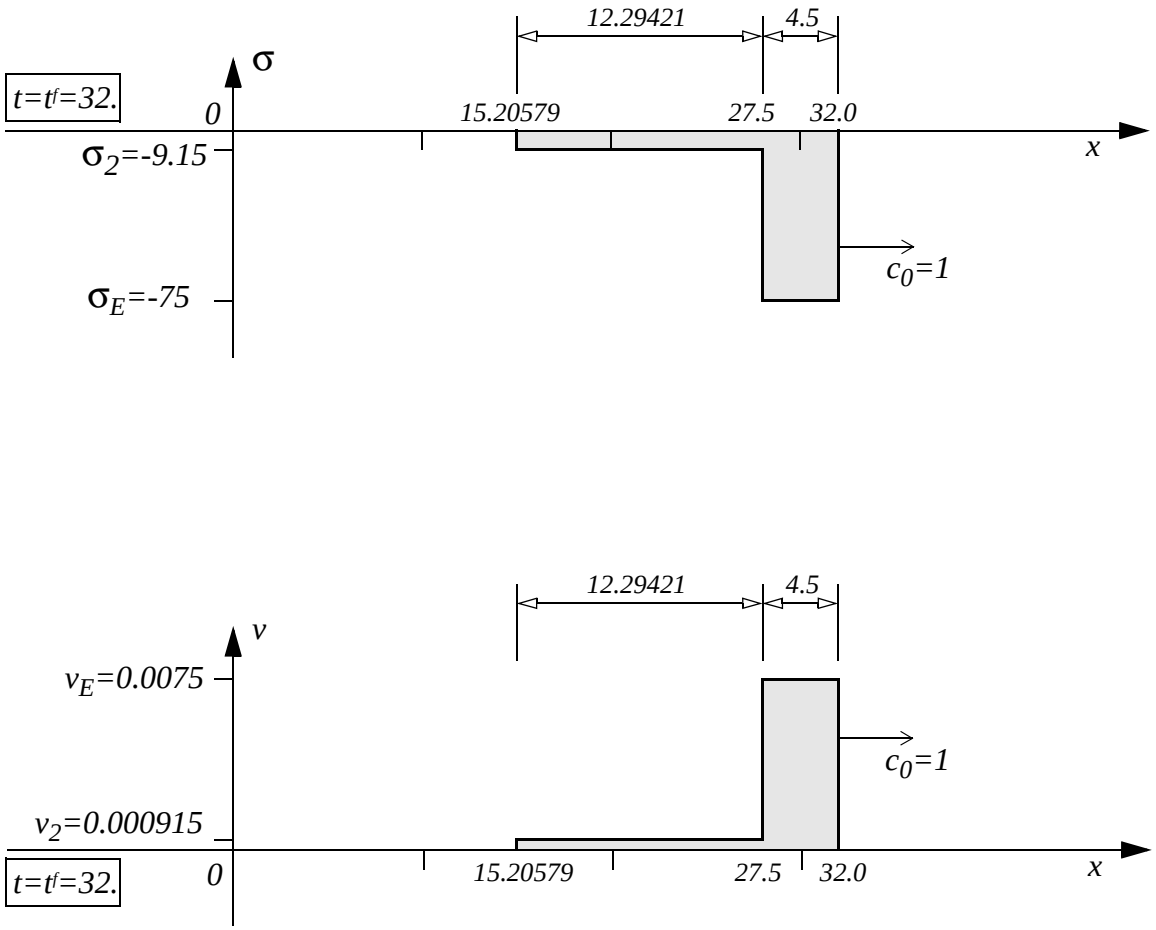

(e)

Elasto-plastic solution at t = 32

Comparison of 1D and 2D elasto-plastic solutions

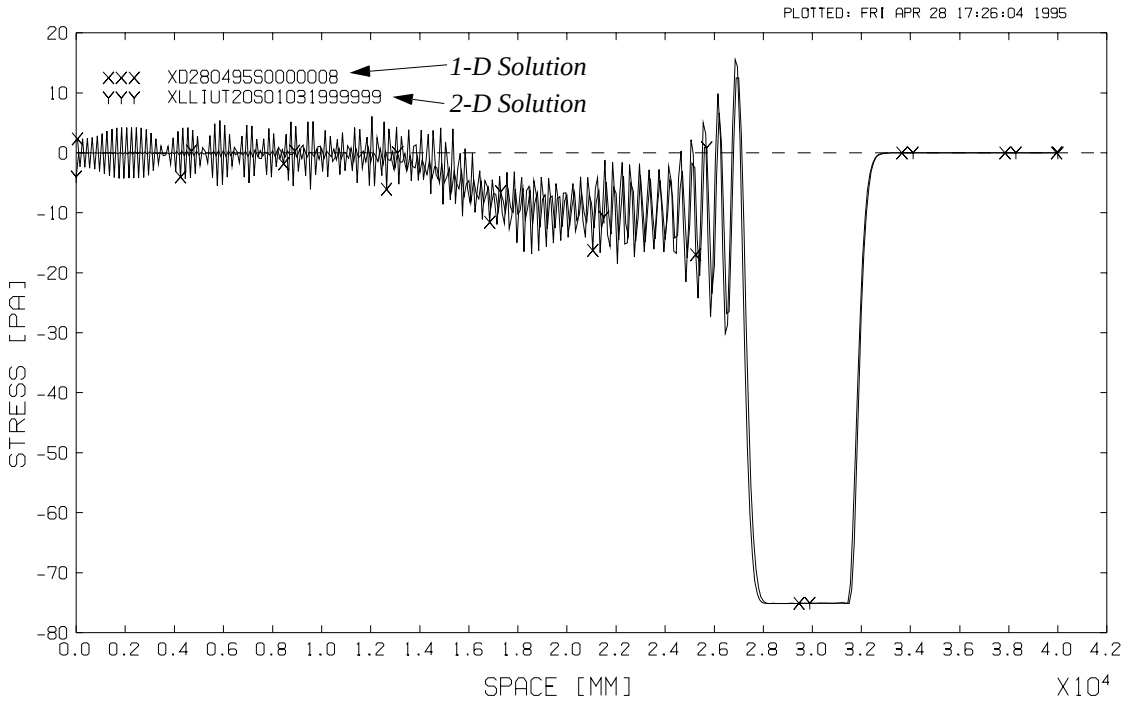

(a)

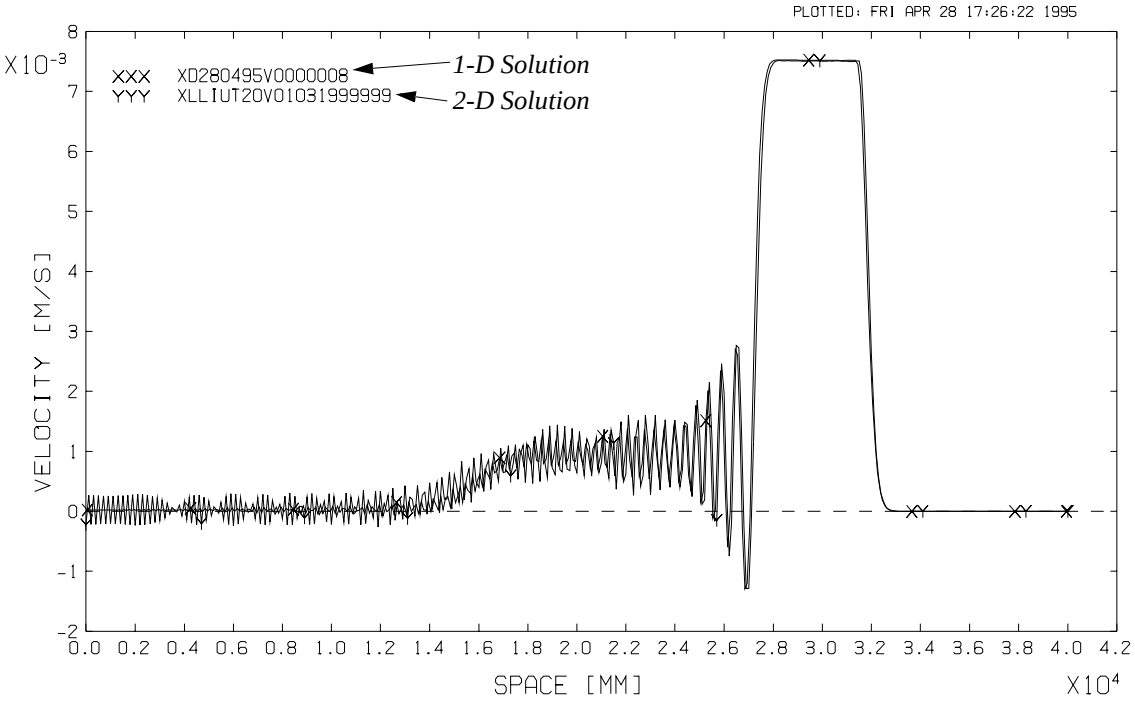

(b)

JOINT RESEARCH CENTRE

European Commission
Institute for the Protection and Security of the Citizen
European Laboratory for Structural Assessment

Cone problem

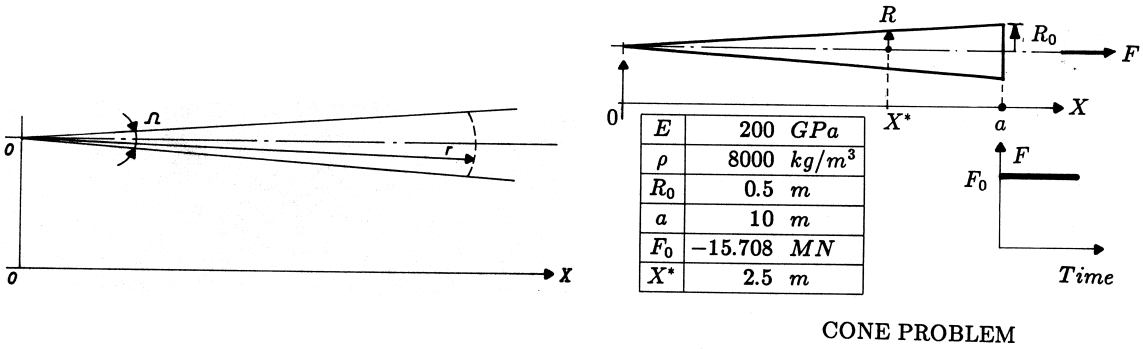

E	200 GPa
ρ	8000 kg/m^3
R_0	0.5 m
a	10 m
F_0	−15.708 MN
X^*	2.5 m

CONE PROBLEM

Problem definition

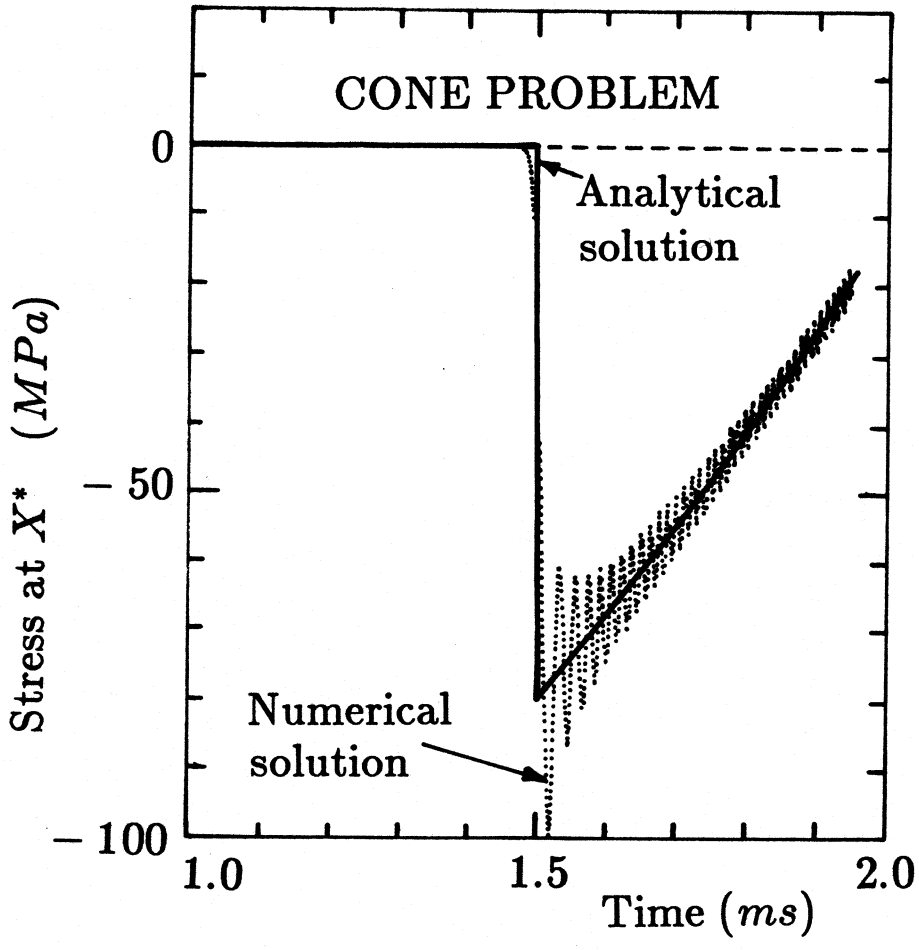

Solutions

Elastic sphere

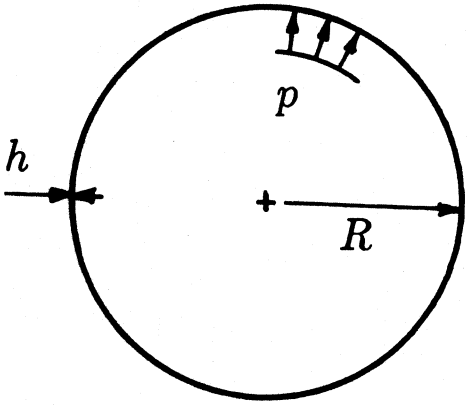

E	200 GPa
ρ	8.E7 kg/m^3
ν	0.3
R_0	0.03 m
p_0	286 MPa
h_0	40 μm
β	0.36282

$$R = R_0(1+\xi) \qquad p = p_0\left[\frac{1-\beta}{(1+\xi)^3-\beta}\right]^{1.24}$$

Problem definition

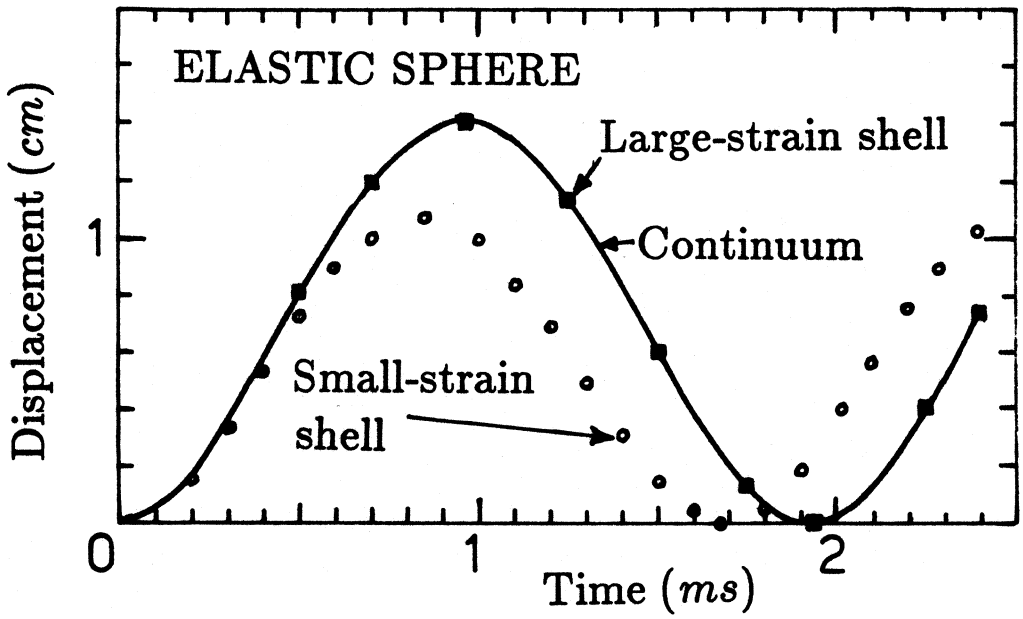

Solutions

JOINT RESEARCH CENTRE
European Commission
Institute for the Protection and Security of the Citizen
European Laboratory for Structural Assessment

Circular plate

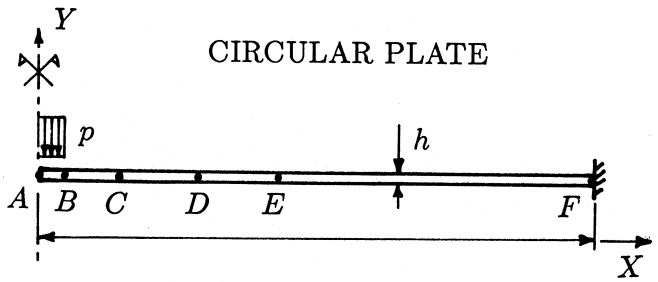

X_A	0 mm
X_B	8.47 mm
X_C	25.4 mm
X_D	50.8 mm
X_E	76.2 mm
X_F	177.8 mm
h	3.175 mm

E	68.95 GPa
ρ	2962 kg/m^3
ν	0.333
σ_y	68.95 MPa
E_p	70 MPa
P_0	18.4957 MPa

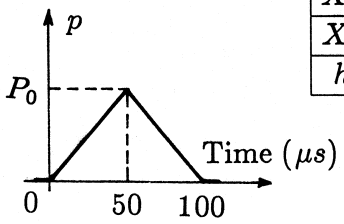

Problem definition

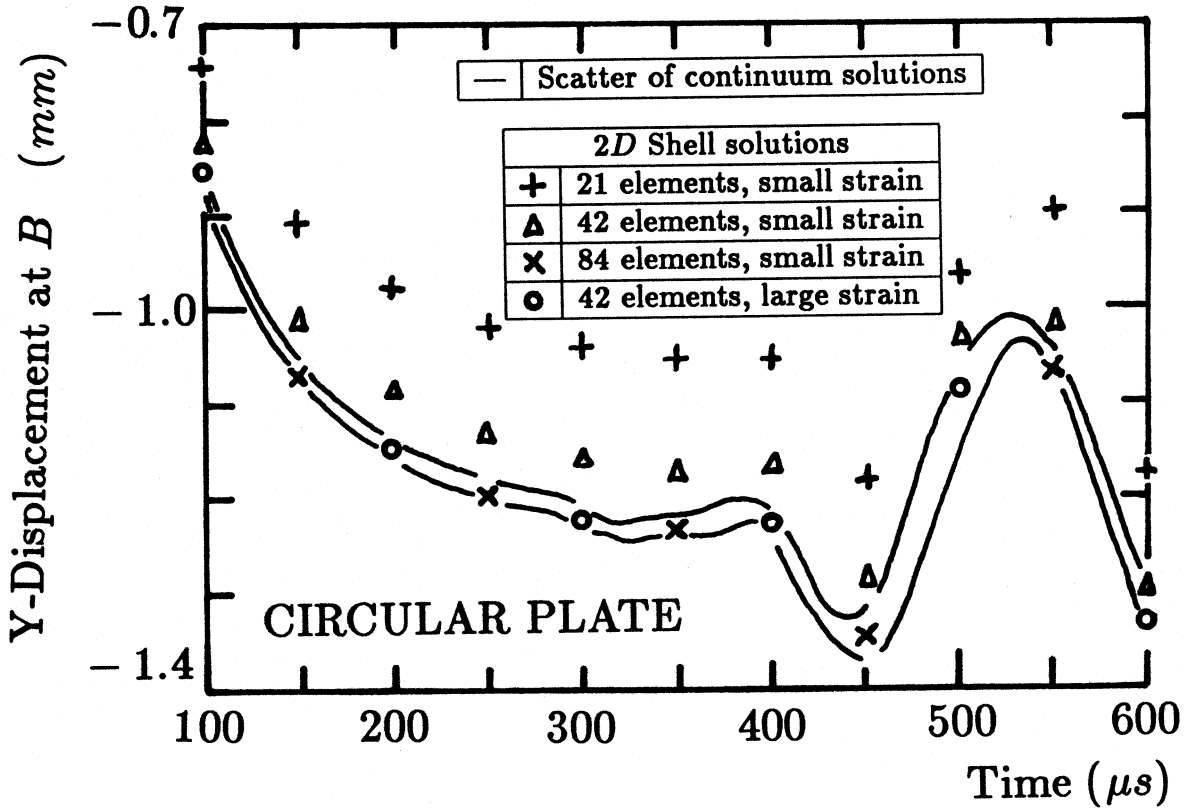

Solutions

JOINT RESEARCH CENTRE
European Commission
Institute for the Protection and Security of the Citizen
European Laboratory for Structural Assessment

Spherical cap

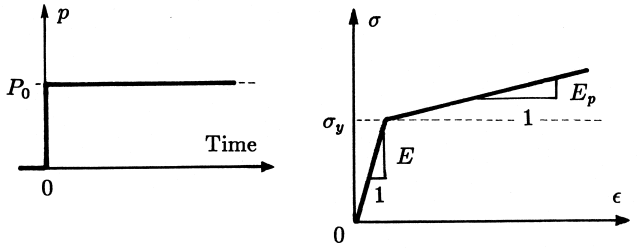

Problem definition

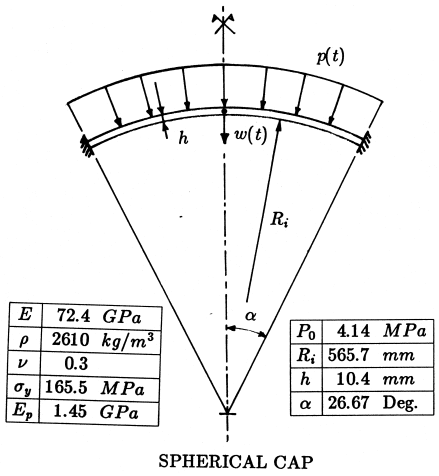

E	72.4 GPa
ρ	2610 kg/m^3
ν	0.3
σ_y	165.5 MPa
E_p	1.45 GPa

P_0	4.14 MPa
R_i	565.7 mm
h	10.4 mm
α	26.67 Deg.

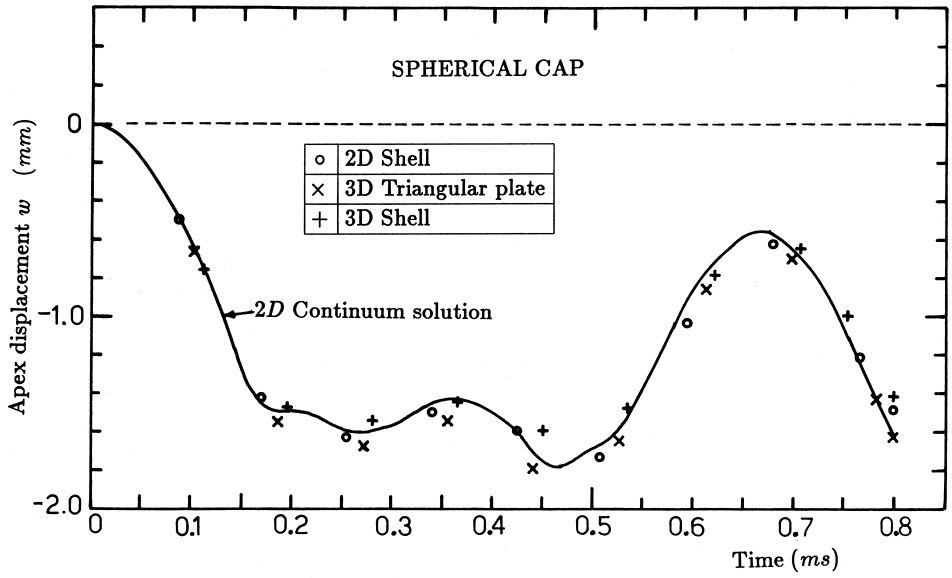

Solutions

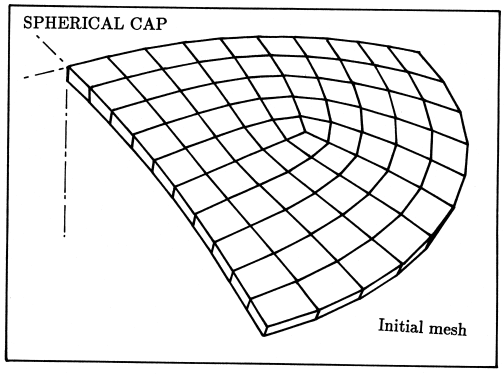

Initial and deformed mesh (3D)

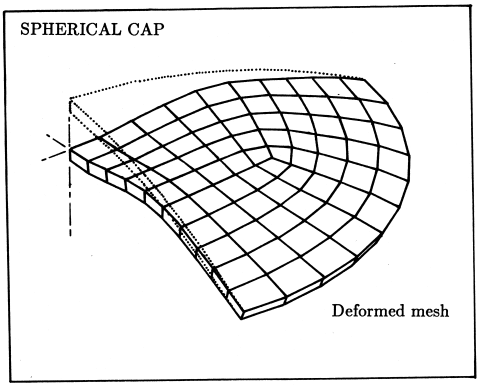

JOINT RESEARCH CENTRE

European Commission
Institute for the Protection and Security of the Citizen
European Laboratory for Structural Assessment

Shock absorber

v_0	13.286	m/s
R	1	m
h	0.005	m
H	2	m
α	45	Deg.

E	210	GPa
ρ	8000	kg/m^3
ρ_2	3819.72	kg/m^3
ν	0.3	
σ_y	480	MPa
E_p	1859	MPa
σ_{y2}	550	MPa
E_{p2}	0	MPa

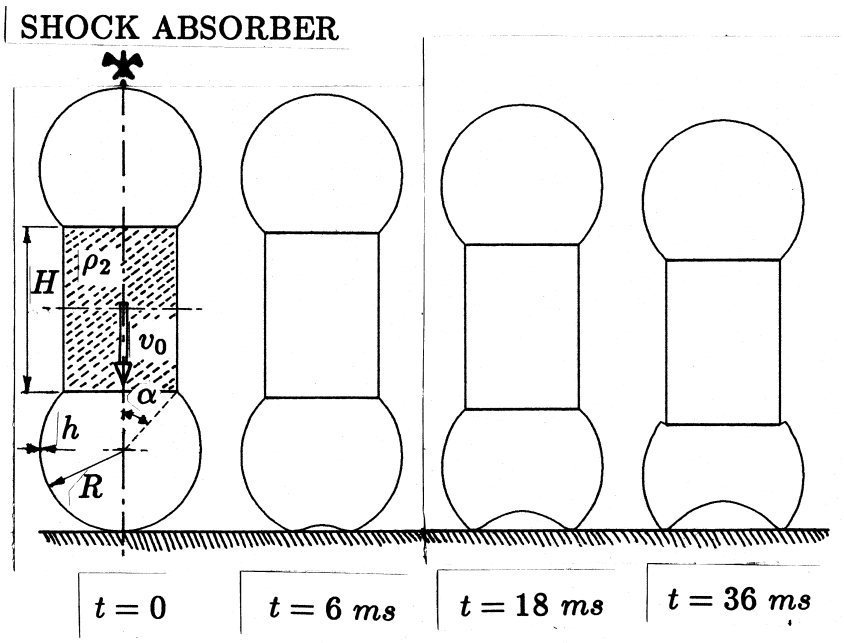

JOINT RESEARCH CENTRE
European Commission
Institute for the Protection and Security of the Citizen
European Laboratory for Structural Assessment

Bar impact

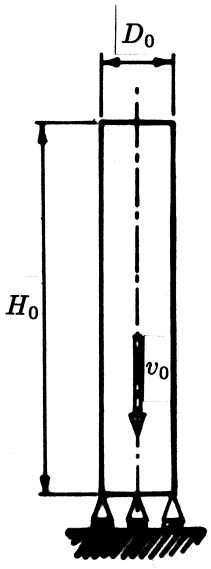

v_0	227 m/s
D_0	6.40 mm
H_0	32.4 mm

E	117 GPa
ρ	8930 kg/m^3
ν	0.35
σ_y	400 MPa
E_p	100 MPa

BAR IMPACT

CODE	Final H	Final R
DYNA-2D	21.47	7.127
NIKE-2D	21.47	7.068
DYNA-3D	21.47	7.034
PLEXIS-3C	21.47	7.113

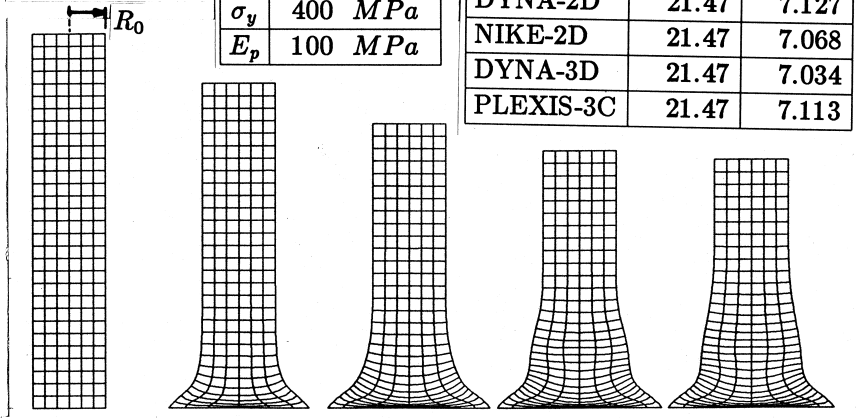

$t = 0$	$t = 20\ \mu s$	$t = 40$	$t = 60$	$t = 80$
$H = 32.40$	$H = 28.06$	$H = 24.56$	$H = 22.22$	$H = 21.47$
$R = 3.200$	$R = 6.159$	$R = 7.049$	$R = 7.115$	$R = 7.113$

Large Dynamic Test Facility (LDTF) [5]-[6]

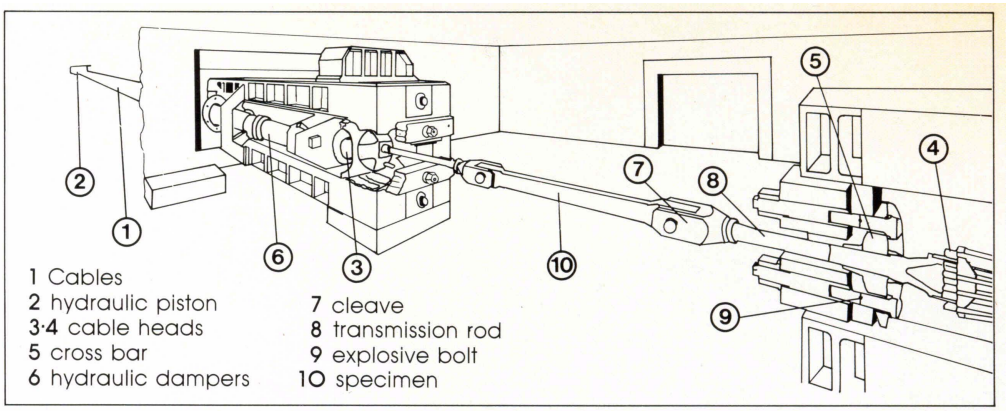

1D model calibration

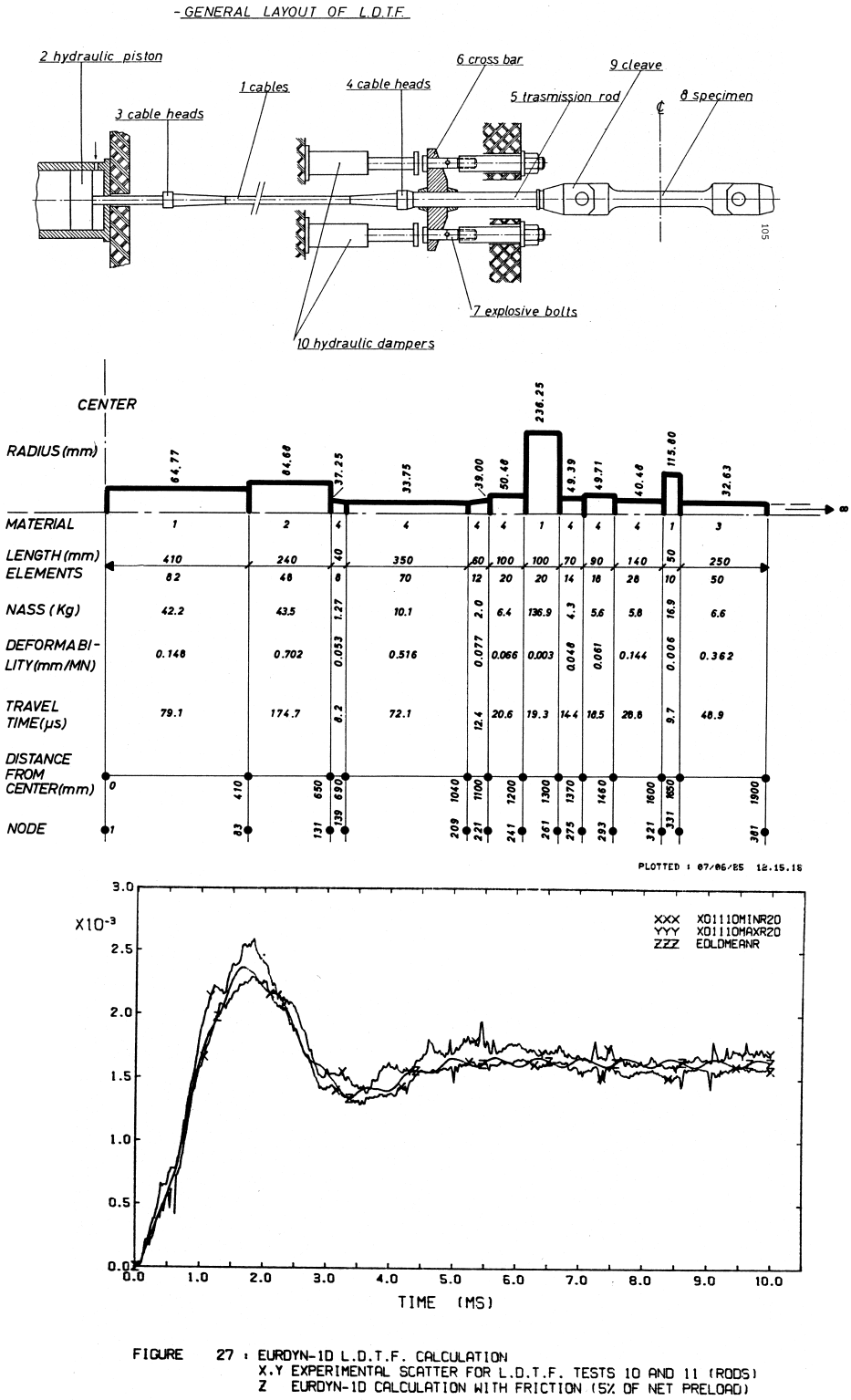

FIGURE 27 : EURDYN-1D L.D.T.F. CALCULATION
X,Y EXPERIMENTAL SCATTER FOR L.D.T.F. TESTS 10 AND 11 (RODS)
Z EURDYN-1D CALCULATION WITH FRICTION (5% OF NET PRELOAD)

LDTF flat specimen

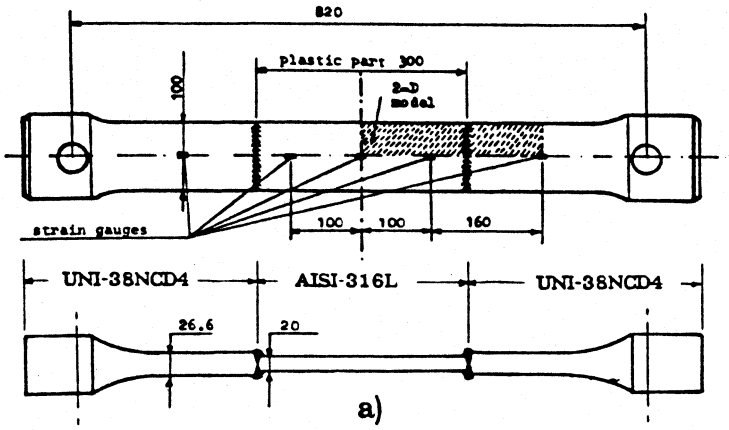

View of the “flat” specimen

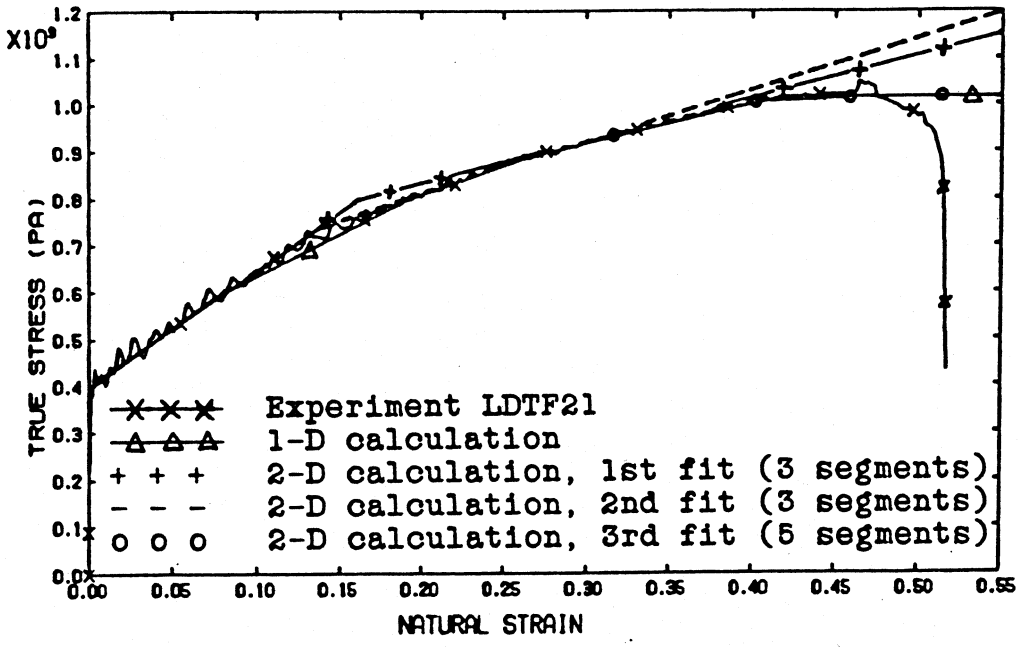

True stress vs. natural strain for test LDTF21 (based on mean strain over a 150 mm span) and multilinear models used in the calculations

Results sensitivity

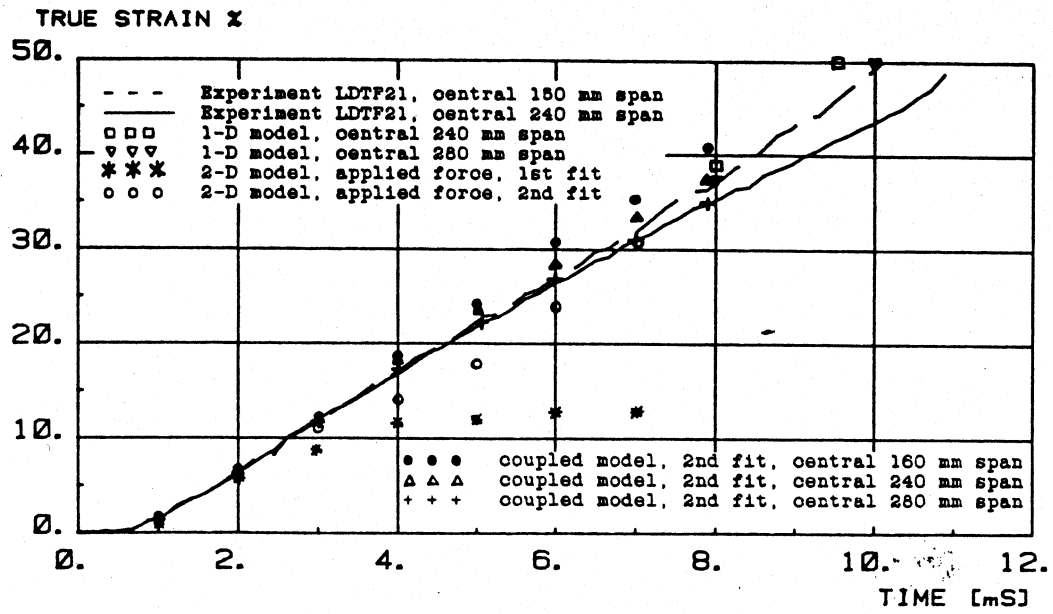

Mean natural longitudinal strain for test LDTF21

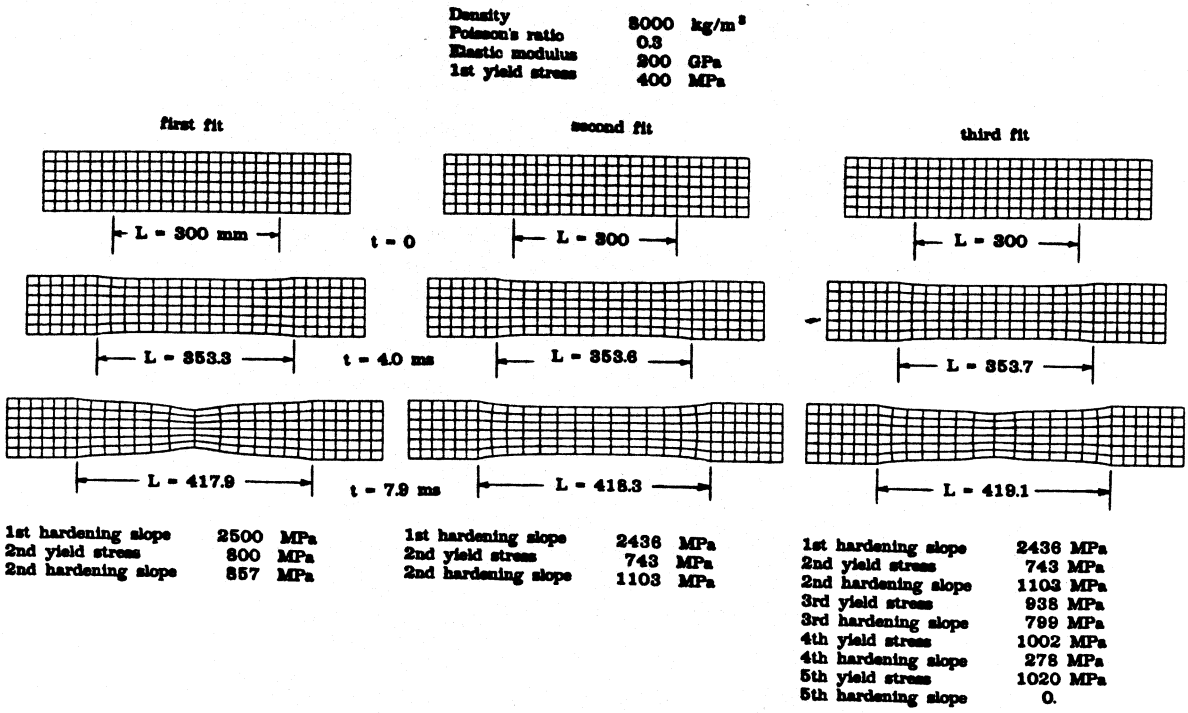

Full-model calculations of test LDTF21. Initial and deformed meshes obtained by the three different assumed material laws

Optimal results

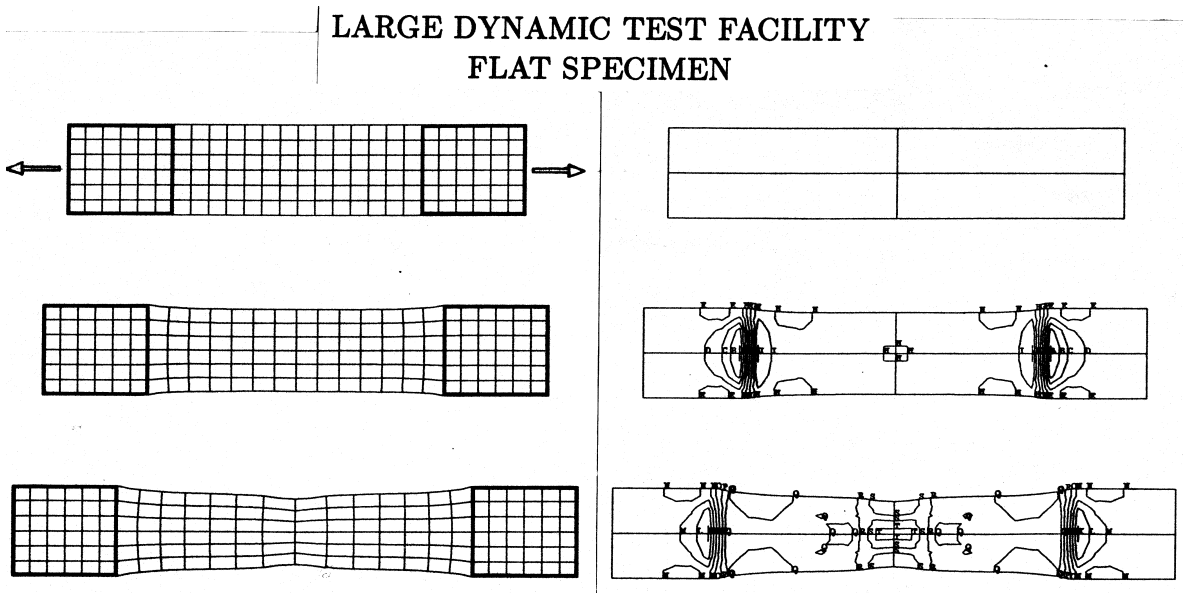

LDTF circular specimen

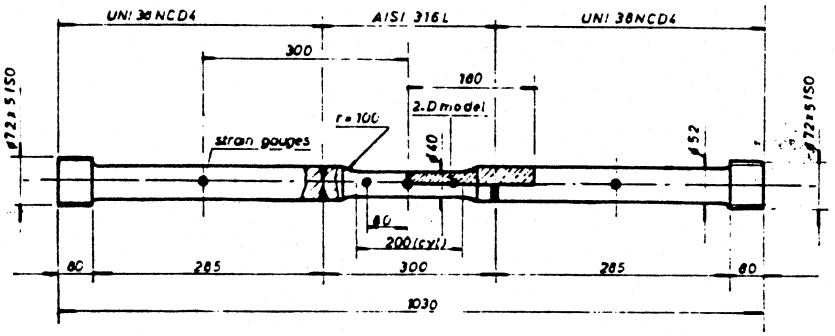

b)

View of the “cykindrical” specimen

LARGE DYNAMIC TEST FACILITY
CYLINDRICAL SPECIMEN

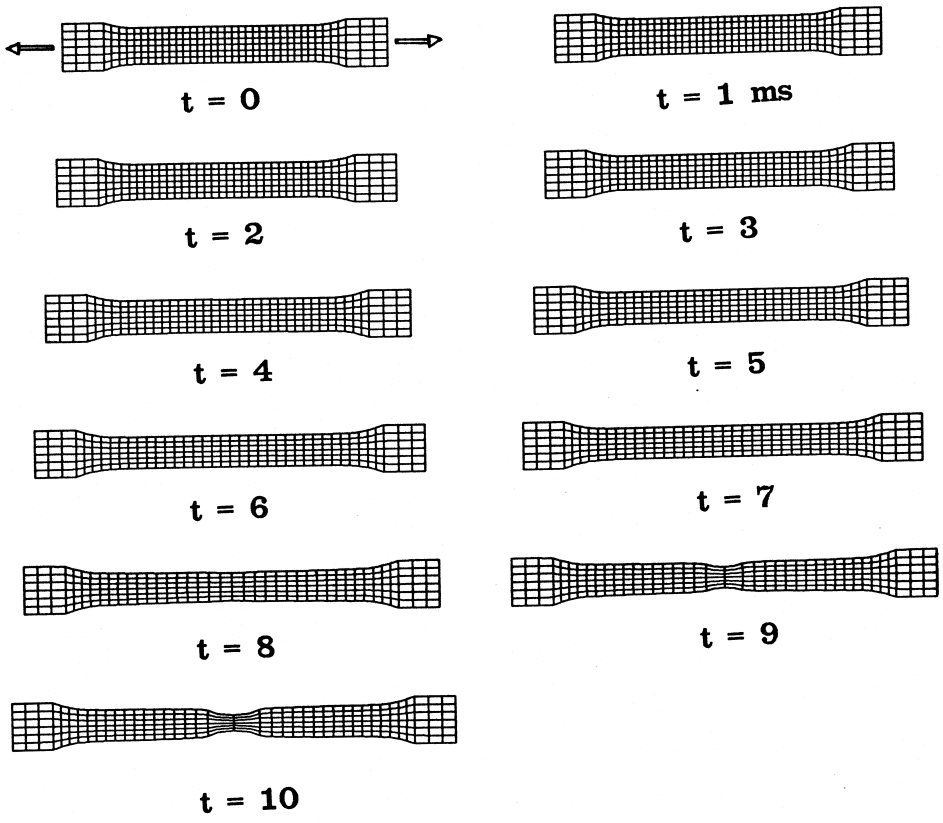

Full-model calculations of test LDTF47. Initial mesh and deformed meshes at various times

JOINT RESEARCH CENTRE
European Commission
Institute for the Protection and Security of the Citizen
European Laboratory for Structural Assessment

Cantilever beam

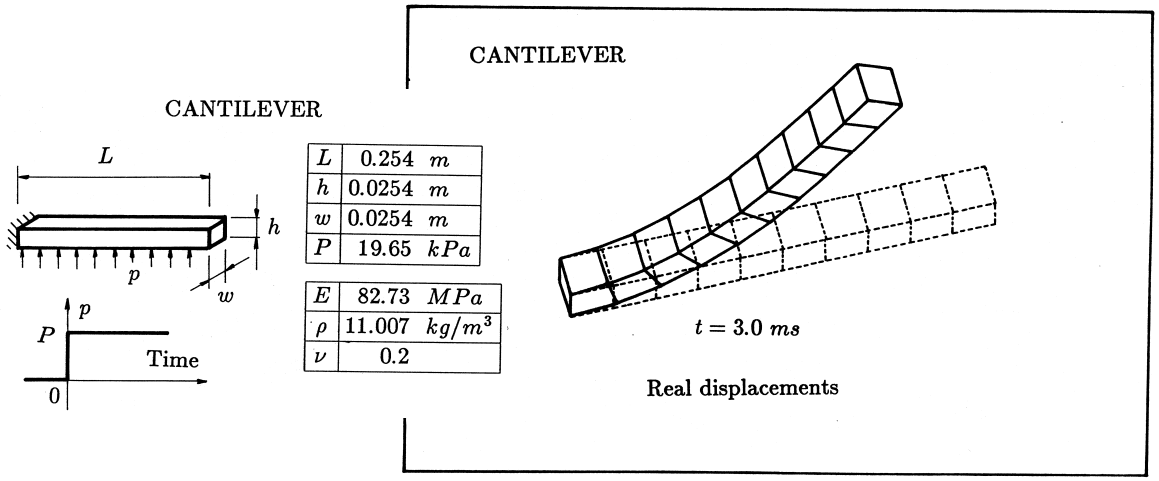

Problem definition

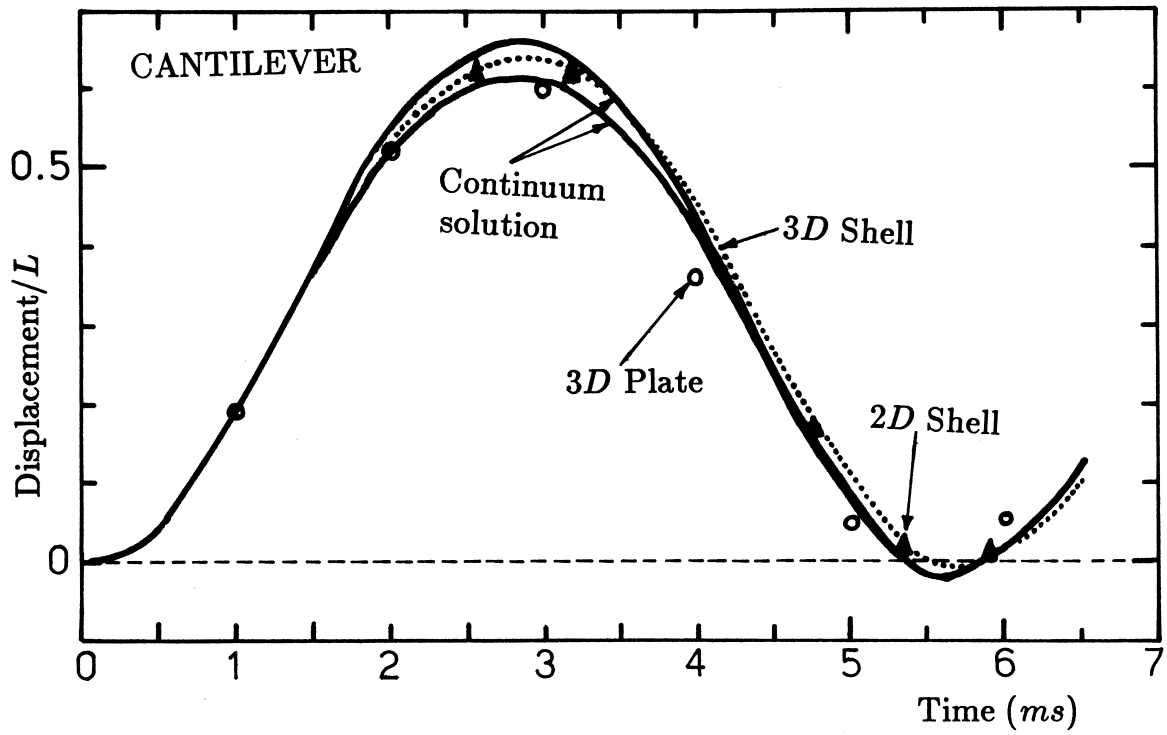

Solutions

JOINT RESEARCH CENTRE
European Commission
Institute for the Protection and Security of the Citizen
European Laboratory for Structural Assessment

Shock absorber

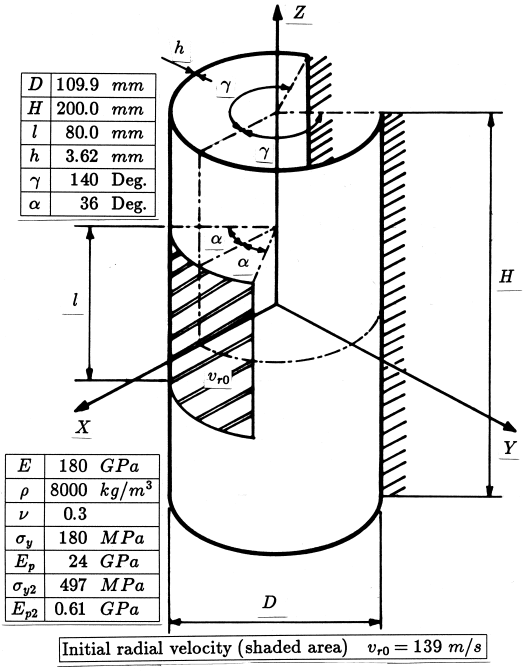

D	109.9 mm
H	200.0 mm
l	80.0 mm
h	3.62 mm
γ	140 Deg.
α	36 Deg.

E	180 GPa
ρ	8000 kg/m^3
ν	0.3
σ_y	180 MPa
E_p	24 GPa
σ_{y2}	497 MPa
E_{p2}	0.61 GPa

Initial radial velocity (shaded area) $v_{r0} = 139\ m/s$

CYLINDRICAL PANEL

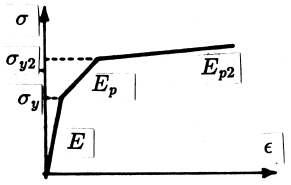

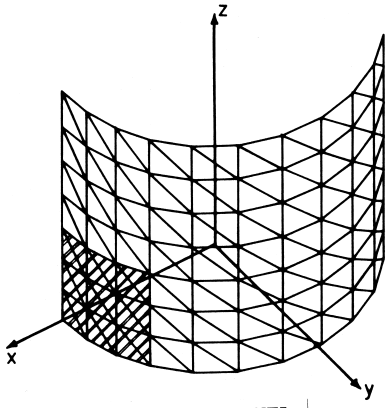

CYLINDRICAL PANEL

Problem definition

Solutions

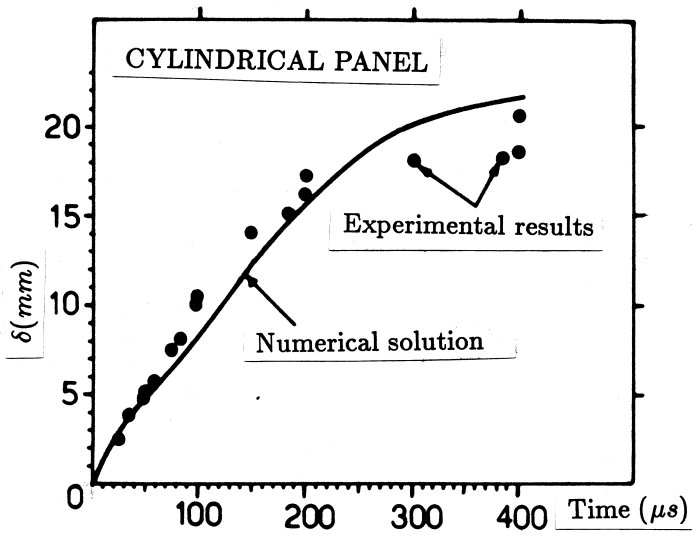

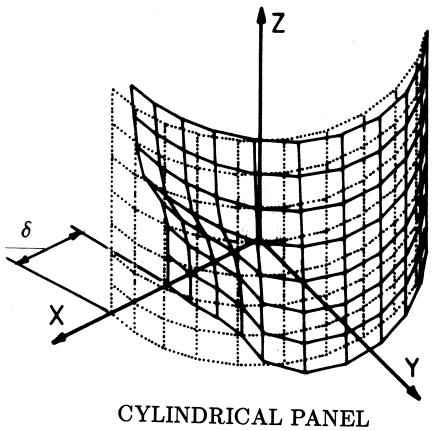

CYLINDRICAL PANEL

JOINT RESEARCH CENTRE

European Commission
Institute for the Protection and Security of the Citizen
European Laboratory for Structural Assessment

Prepared for the Course “Fluid-Structure Interaction in Fast Transient Dynamics”
Organised by UPC, Barcelona (E) 4-7 May 2004.

Course Notes

Part II

ALE Formulation

Folco Casadei

Joint Research Centre - IPSC
European Laboratory for Structural Assessment, T.P. 480
21020 Ispra (Varese) - Italy
E-mail: folco.casadei@jrc.it
Web: http://europlexus.jrc.it

JOINT RESEARCH CENTRE

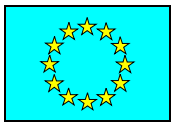

European Commission
Institute for the Protection and Security of the Citizen
European Laboratory for Structural Assessment

ALE description

The fluid domain is assumed to be ***compressible*** and ***inviscid***. Both assumptions are related to the fact that in the class of problems of interest here (fast transient phenomena such as impacts, explosions, etc.) relatively ***high pressures and pressure gradients*** are usually present. As a consequence, even liquid materials exhibit some compressibility and the viscous forces due to friction phenomena always present in real fluids are usually negligible compared with pressure and inertia forces.

The governing equations for the fluid domain are the so-called ***Euler equations***, which express the conservation of mass, momentum and energy. In the ALE formulation, these are written in mixed coordinates, i.e. with respect to a ***referential domain*** that coincides neither with the fixed (Eulerian) reference, nor with the moving particles (Lagrangian), but can be arbitrarily defined and moved in time.

The equations can be conveniently expressed in integral form:

$$\frac{dM}{dt} = \frac{d}{dt}\int_{V(t)} \rho\, dV = \oint_{S(t)} \rho(\underline{w}-\underline{v})\cdot\underline{n}\, dS \qquad \text{(Mass)} \qquad (49)$$

$$\frac{d\underline{Q}}{dt} = \frac{d}{dt}\int_{V(t)} \rho\underline{v} dV = \oint_{S(t)} \rho\underline{v}(\underline{w}-\underline{v})\cdot\underline{n}\, dS - \int_{V(t)} \underline{\nabla} p dV + \int_{V(t)} \rho\underline{g} dV \quad \text{(Momentum)}$$

$$\frac{dE}{dt} = \frac{d}{dt}\int_{V(t)} \rho e dV = \oint_{S(t)} \rho e(\underline{w}-\underline{v})\cdot\underline{n}\, dS - \oint_{S(t)} p\underline{v}\cdot\underline{n} dS + \int_{V(t)} \rho\underline{g}\cdot\underline{v} dV \quad \text{(Energy)}$$

Here ρ is the fluid mass density, p the pressure, $\underline{v}$ the fluid velocity, $\underline{g}$ the acceleration of gravity and e the total specific energy. The symbol $\cdot$ denotes scalar (dot) product and $\underline{\nabla}$ the gradient operator.

The quantities M, Q and E are the total mass, total momentum and total energy, respectively, of a control volume $V(t)$, bounded by a surface S, which moves in the fluid with an arbitrary velocity $\underline{w}$ which may be zero (Eulerian coordinates), or $\underline{v}$ (Lagrangian coordinates) or have any other value (mixed coordinates). The vector $\underline{n}$ is the outwards unit normal to the surface S.

Furthermore, for a compressible fluid, the total specific energy e is equal to:

$$e = i + \frac{1}{2}v^2 \tag{50}$$

where i is the specific internal energy and the pressure p is given by the ***equation of state***:

$$p = p(\rho, i) \tag{51}$$

In place of the third of Eqs. (49) one may also consider an integral expression governing the time rate of change of the internal energy I contained in the control volume $V(t)$:

$$\frac{dI}{dt} = \frac{d}{dt}\int_{V(t)} \rho i dV = \oint_{S(t)} \rho i(\underline{w} - \underline{v}) \cdot \underline{n}\, dS - \int_{V(t)} p\underline{\nabla} \cdot \underline{v} dV \tag{52}$$

In Eqs. (49) and (52), the first term in the right-hand side is a transport term (depending on the relative velocity $\underline{w} - \underline{v}$), the second (when present) is a fluid pressure term and the third a body force term.

To achieve the discretization of two- or three-dimensional fluid domains, simple elements with rectilinear sides and multilinear local velocity fields are used. The density and the specific internal energy (and consequently the pressure) are assumed uniform over each one of these elements.

Therefore, direct use can be made of the integral forms (49, first Eq.) and (52) of mass and internal energy conservation to update the element density and specific internal energy, provided $V(t)$ represents the current volume of the element.

The treatment of the conservation of momentum is more complicated and the interested reader is addressed to references [8-9] for further details. For the scope of the present work, it is sufficient to recall that the resulting time integration scheme for the fluid domain consists of three distinct phases, as originally proposed by Hirt *et al* [10].

- In the first phase, an ***explicit Lagrangian*** calculation is performed by noting that the convective terms in the conservation equations vanish when $\underline{w} - \underline{v} = 0$.

- Then, pressure is iteratively refined (also in order to stabilize the solution) in the second phase, an ***implicit Lagrangian*** calculation. To this end only a fixed, small number of iterations is actually required.

- Finally, transport terms contributions are added separately in the third phase, a ***convective flux*** calculation.

This time integration scheme is not as limpid as the one presented in the flowchart for the structural domain (Lesson 3), but in practice the two algorithms are combined quite effectively in the program. The few modifications required are shown below.

Note that the grid velocity, indicated with $\underline{w}$, is arbitrary, therefore it has to be provided in some way to the code. An efficient automatic algorithm for the evaluation of $\underline{w}$ so as to minimize mesh distortions in the fluid is available, see [11-12].

A first-guess value for $\underline{w}$ is estimated as a function of the mesh geometry (current coordinates $\underline{x}$) and then corrected to take into

account the local fluid velocity $\underline{v}$. The configuration is updated by using the grid velocity, see the flowchart below, which for the structural domain coincides of course with the velocity of the particles.

Finally, note that the subdivision of the step into three separate phases requires a double loop on the fluid elements when computing the internal forces. All remaining steps of the integration algorithm remain unchanged, including the determination of reaction forces due to essential boundary conditions.

Time integration scheme (fluid)

Modifications to the time integration scheme (see Lesson 3) necessary for treating also the fluid domain

1-2. Unchanged;
3. Immediately after the computation of the new mid-step velocity in the fluid, add the computation of the grid velocity, $\underline{w}^{n+1/2}$, which is performed by the automatic rezoning algorithm: $\underline{w}^{n+1/2} = F(\underline{x}^{n}, \underline{v}^{n+1/2})$;
4. The update of the configuration now reads: $\underline{x}^{n} = \underline{x}^{n-1} + \Delta t \underline{w}^{n-1/2}$;
5. The computation of the internal forces now requires *two* loops on the (fluid) elements: 5.1 explicit Lagrangian phase and the implicit Lagrangian iteration on the pressure; 5.2 convective flux calculations;
6-10. Unchanged.

Kinematics of the ALE description

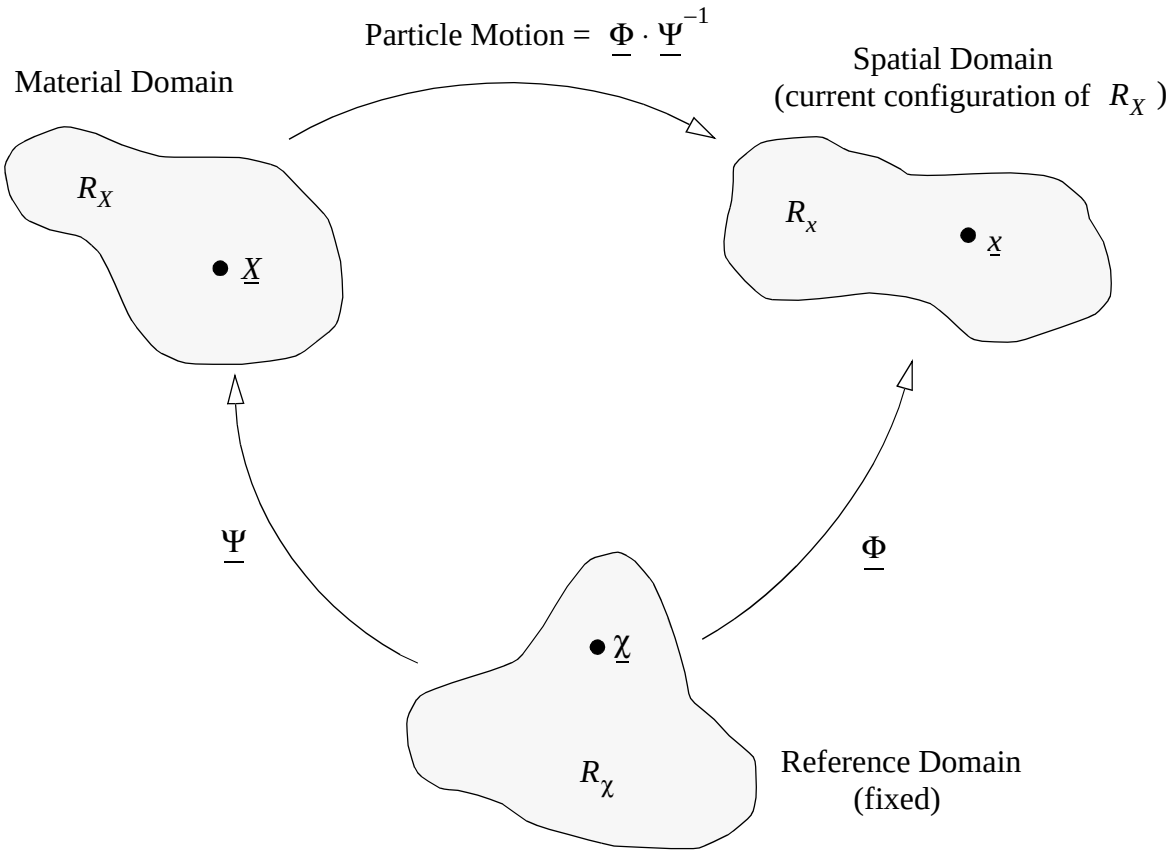

Schematic diagram for the domains and mappings in the ALE description

Let $\underline{v}$ be the ***particles velocity*** and $\underline{w}$ the ***grid velocity***. Then:

- When $\underline{w} \equiv \underline{v}$ the description is ***Lagrangian***;
- Else when $\underline{w} \equiv 0$ the description is ***Eulerian***;
- Else the description is ***ALE***.

One-dimensional example

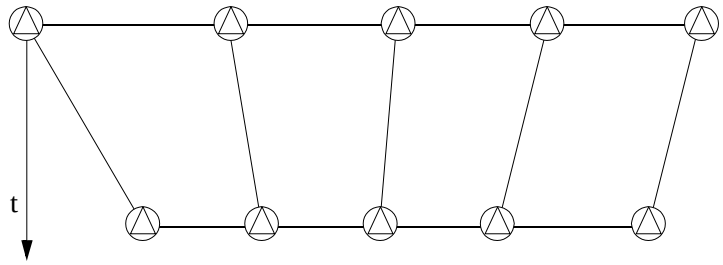

LAGRANGIAN $\underline{\chi}_1 = \underline{X}_1$

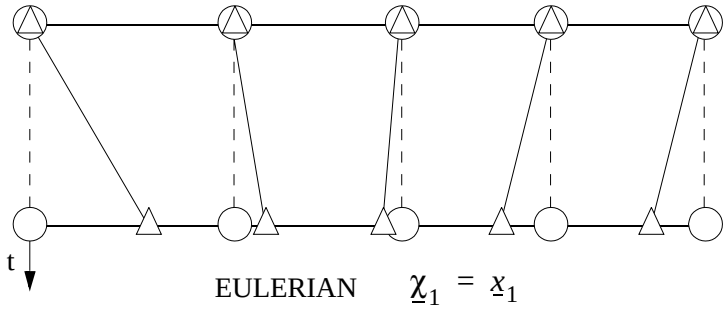

EULERIAN $\underline{\chi}_1 = \underline{x}_1$

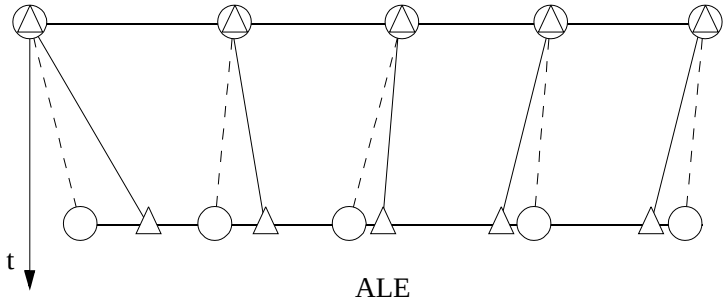

ALE

△ material point (particle) ——— particle motion

○ mesh node - - - - - - mesh motion

One-dimensional example of Lagrangian, Eulerian and ALE mesh and particle motions

JOINT RESEARCH CENTRE

European Commission
Institute for the Protection and Security of the Citizen
European Laboratory for Structural Assessment

Finite Volume Formulation

The same FSI techniques to be described below in a Finite Element context may be applied, with appropriate adjustments, also to Finite Volume formulations.

We use a ***node-centered FV fluid model***, which employs an approximate Riemann solver combined with a MUSCL-like technique to obtain second-order accuracy in space and time in the computation of numerical fluxes.

An ALE formulation [13] is adopted, based on a fully unstructured FV grid that is automatically built by the program starting from a FE-like discretisation of the fluid domain. The FV model, initially implemented in two space dimensions [14], has been recently extended to axisymmetric and full 3D geometry [15].

The governing Euler equations for the fluid domain are written in the form:

$$\frac{\partial \underline{U}}{\partial t} + \underline{\nabla} \cdot \underline{F}(\underline{U}) = 0 \tag{53}$$

with:

$$\begin{aligned} \underline{U} &= \{\rho, \rho\underline{\dot{u}}, \rho E\} \\ \underline{F}(\underline{U}) &= \{\rho\underline{\dot{u}}, \rho\underline{\dot{u}}\underline{\dot{u}} + p\underline{I}, (\rho E + p)\underline{\dot{u}}\} \end{aligned} \tag{54}$$

where $\underline{U}$ is the vector of the so called ***conserved variables***, and $\underline{F}(\underline{U})$ is the flux of $\underline{U}$; ρ is the total density, $E = e + |\underline{\dot{u}}|^2/2$ the total energy per unit mass, e the internal energy per unit mass, $|\underline{\dot{u}}|^2/2$ the kinetic energy per unit mass, $\underline{\dot{u}}\underline{\dot{u}}$ is the tensor of components $\dot{u}_i\dot{u}_j$ $(i, j = 1, \ldots, 3)$ and p the pressure.

The conserved variables $\underline{U} = U(\underline{x}, t^n)$, $t^n > 0$, $\underline{x} \in R^3$ are defined in a series of instants $\{t^n\}$ by a set of discrete constant values $\{\underline{U}^n\}$ expressing integral means on the generic control volume Ω:

$$\underline{U}^n = \frac{1}{|\Omega|}\int_\Omega \underline{U} dV \tag{55}$$

where $|\Omega|$ represents the measure of the control volume. The weak form of Eq. (55) is:

$$\frac{d}{dt}\int_\Omega \underline{U} dV = -\int_{\partial\Omega} [\underline{n} \cdot \underline{F}(\underline{U})] dS \tag{56}$$

where $\underline{n}$ is the outward normal to the control volume surface $\partial\Omega$. By using a ***first-order explicit*** time integration, Eq. (56) yields, by denoting the numerical flux as $\underline{\Phi}$:

$$|\Omega|^{n+1}\underline{U}^{n+1} - |\Omega|^n \underline{U}^n = \Delta t \sum_{\partial\Omega} (\underline{n} \cdot \underline{\Phi}) \tag{57}$$

This first-order relation is used to advance in time the solution in the FV subdomain.

For the enforcement of *essential boundary conditions* (BC) in the Finite Volume model—and in particular for dealing with FSI—a mixed weak/strong approach is adopted.

A *weak* enforcement is chosen for the *energy terms*, i.e. boundary fluxes of these terms are added to the balance of those nodal control volumes which lay on any moving edge of the fluid domain. However, *strong* enforcement is preferred for the *momentum terms*, in the sense that the related contributions are represented by external nodal reaction forces. Essential boundary conditions are treated in the same manner for all concerned nodes—both FE and FV—in the computer code.

To achieve strong enforcement of BCs related to momentum terms, *two sources of inaccuracy* are introduced. The first one is due to the assumption that velocity is a *nodal* quantity, whose component normal to the boundary is null. This assumption, quite natural in the FE context, is somewhat constraining for a FV model where all quantities are actually related to the entire nodal control volume, and not particularly to the node.

A second inaccuracy in BC application stems from the choice of adhering to the general framework of FSI algorithms in the code, and will be detailed below.

Why mesh rezoning?

Rezoning is necessary because ***Lagrangian*** solutions of fluid problems suffer from ***excessive mesh distortions*** and ***entanglement***:

TYPICAL POOL TYPE LMFBR
FOR
«CONT» BENCHMARK CALCULATIONS
(Dimensions in meters)

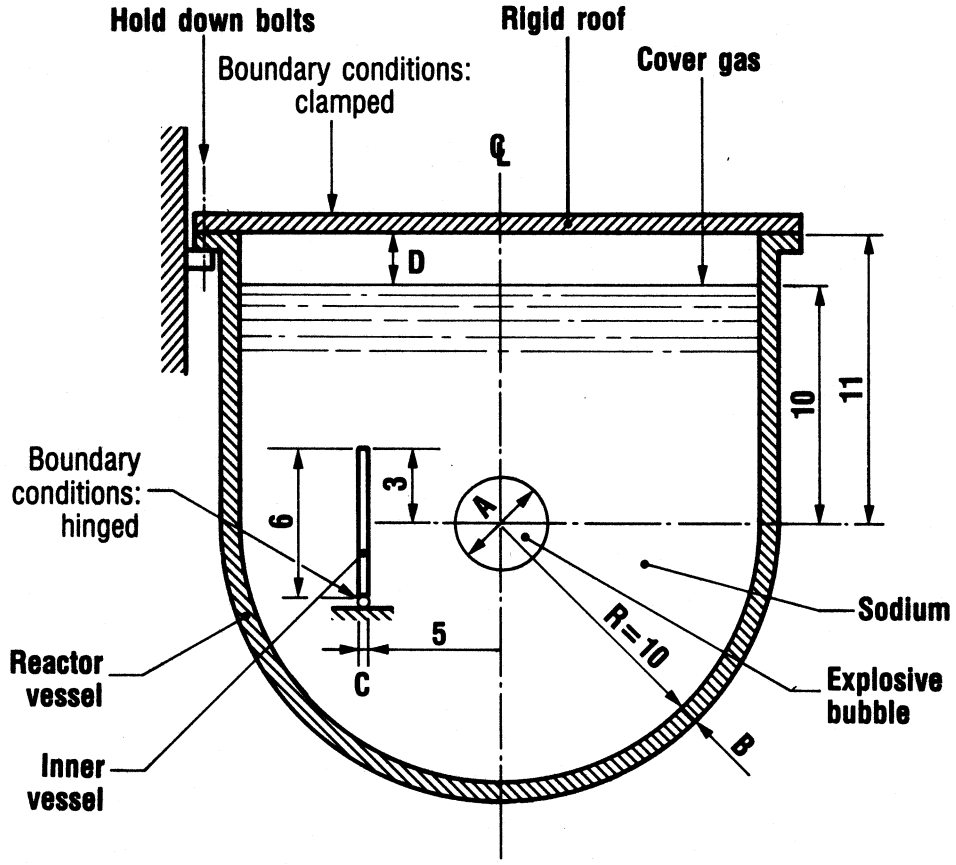

A	1.989	*m*
B	0.025	*m*
C	0.025	*m*
D	1.000	*m*
Temp.	723	*K*

Early solution attempts [16]

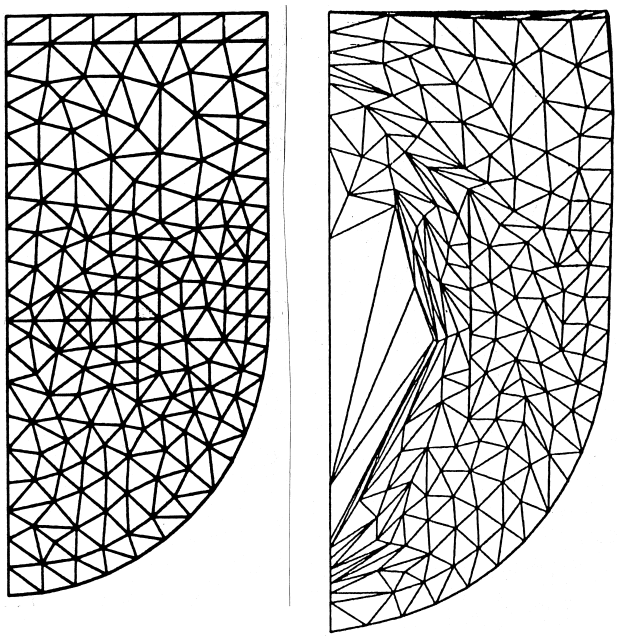

Lagrangian, triangular elements

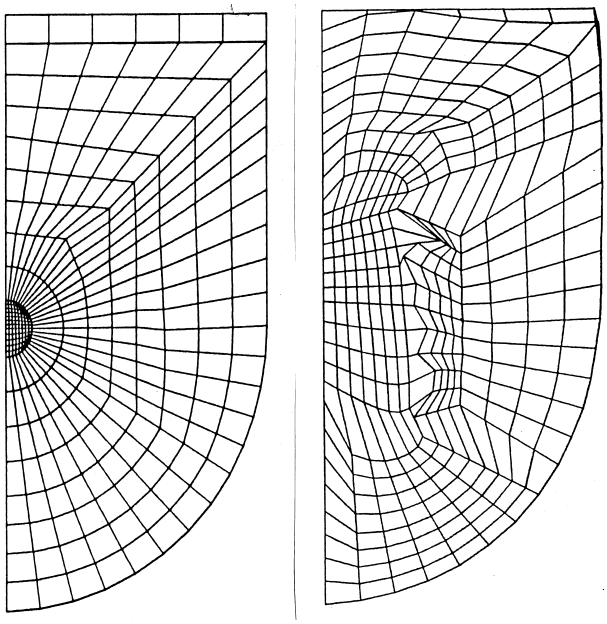

ALE, "manual" rezoning, quadrilateral elements

JOINT RESEARCH CENTRE

European Commission
Institute for the Protection and Security of the Citizen
European Laboratory for Structural Assessment

ALE solution with ***automatic rezoning*** (Giuliani, see [11])

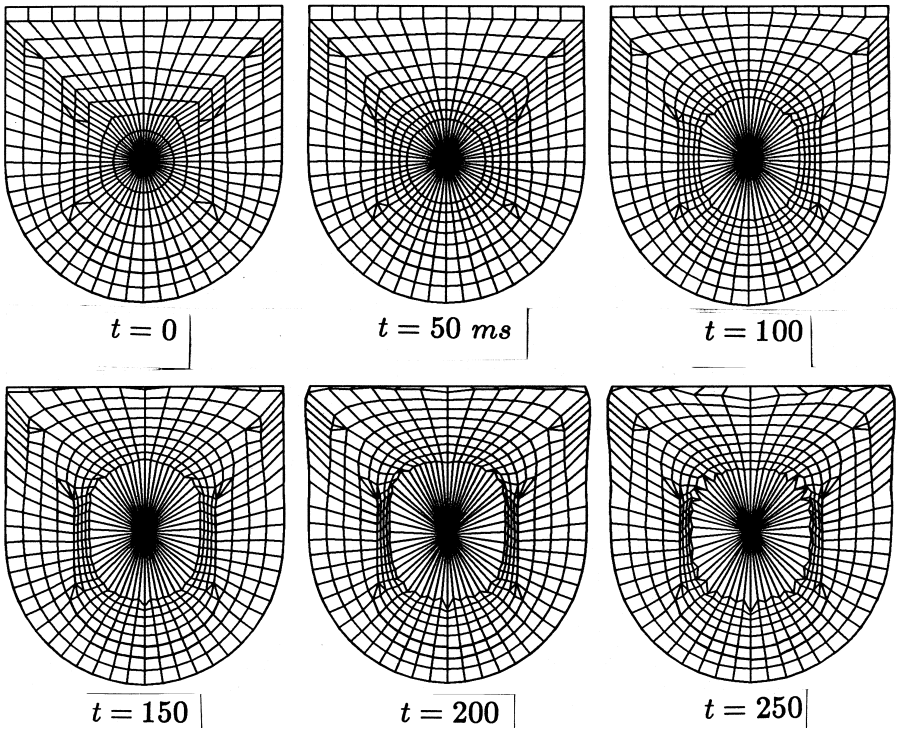

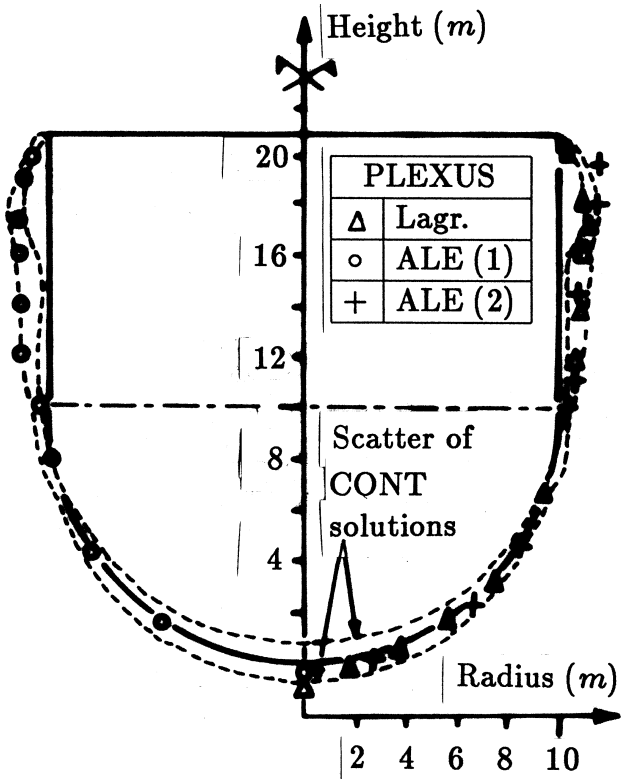

Mesh rezoning algorithms

It should be stressed that in the present context by ***rezoning*** we intend the motion of (nodes belonging to) an ALE mesh, ***with the mesh topology being kept constant***. In other words, the position of nodes changes in time, but the nodes, finite elements and element compositions in terms of nodes do not change in time.

This should not be confused with ***adaptive*** algorithms, which change the number of nodes and elements in a mesh as well as their positions.

Rezoning algorithms may tentatively be subdivided into:

- Purely ***kinematic***, e.g:
  - A (slave) node follows the motion of a (master) node;
  - Nodes initially along a line remain on the same line (master end-points) by maintaining the ratios of inter-node distances;
  - Nodes within a triangle or quadrilateral (identified by suitable master corner nodes) move by homeomorphic deformation,
  - etc. etc.
- ***Geometric***:
  - Giuliani's method based upon minimization of triangles (or tetrahedra) distortion [11];
  - Mean value algorithm;
  - etc. etc.
- ***Mechanical***:
  - Solve elasticity equations for a (dual) mesh coinciding with the ALE grid and considered as a solid body (continuum, or bar assembly etc.).

The mean value algorithm

In its simplest formulation, the mean value algorithm states that the optimal ***position*** of any node coincides with the arithmetic mean of the positions of its neighbour nodes. In the 2D case, we have then:

$$\underline{x}_I^r = \frac{1}{N} \sum_{J=1}^{N} \underline{x}_J \qquad (58)$$

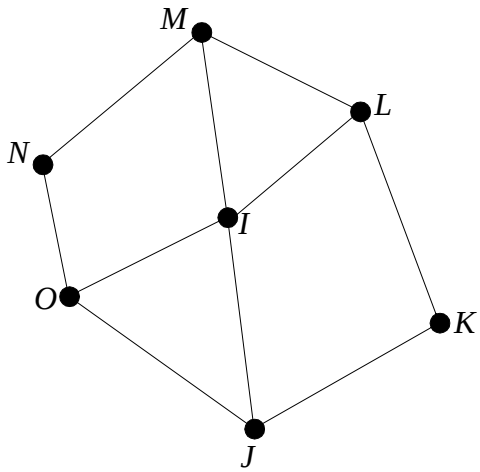

The mean position algorithm

Alternatively, one can use nodal (total) ***displacements*** $\underline{u}$, in place of nodal positions $\underline{x}$.

Drawbacks:

- Rapidly tends to produce a uniform mesh (may be bad in some cases);
- Fails in some particular configurations, due to local mesh “curvature” (see example next).

Failure of the mean value algorithm

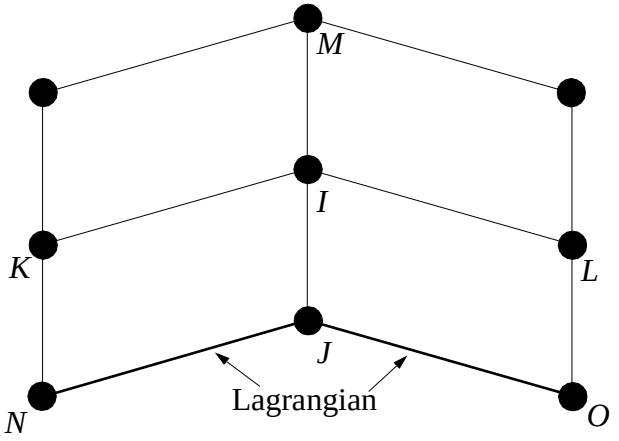

$$\underline{x}_I^r = \frac{1}{4}(\underline{x}_J + \underline{x}_K + \underline{x}_L + \underline{x}_M)$$

A curved mesh

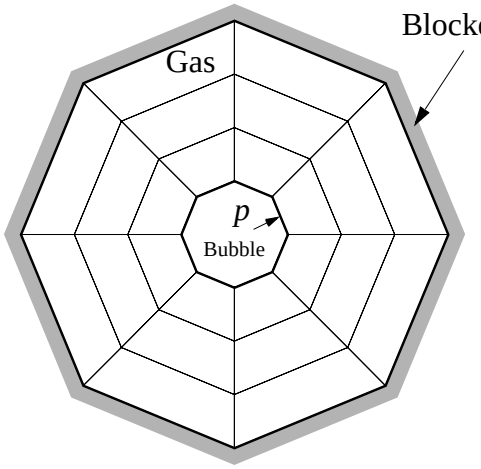

Test problem

Solution

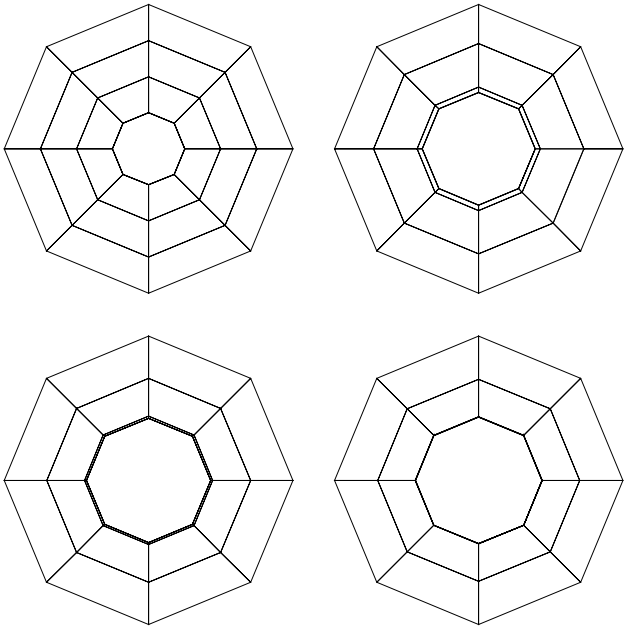

JOINT RESEARCH CENTRE

European Commission
Institute for the Protection and Security of the Citizen
European Laboratory for Structural Assessment

Giuliani's automatic rezoning

This is fully automatic and based upon ***geometric*** considerations [11].

For each node to be rezoned, an ***influence domain*** is identified, composed of the neighbouring triangles in 2D (tetrahedra in 3D):

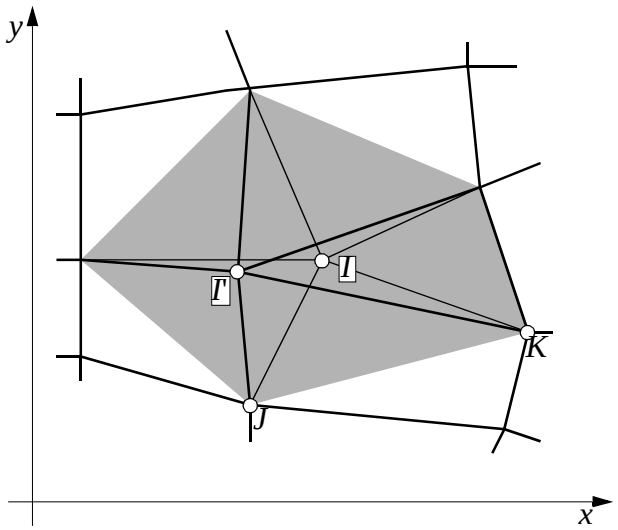

Influence domain of a node I in a two-dimensional element mesh

The "***shear***" and "***stretch***" of each triangle in the domain is measured:

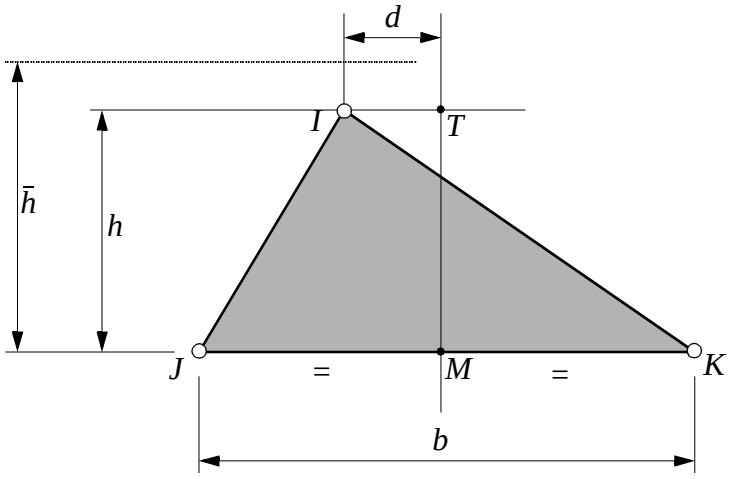

shear $= f(d)$

stretch $= g(h)$

$\bar{h}$ is the mean height of triangles in the influence domain

Generic triangle in the influence domain of node I

JOINT RESEARCH CENTRE

European Commission
Institute for the Protection and Security of the Citizen
European Laboratory for Structural Assessment

A function of the total shear and stretch over all triangles in the influence domain is ***minimised***:

$$E = \sum_{i=1}^{N} \left(\frac{h_i - \bar{h}}{\bar{h}} \right)^2 + \sum_{i=1}^{N} \left(\frac{2d_i}{\bar{b}} \right)^2 = \text{minimum} \qquad (59)$$

Special care is taken for nodes subjected to ***boundary conditions*** (e.g. on an axis or plane of symmetry):

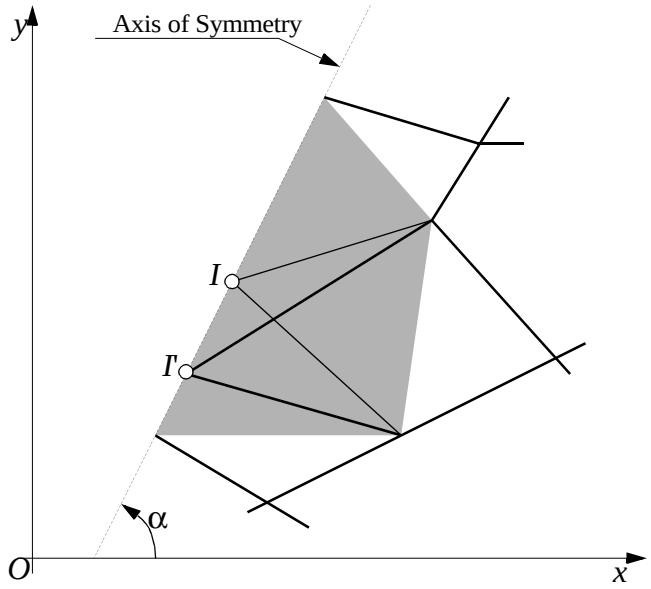

Influence domain of a node I located on a symmetry axis.

It is important to ***constrain*** the resulting grid velocity somehow:

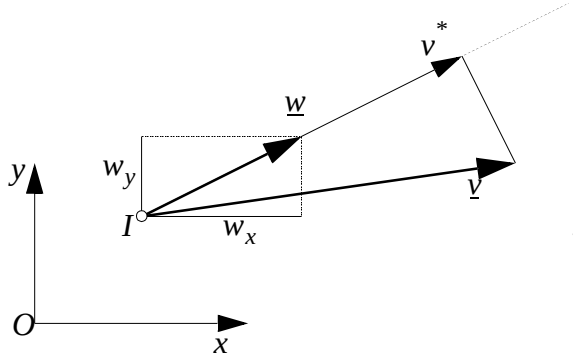

Grid velocity restriction

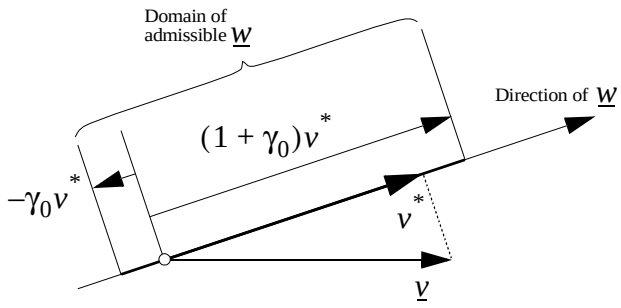

Domain of admissible mesh velocities (2D case).

Validation of fluid models

The shock tube

Following Harlow & Amsden [7], we consider a rigid cylinder divided into two semi-infinite sections by a diaphragm, as shown below.

Problem geometry and initial conditions

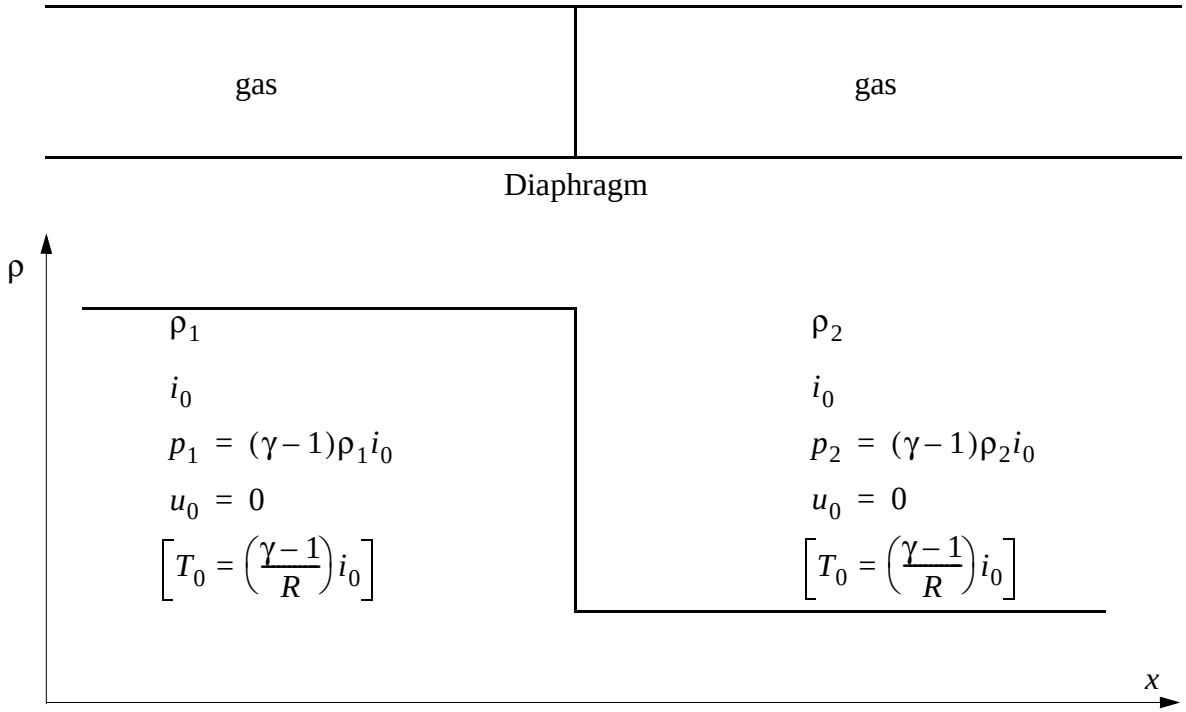

Initially, an ideal gas is considered to be at rest (particle velocity $u_0 = 0$) on both sides, and the same temperature T_0 is assumed all over. To the left of the diaphragm, the gas is initially at higher density and pressure, ρ_1 and p_1, than those to the right, ρ_2 and p_2. The initial internal energy is i_0 on both sides.

For a polytropic gas the equation of state reads:

$$p = (\gamma - 1)\rho i \qquad (60)$$

where $\gamma = c_p/c_v$ is a gas property, c_p and c_v are the specific heats at constant pressure and volume. This may also be written as:

$$p = R\rho T \tag{61}$$

where R is the gas constant.

The problem is to determine the variation in time and space of the thermodynamic quantities involved, once the diaphragm is removed.

Analytical solution

At time $t = 0$ the diaphragm is removed and at any later time there is observed a ***shock*** *S*, moving to the right, a ***contact discontinuity***, *C*, moving to the right (this follows the motion of the particles that were initially at the diaphragm) and a ***rarefaction wave***, *R*, bounded by points a and b, moving to the left, as shown below. There is no significant length to the system: the appearance of the configuration at a later time is a magnification of an earlier appearance.

Density distribution after removal of the diaphragm

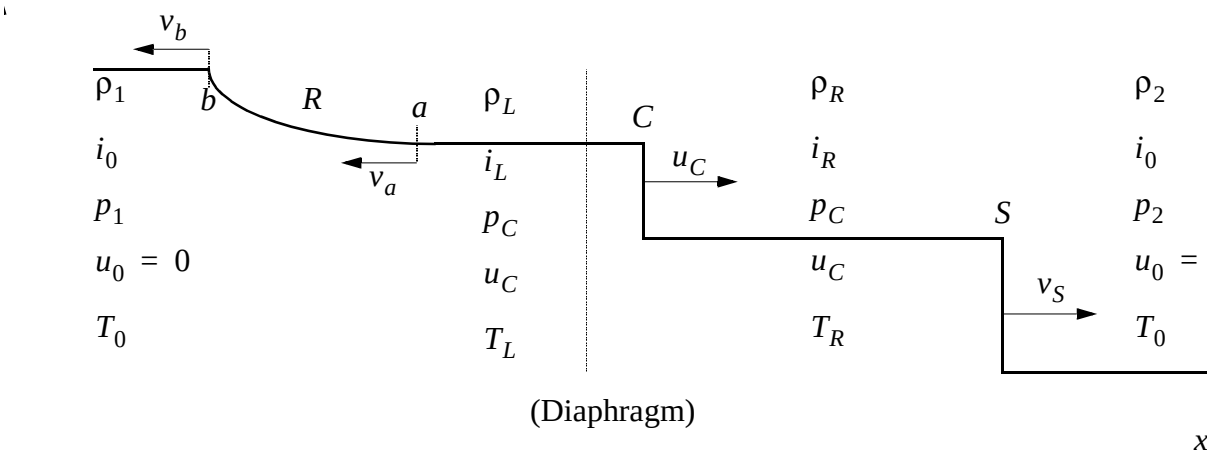

Both the velocity u_C (since no gas passes over the discontinuity) and the pressure p_C (otherwise there would be an infinite acceleration) across the contact discontinuity are continuous, but the density passes

from ρ_L to ρ_R. Through the equation of state (60), the internal energies i_L, i_R (and the temperatures T_L, T_R) may be determined if p_C, ρ_L and ρ_R are known.

Thus, the four unknowns of the problem are ρ_L, ρ_R, u_C and p_C. If one defines:

$$\lambda \equiv \frac{\rho_1}{\rho_2} = \frac{p_1}{p_2} \tag{62}$$

$$P \equiv \frac{p_C}{p_2} \tag{63}$$

so that λ is known from the initial configuration, then P may be determined from the following equation, in terms of λ an γ:

$$\frac{(1-P)^2}{\gamma(1-P)-1+P} = \frac{2\gamma}{(\gamma-1)^2}\left[1-\left(\frac{P}{\lambda}\right)^{\frac{1}{2}\left(1-\frac{1}{\gamma}\right)}\right]^2 \tag{64}$$

The pressure ratio P is determined iteratively from this equation as:

$$P^{\text{new}} = 1 + \sqrt{[\gamma(1-P)-1+P]\frac{2\gamma}{(\gamma-1)^2}\left[1-\left(\frac{P}{\lambda}\right)^{\frac{1}{2}\left(1-\frac{1}{\gamma}\right)}\right]^2} \tag{65}$$

An initial value for P, $P_0 = 1.0$, is used for the first iteration and the iterative process is stopped when:

$$\frac{\left|P^{\text{new}} - P\right|}{\min(|P|, \left|P^{\text{new}}\right|)} < \varepsilon \tag{66}$$

where ε is a tolerance (we take $\varepsilon = 1\times10^{-5}$). The process usually converges in a few iterations.

Once P determined, the remaining unknown quantities are:

$$p_C = p_2 P \tag{67}$$

$$\rho_R = \rho_2 \frac{\gamma(1+P)+(P-1)}{\gamma(1+P)-(P-1)} \tag{68}$$

$$\rho_L = \rho_2 (P\lambda^{\gamma-1})^{1/\gamma} \tag{69}$$

Then, from the equation of state (60):

$$\begin{aligned} i_R &= \frac{p_C}{(\gamma-1)\rho_R} \\ i_L &= \frac{p_C}{(\gamma-1)\rho_L} \end{aligned} \tag{70}$$

but, since:

$$i_0 = \frac{p_2}{(\gamma-1)\rho_2} \tag{71}$$

we have:

$$\frac{1}{\gamma-1} = i_0 \frac{\rho_2}{p_2} \tag{72}$$

which, substituted in (71) yields:

$$i_R = i_0 \frac{p_C}{p_2}\frac{\rho_2}{\rho_R} = i_0 P \frac{\rho_2}{\rho_R}$$
$$i_L = i_0 \frac{p_C}{p_2}\frac{\rho_2}{\rho_L} = i_0 P \frac{\rho_2}{\rho_L} \qquad (73)$$

Finally:

$$u_C = 2\sqrt{\frac{\gamma}{\gamma-1}i_0}\left(1-\sqrt{\frac{i_L}{i_0}}\right) \qquad (74)$$

The absolute speed of the shock is:

$$v_S = \frac{u_C \rho_R}{\rho_R - \rho_2} \qquad (75)$$

that of the contact discontinuity is u_C as given by Eq. (74), and those of points a and b are:

$$v_a = u_C - \sqrt{\gamma(\gamma-1)i_L}$$
$$v_b = -\sqrt{\gamma(\gamma-1)i_0} \qquad (76)$$

Problem parameters

Table 1: Specifications assumed for the numerical solutions

ρ_1	1.22
ρ_2	0.1237
γ	1.269
p_1	1.0×10^{6}
p_2	1.013×10^{5}
$i_1 = i_2$	3.046×10^{6}

Analytical solution

Table 2: Analytical solution

λ	9.863	u_C	925.4
P	2.888	v_S	1672.
p_C	2.927×10^{5}	v_a	30.12
ρ_R	0.2771	v_b	–1020.
ρ_L	0.4635	c_0	1020.
i_R	3.928×10^{6}	c_a	895.2
i_L	2.348×10^{6}	c_b	1020.

Numerical solutions

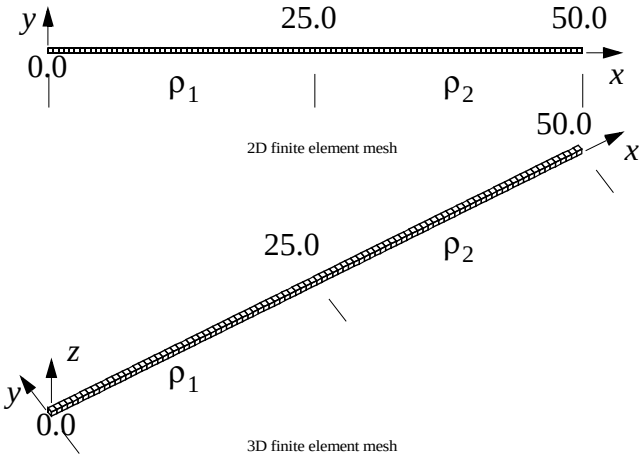

Eulerian solution

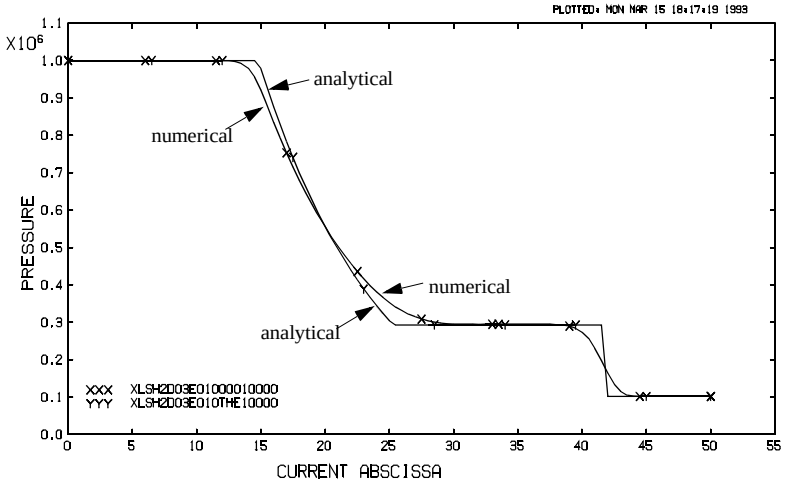

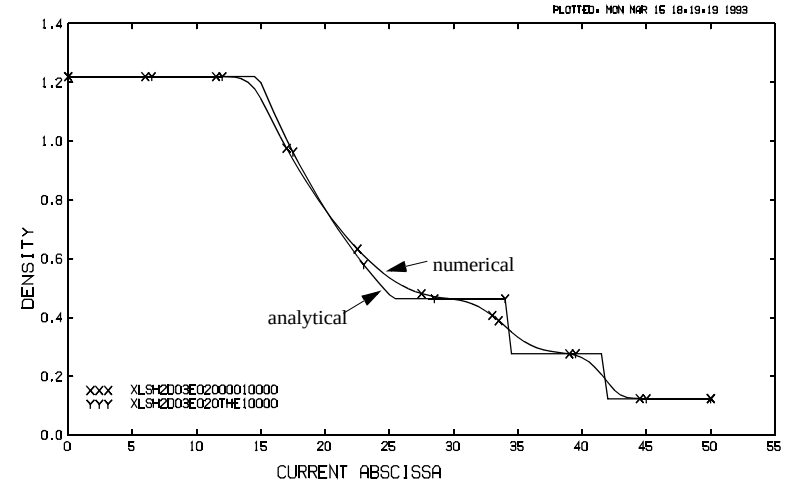

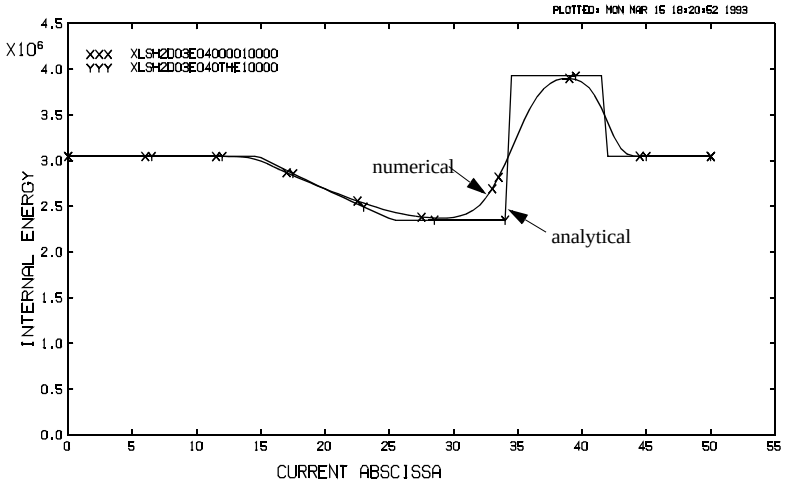

Eulerian solution with optimised parameters

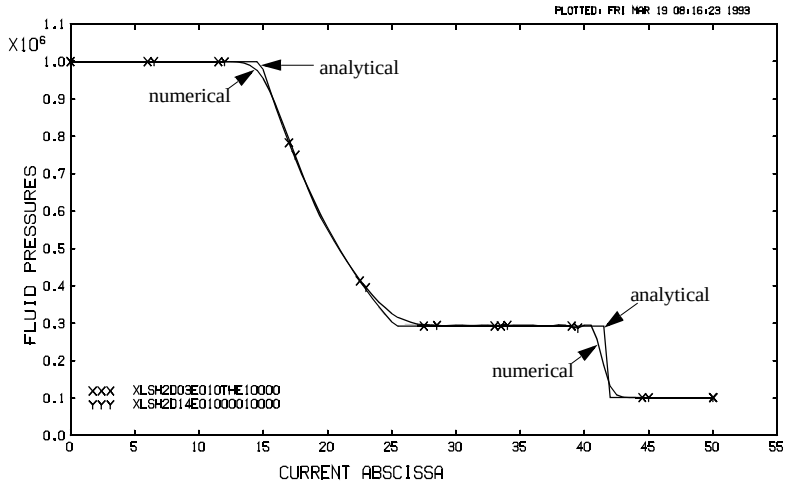

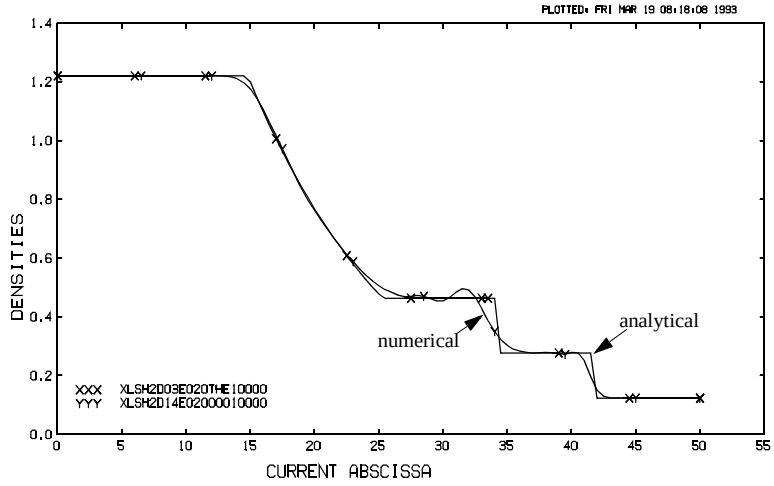

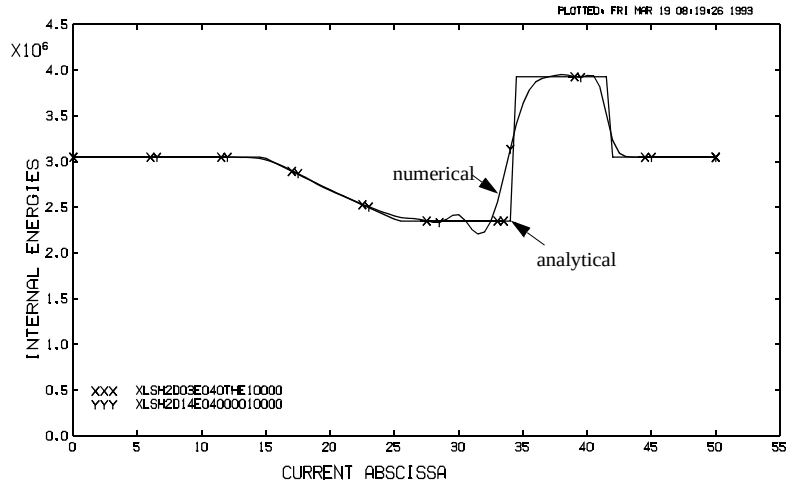

Influence of pseudoviscosity and upwinding

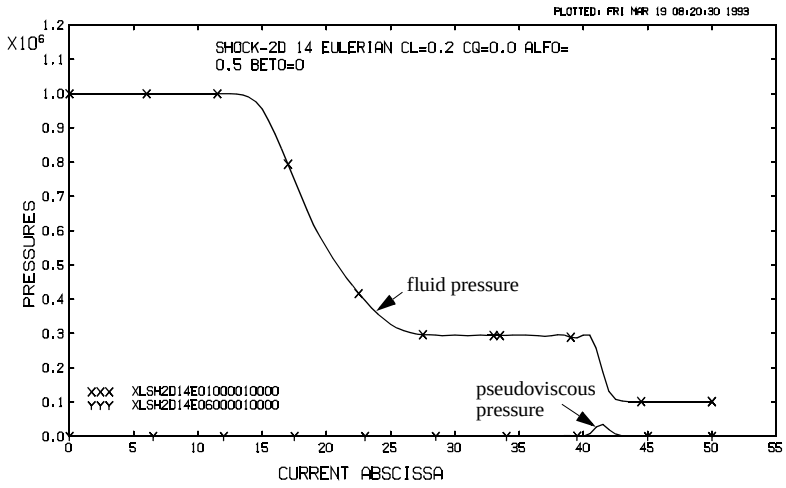

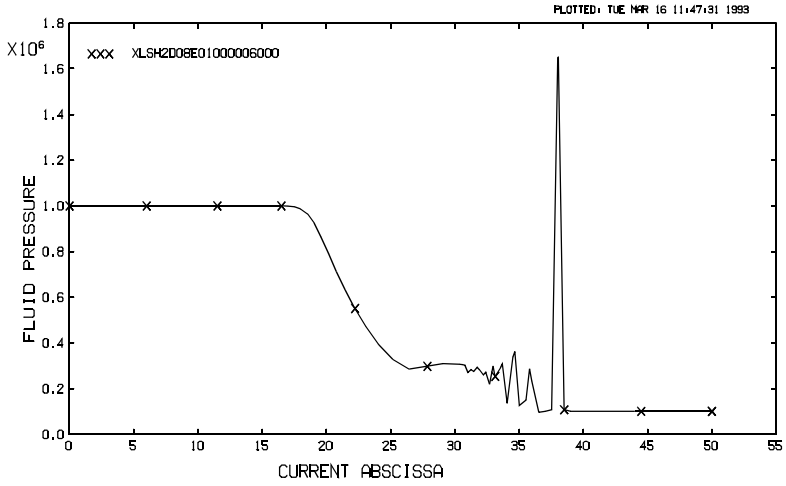

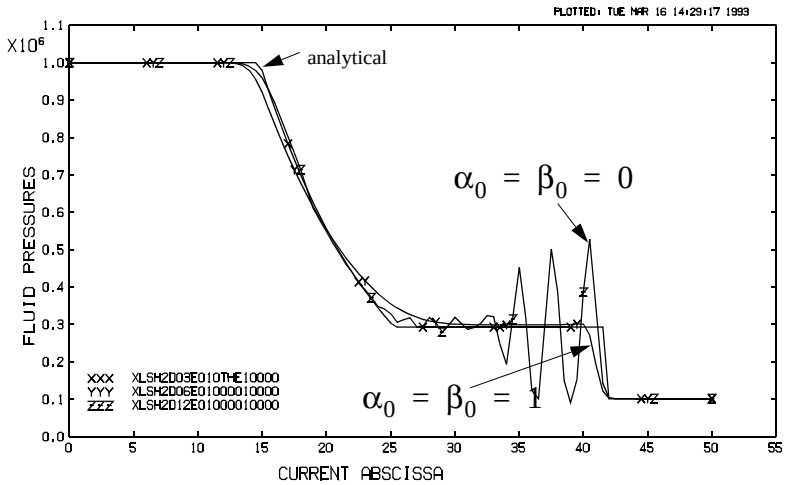

Prepared for the Course “Fluid-Structure Interaction in Fast Transient Dynamics”
Organised by UPC, Barcelona (E) 4-7 May 2004.

Course Notes

Part III

ALE Fluid-Structure Interaction

Folco Casadei

Joint Research Centre - IPSC
European Laboratory for Structural Assessment, T.P. 480
21020 Ispra (Varese) - Italy
E-mail: folco.casadei@jrc.it
Web: http://europlexus.jrc.it

JOINT RESEARCH CENTRE

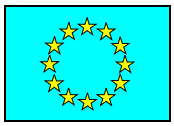

European Commission
Institute for the Protection and Security of the Citizen
European Laboratory for Structural Assessment

Why Fluid-Structure Interactions?

Problems involving interaction phenomena between ***compressible, inviscid fluids*** and ***deformable structures*** can be tentatively solved in two ways: uncoupled solution or fully coupled solution.

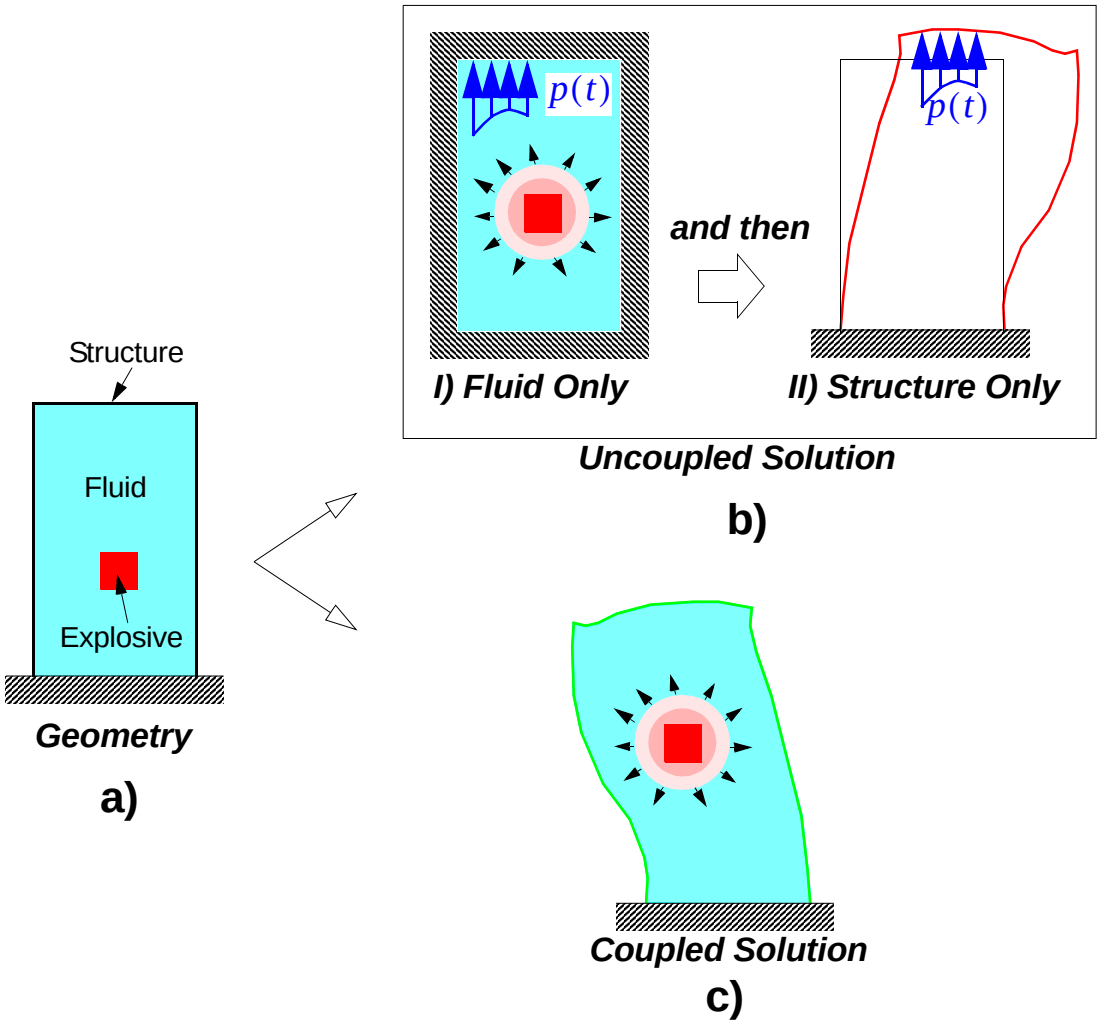

A simple FSI problem: a) Geometry; b) Solution by uncoupled analysis; c) Solution by coupled analysis

Fully coupled analysis is mandatory in at least ***two classes*** of problems:

- In the presence of ***nearly incompressible fluids***:

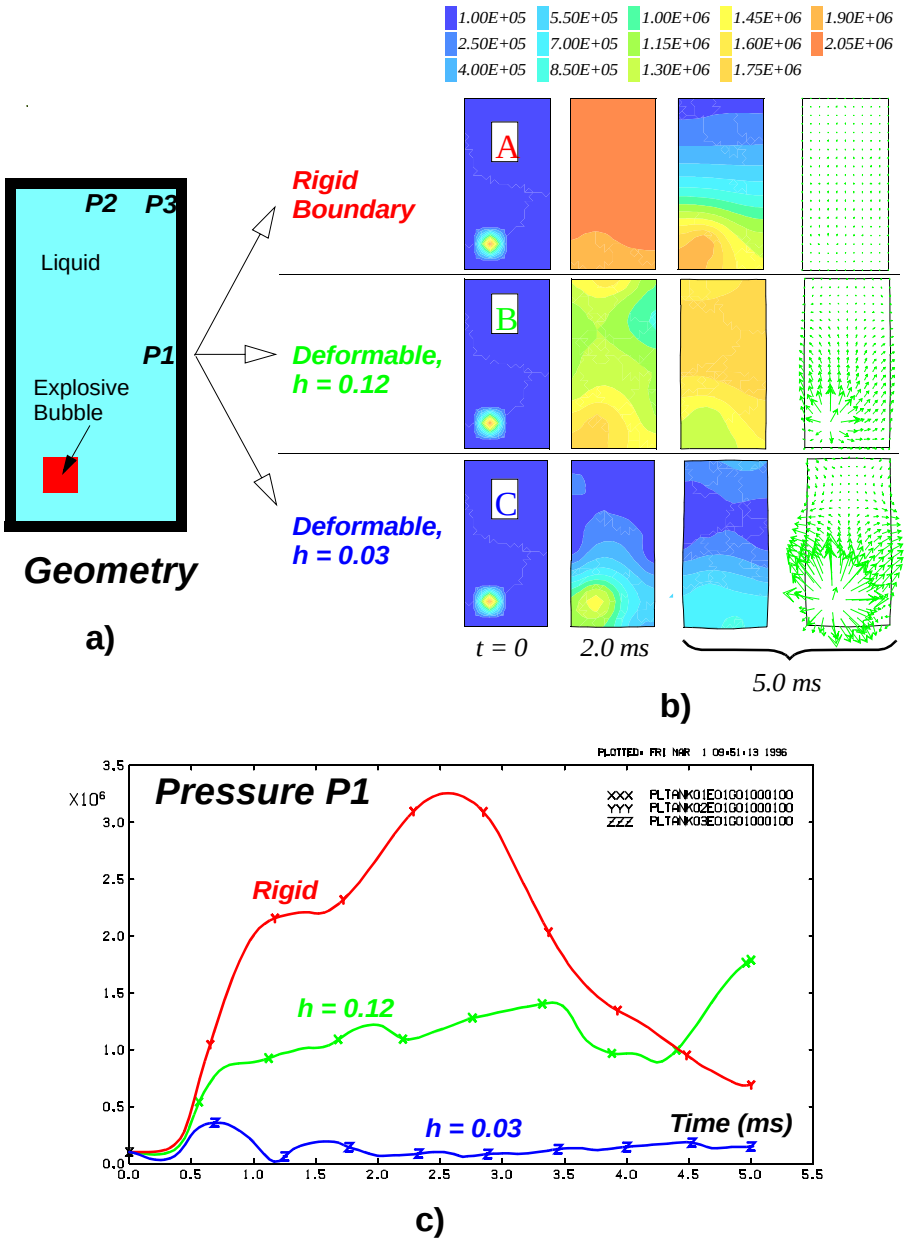

FSI problem with nearly incompressible fluid: a) Geometry; b) Fluid pressures and velocities; c) Transient fluid pressures at the P1 location

- For ***very deformable structures***:

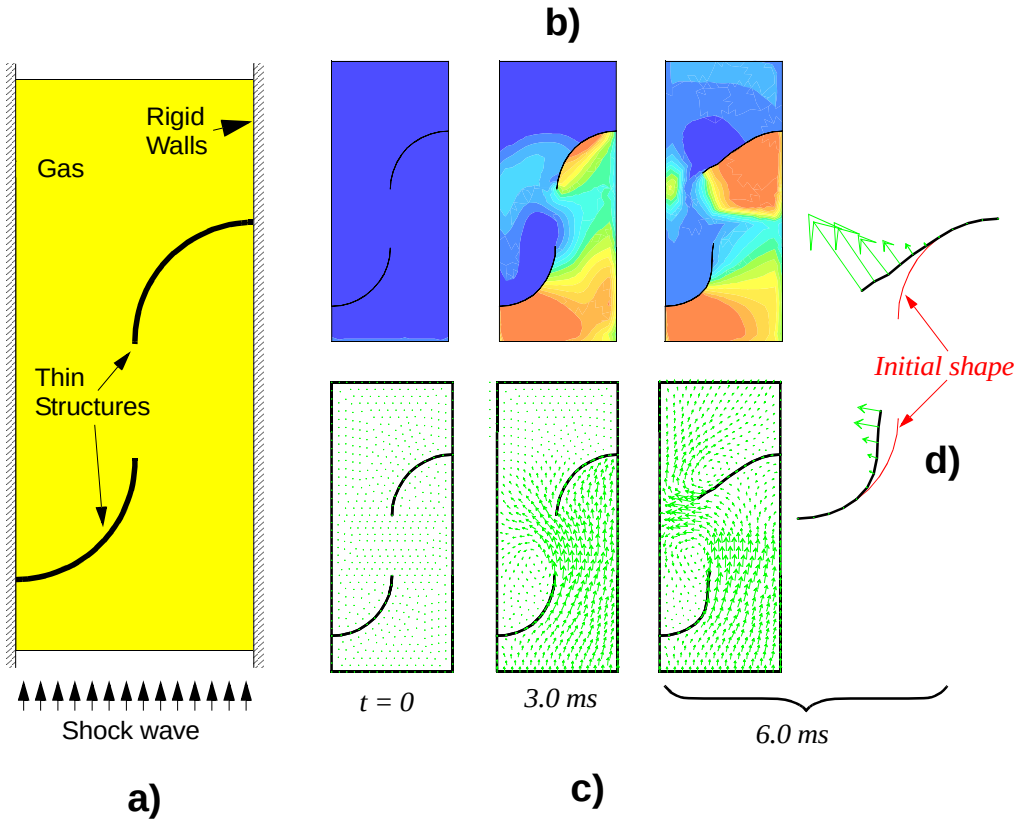

FSI problem with very deformable structures: a) Geometry; b) Fluid pressure; c) Fluid velocities; d) Structure deformations

Furthermore, consider following ***practical issues***:

- Amount of data to be transferred in uncoupled analysis;
- Probability of errors;
- Verification of solution requires deep insight and may be done only *a posteriori*.

Fluid-Structure Interactions

The interaction phenomena between ***compressible, inviscid fluids*** and ***deformable structures*** can be tentatively subdivided into two broad classes: permanent and non-permanent.

- By ***permanent*** contact we indicate the case of a structure in contact with a fluid: a) during the entire time interval of interest, and b) when the fluid is always of the same type.

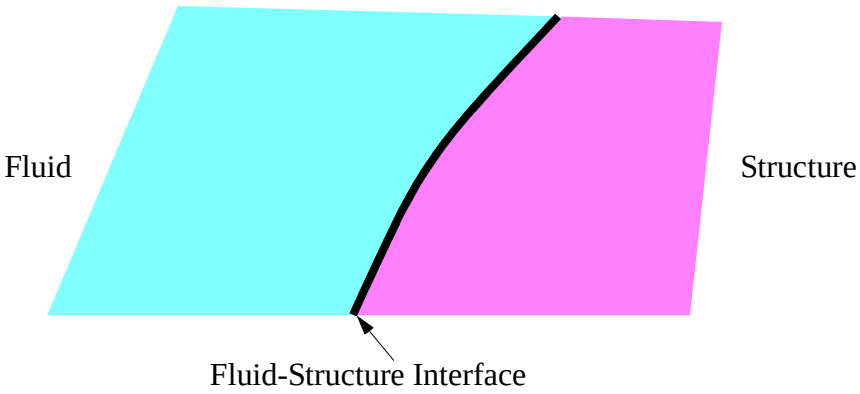

- On the other hand, the contact is ***non-permanent*** if any of the above conditions is violated, such as e.g. in the presence of free surfaces or of immiscible fluid-fluid interfaces.

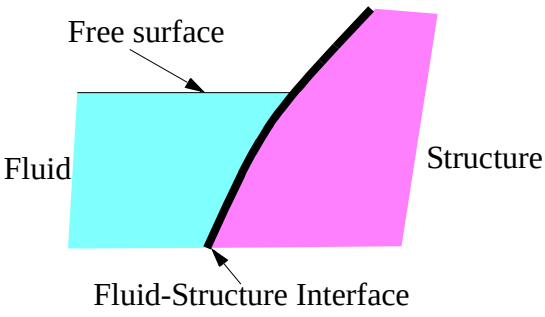

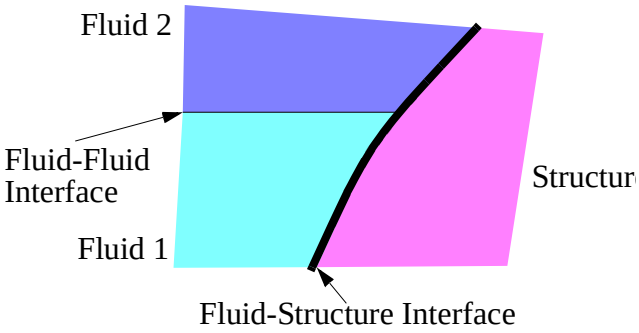

F-S Interaction of the Permanent Type

The permanent contact may be quite naturally and effectively treated by the ALE formulation and is also referred to as F-S interaction of the ALE type.

- Structure and fluid transmit to each other a mutual interaction in the form of a ***contact pressure*** at each point along the interface.

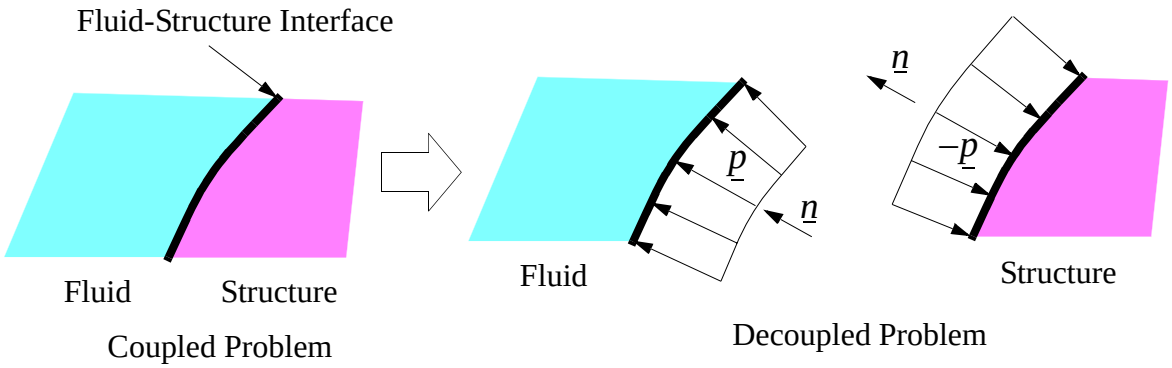

- Since the fluid is inviscid, the interaction pressure is directed along the normal $\underline{n}$ to the interface.

- In the finite element formulation, the continuous interface is substituted by a discrete approximation and instead of an interaction pressure we consider its resultant at each interface node, the ***interaction force*** $\underline{r}$.

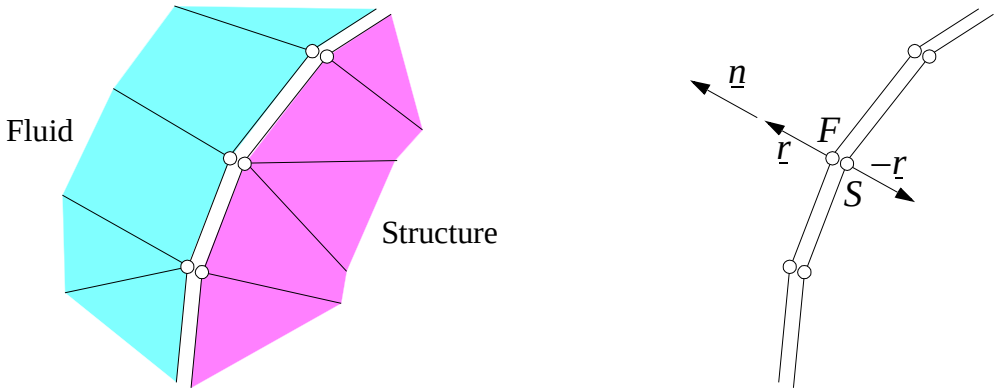

JOINT RESEARCH CENTRE

European Commission
Institute for the Protection and Security of the Citizen
European Laboratory for Structural Assessment

Conditions on Velocities

- Mesh velocity is identical in the two sub-domains along the F-S interface:

$$\underline{w}_F = \underline{w}_S$$

- Material velocity components normal to the F-S interface must be equal (***compatibility condition***) to ensure that the fluid and solid domains neither detach nor overlap during the motion:

$$\underline{v}_F \cdot \underline{n} = \underline{v}_S \cdot \underline{n} \qquad (77)$$

Tangential components, on the other hand, are arbitrary.

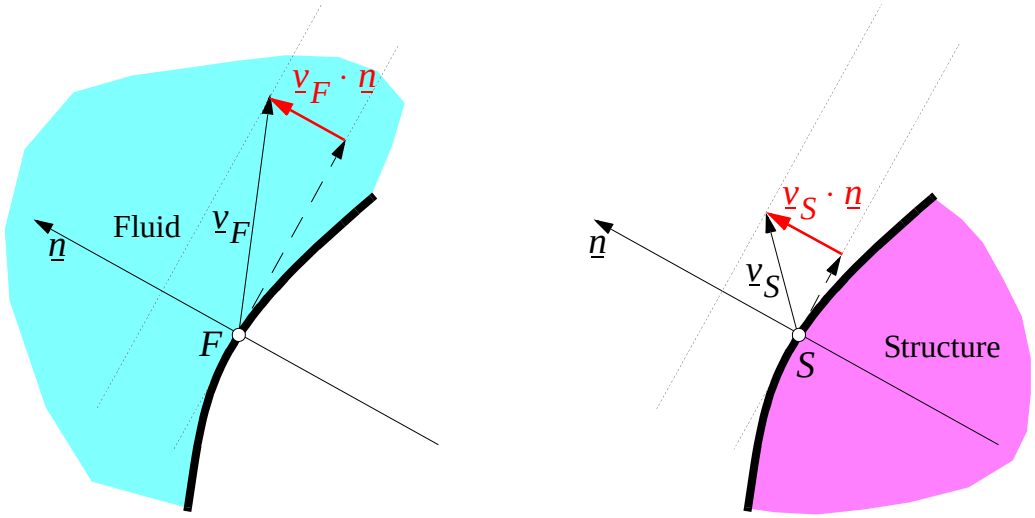

- Condition (77) is precisely of the form $\underline{C}\underline{v} = \underline{b}$ (see Eq. 7) and therefore may be imposed via the method of Lagrange multipliers.

- However, the following ***apparently simple*** question arises:

How does one define "the" normal to a *discrete* interface?

Geometrically Complex Cases

Traditionally complex cases of large practical importance are:

- Bilateral fluid contact (i.e., along both sides of a structure)

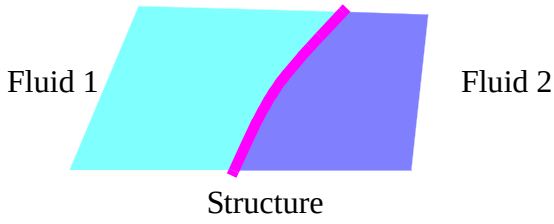

- Bifurcations (joints) in the structure

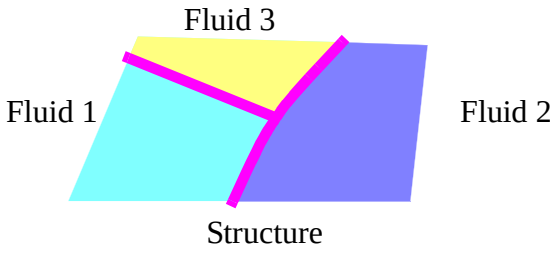

- Submerged structural edges

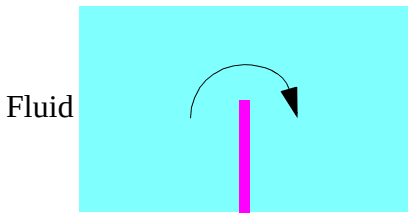

The difficulties arise from the use of ***structural elements without a topological thickness*** (beams, plates, shells) in the F.E. model.

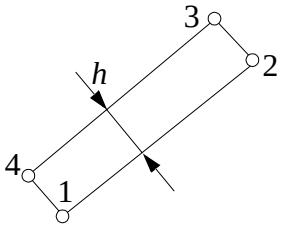

element with a topological thickness

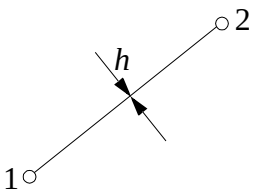

element without a topological thickness

JOINT RESEARCH CENTRE

European Commission
Institute for the Protection and Security of the Citizen
European Laboratory for Structural Assessment

Examples of 3-D Box-Like Structures

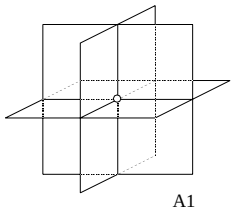

A1

a) basic geometry: 12 mutually orthogonal slabs completely embedded in a fluid

B1

b) one-slab case

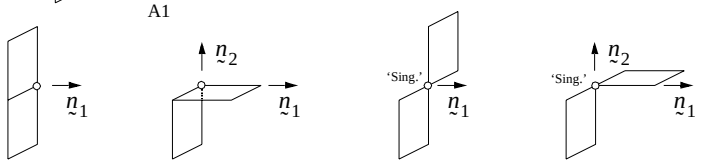

C1 C2 C3 C4

c) two-slab cases

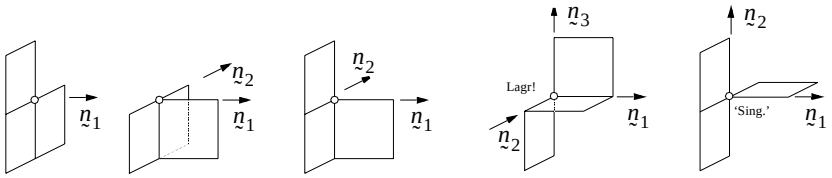

D1 D2 D3 D4 D5

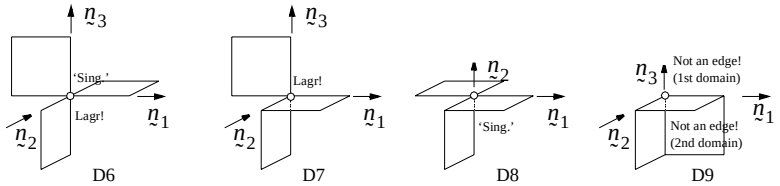

D6 D7 D8 D9

d) three-slab cases

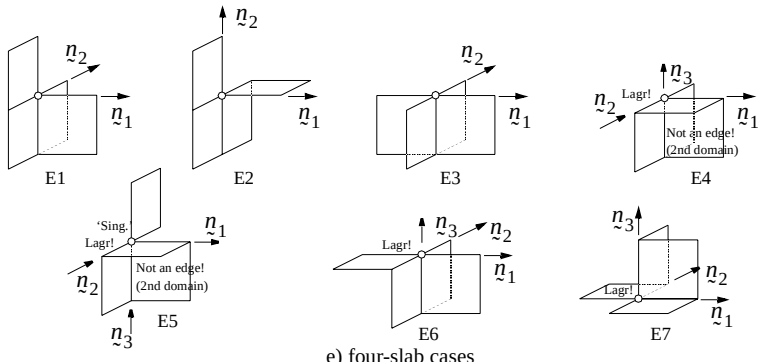

E1 E2 E3 E4 E5 E6 E7

e) four-slab cases

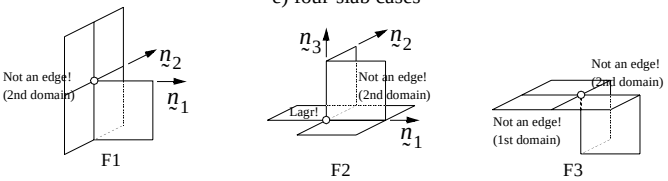

F1 F2 F3

f) five-slab cases

JOINT RESEARCH CENTRE

European Commission
Institute for the Protection and Security of the Citizen
European Laboratory for Structural Assessment

Determination of the normal to a discrete interface

Methods may be subdivided into two classes:

- ***Non-geometrical*** Methods, based e.g. on equilibrium considerations.

  Example: the ***UP*** (Uniform Pressure) algorithm.

- ***Geometrical*** Methods, based upon the topology of the discrete F-S interface in the vicinity of the point (node) under consideration.

  Example: the ***FSA*** (Fluid-Structure ALE) algorithm.

JOINT RESEARCH CENTRE

European Commission
Institute for the Protection and Security of the Citizen
European Laboratory for Structural Assessment

The Uniform Pressure (UP) Method

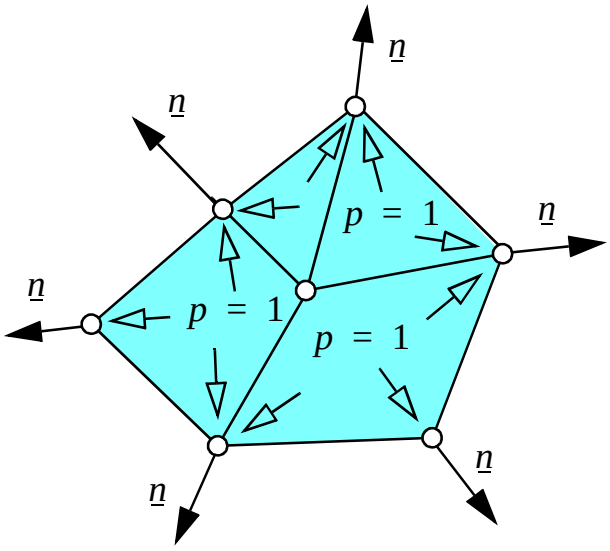

→ Element's pressure forces

The method simply relies upon the observation that:

> *The direction of the discrete normal is exactly prescribed, in a variational sense, by the resultant of internal forces due to an arbitrary but uniform pressure in the whole fluid domain.*

$$(\underline{f}_p^i)_{\text{element}} = \frac{1}{p}(\underline{f}^i)_{\text{element}} \quad \overset{\text{Assembly}}{\rightarrow} \quad \underline{n} = \underline{f}_p^i / \left\| \underline{f}_p^i \right\| \qquad (78)$$

Advantages:

- Computationally ***inexpensive***
- By automatically accounting for fluid element formulation, it avoids onset of spurious velocities due to lack of equilibrium that may affect purely geometric methods (e.g. ***warped faces***, etc.)

Shortcomings of The UP Method

- In the presence of fully submerged structural edges with no topological thickness, the UP method yields ***zero force***, since the node is completely surrounded by fluid. Therefore, the direction of the normal (78) is ***undetermined***.

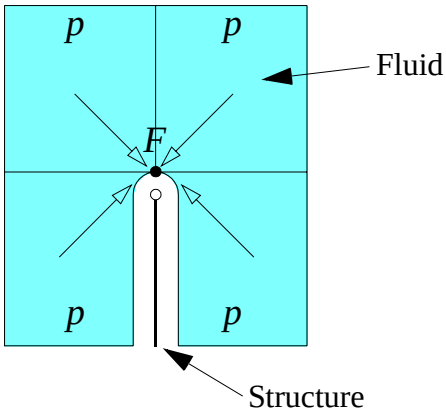

Element's pressure forces in node F

The assembled force for uniform pressure in node F is zero

- It may yield ***at most one*** normal per node. However, there are situations in 3D where ***two distinct normals*** are required, since the fluid motion is tied to the structure along two different components.

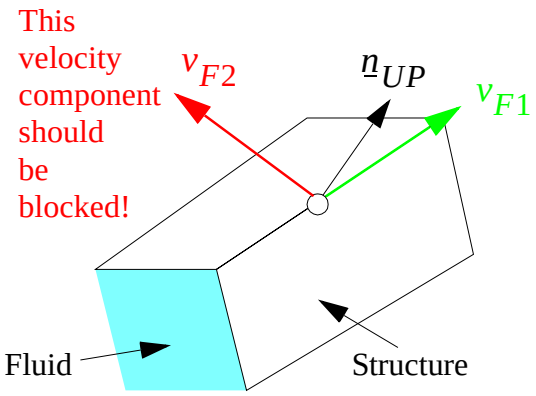

UP Method:
One Normal

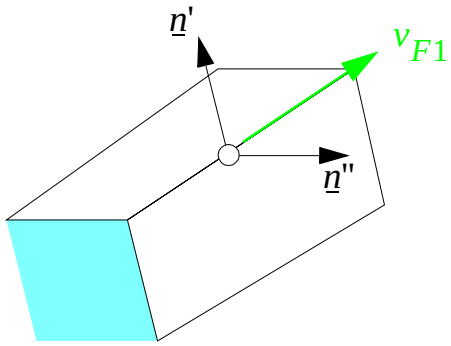

Geometric Method:
Two Normals

JOINT RESEARCH CENTRE

European Commission
Institute for the Protection and Security of the Citizen
European Laboratory for Structural Assessment

The FSA Method

The method is purely geometrical:

- To determine the local normal to the discrete interface in a generic fluid node only the ***shape of the fluid domain*** is considered in the vicinity of the node. By completely neglecting the solid domain, we avoid topological ambiguities due to zero-thickness elements.

- The normal direction is obtained by imposing ***zero net velocity flux*** across the discrete interface, so as to avoid artificial gains or losses of fluid:

$$\underline{n} = \underline{\Delta} / \left\| \underline{\Delta} \right\| \qquad \text{with} \qquad \underline{\Delta} = \sum_{k=1}^{n} \underline{S}_k \tag{79}$$

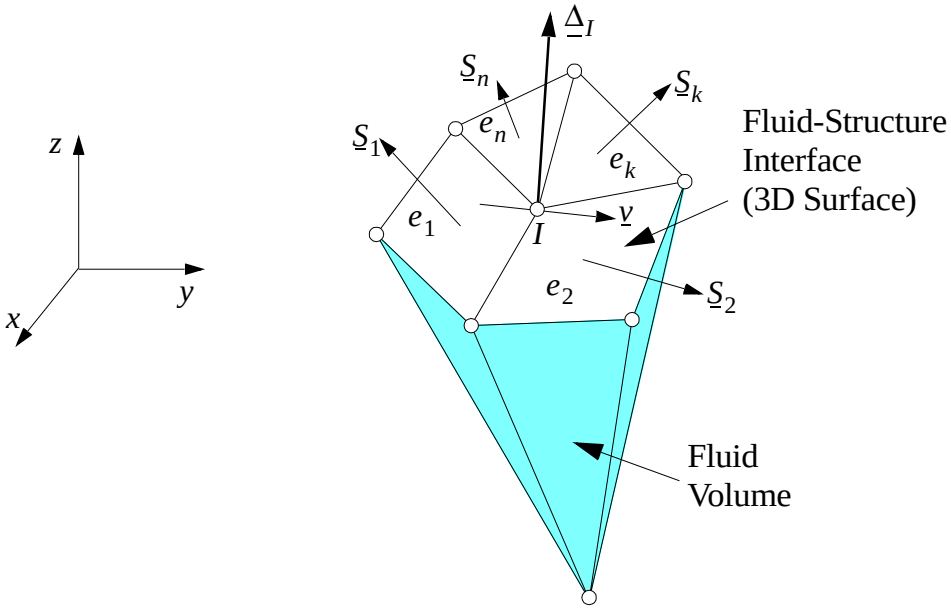

Here $\underline{\Delta}$ is the influence domain of the node, composed by all surrounding element faces $\underline{S}_k$ along the F-S interface.

- The method is easily adapted so as to avoid the undefined normal in the case of submerged structural edges, and also to yield 2 normals in 3D cases when this is relevant (see [17-20] for technical details).

The FSA algorithm

Table 3 - The FSA algorithm (from [18])

The basic tasks to be performed are summarized hereafter:

Algorithm A

For each fluid node F declared subjected to FSA conditions:

A1 Determine the corresponding 'structural' node S;

A2 Find the normal(s) $\underline{n}$ to the interface;

A3 'Write down' the relation(s) $v_{Fn} = v_{Sn}$ to be inserted in the system of linear relations between degrees of freedom;

Once all such relations are written, solve the system to determine the Lagrange multipliers and the reactions.

Definition: The master node S corresponding to a fluid slave node F subjected to FSA sliding conditions is the node (structural or fluid) that has the same initial coordinates as F and is declared to be Lagrangian. It must be unique in the mesh.

Algorithm A2

A2.1 Find the influence domain Δ of the slave node F;

A2.2 Compute the normal $\underset{\sim}{n}$ to the influence domain.

Table 3 - The FSA algorithm (from [18]) (Continued)

Algorithm A2.1

To find the influence domain(s) of a slave fluid node F, we proceed as follows:

A2.1.1 Loop over all elements to find those ***fluid*** elements that contain node F;

A2.1.2 For each such element, determine the faces that contain node F;

A2.1.3 Of these faces, retain only those that do not have another fluid element on the other 'side' of the face;

The set of all such faces is a 'trial' influence domain Δ^*.

A2.1.4 Subdivide the domain Δ^* into two (possibly empty) subdomains: Δ_1 contains N_1 single (i.e., uncoupled) element faces, while Δ_2^* contains N_2 ***couples*** of mutually opposite element faces (i.e., $2N_2$ faces altogether);

A2.1.5 Consider subdomain Δ_1 of single faces, and determine one or more normals to the domain (see details below);

A2.1.6 Consider subdomain Δ_2^* of coupled faces and extract from it a (sub-)subdomain Δ_2 that contains one and only one face from each couple (i.e., N_2 faces) (see details below);

A2.1.7 Consider subdomain Δ_2 and determine one or more normals to the domain by exactly the same procedure as in step 5 above;

A2.1.8 Collect all the normals produced in steps 5 and 7 above, perform consistency checks and determine the final number of distinct normals found.

Algorithm A2.1.5

Determine the normal(s) to the domain Δ.

A2.1.5.1 Set all faces in Δ as 'free';

A2.1.5.2 Repeat until no free faces are left:

- Take the first free face; this is the 'reference';
- Consider the next free face: if it forms an angle of less than α_0 with the reference, retain it (it is no longer free), otherwise skip it;
- When all faces have been considered, the retained ones form a subset of Δ from which one normal can be determined;
- The element/face information for each such group should be memorized for future reference (see below).

Algorithm A2.1.6

A2.1.6.1 Pick up one of the two faces of the first couple (say the first one) and keep it as a reference; reject the other face;

A2.1.6.2 For each other couple, keep the face of the couple that forms the smallest angle with the reference, and reject the other one.

Example: finding the normal to the interface in plane geometry

As an example, let us consider a generic discrete fluid-structure interface as shown below, consisting of two straight sides of lengths L_1 and L_2, that meet at node I forming an angle γ.

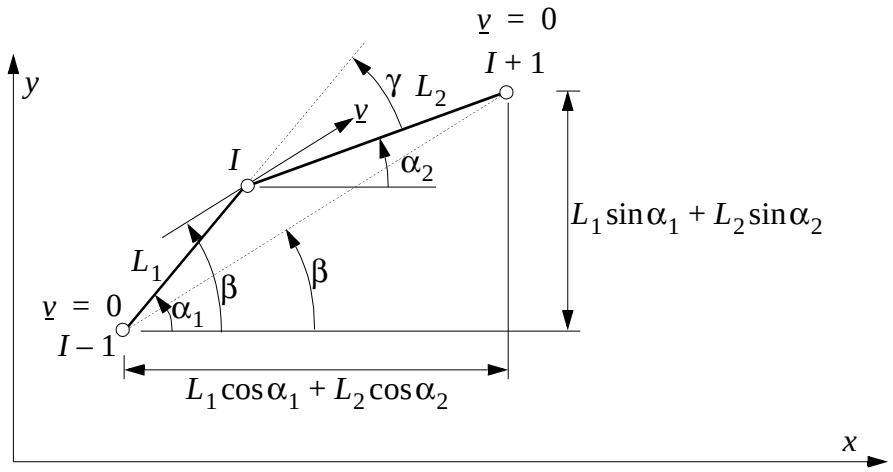

A generic discretized fluid-structure interface in two dimensions (plane situation)

In their early work, Donea and co-workers adopted an approximated technique to determine the normal based on physical intuition. It was simply assumed that the tangent to the interface at I would be the average of the directions of the two sides, i.e.:

$$\beta^* = \frac{\alpha_1 + \alpha_2}{2} \qquad (80)$$

which, as we will see hereafter, is satisfactory only in the particular case of sides of equal length ($L_1 = L_2$) and for a plane geometry. Later on, they observed [8,9] that in general situations the mass balance was incorrect when (80) was assumed because some fluid was 'gained' or 'lost' at the corners of the interface.

In fact, consider for simplicity that the structure is fixed and that the fluid velocity is null at nodes $I-1$ and $I+1$. The case of non-fixed structure can be treated similarly by using the relative (fluid -

structure) velocity in place of the fluid velocity. Assuming a generic fluid velocity $\underline{v}$ of slope β at node I induces a flux of fluid flowing 'out of' side L_1 which is proportional (for a *plane* 2D geometry) to $\Phi_1 = \|\underline{L}_1 \times \underline{v}\| = L_1 v \sin(\alpha_1 - \beta)$, while the flux flowing 'into' side L_2 is proportional to $\Phi_2 = \|\underline{L}_2 \times \underline{v}\| = L_2 v \sin(\beta - \alpha_2)$, where $\times$ denotes a vector product and $\| \ \|$ the modulus of a vector. Thus, in order to have compensation (no fluid 'lost' or 'gained' at I), it must be $\Phi_1 = \Phi_2$, or:

$$L_1 v \sin(\alpha_1 - \beta) = L_2 v \sin(\beta - \alpha_2) \tag{81}$$

Simplifying and dividing by $\cos\beta$, thereby assuming $\cos\beta \neq 0$, we obtain finally:

$$\tan\beta = \frac{L_1 \sin\alpha_1 + L_2 \sin\alpha_2}{L_1 \cos\alpha_1 + L_2 \cos\alpha_2} \tag{82}$$

Thus, β ***is precisely the slope of the line connecting nodes*** $I-1$ ***and*** $I+1$, as shown in the above figure. When $L_1 = L_2 = L$, this expression reduces to:

$$\tan\beta = \frac{\sin\alpha_1 + \sin\alpha_2}{\cos\alpha_1 + \cos\alpha_2} \tag{83}$$

which is verified for $\beta = (\alpha_1 + \alpha_2)/2$, that coincides with (80).

Example 2: the normal in axisymmetric geometry

The arguments invoked in an intuitive manner in the previous Section for plane situations may be more precisely defined and applied to more complex geometries, such as axisymmetric cases.

The flux of a generic vector $\underline{\delta}$ across a rectilinear side or segment I-J as shown below is given by:

$$\Phi = \int_I^J (\underline{\delta} \cdot \underline{n}) dl \tag{84}$$

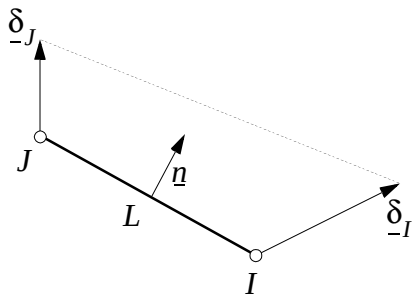

Flux of a vector across a rectilinear side

One readily obtains in the axisymmetric case:

$$\Phi^{ax} = \frac{1}{2}\left[\left(\frac{2x_I + x_J}{3}\delta_{xI} + \frac{x_I + 2x_J}{3}\delta_{xJ}\right)(y_J - y_I) + \left(\frac{2x_I + x_J}{3}\delta_{yI} + \frac{x_I + 2x_J}{3}\delta_{yJ}\right)(x_I - x_J)\right] \tag{85}$$

The situation of interest here is that of two adjacent sides with a velocity $\underline{v}$ at the common node and zero velocities at the other nodes, as shown in the next figure.

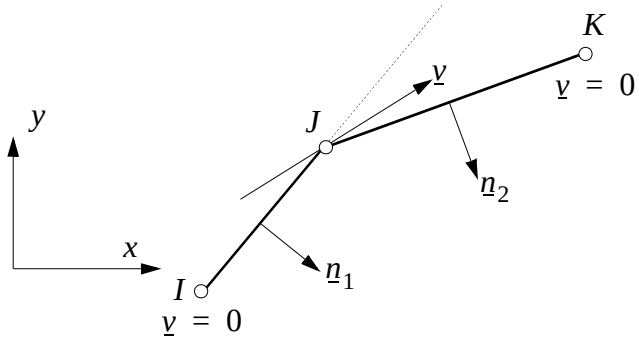

Two adjacent sides

JOINT RESEARCH CENTRE
European Commission
Institute for the Protection and Security of the Citizen
European Laboratory for Structural Assessment

By applying (85), we have:

$$\Phi^{ax} = \Phi_1^{ax} + \Phi_2^{ax} = \frac{1}{2}\left[\frac{x_I + 2x_J}{3} v_x (y_J - y_I) + \frac{x_I + 2x_J}{3} v_y (x_I - x_J)\right] + \\ + \frac{1}{2}\left[\frac{2x_J + x_K}{3} v_x (y_K - y_J) + \frac{2x_J + x_K}{3} v_y (x_J - x_K)\right] \tag{86}$$

We proceed as usual imposing a zero net flux and obtain after some algebraic simplifications the condition:

$$\frac{v_y}{v_x} = \frac{x_I (y_J - y_I) + 2x_J (y_K - y_I) + x_K (y_K - y_J)}{x_K (x_J + x_K) - x_I (x_I + x_J)} \tag{87}$$

It may be verified that this expression tends to the expression found above for plane geometry when the radius becomes very large. In fact, for $x_I \to x_\infty$, $x_J \to x_\infty$, $x_K \to x_\infty$ (where x_∞ is a very large quantity) the numerator tends to $3(y_K - y_I)x_\infty$. At the same time the denominator, that may be re-written as $(x_I + x_J + x_K)(x_K - x_I)$, tends to $3(x_K - x_I)x_\infty$, therefore:

$$\frac{v_y}{v_x} \to \frac{y_K - y_I}{x_K - x_I} \tag{88}$$

which is equivalent to (83), as anticipated.

Shortcomings of The FSA Method

- Use of FSA alone may lead to the onset of spurious, ***non-physical velocities*** in 3D models with warped element faces along the F-S interface, as shown in the simple ***patch test***:

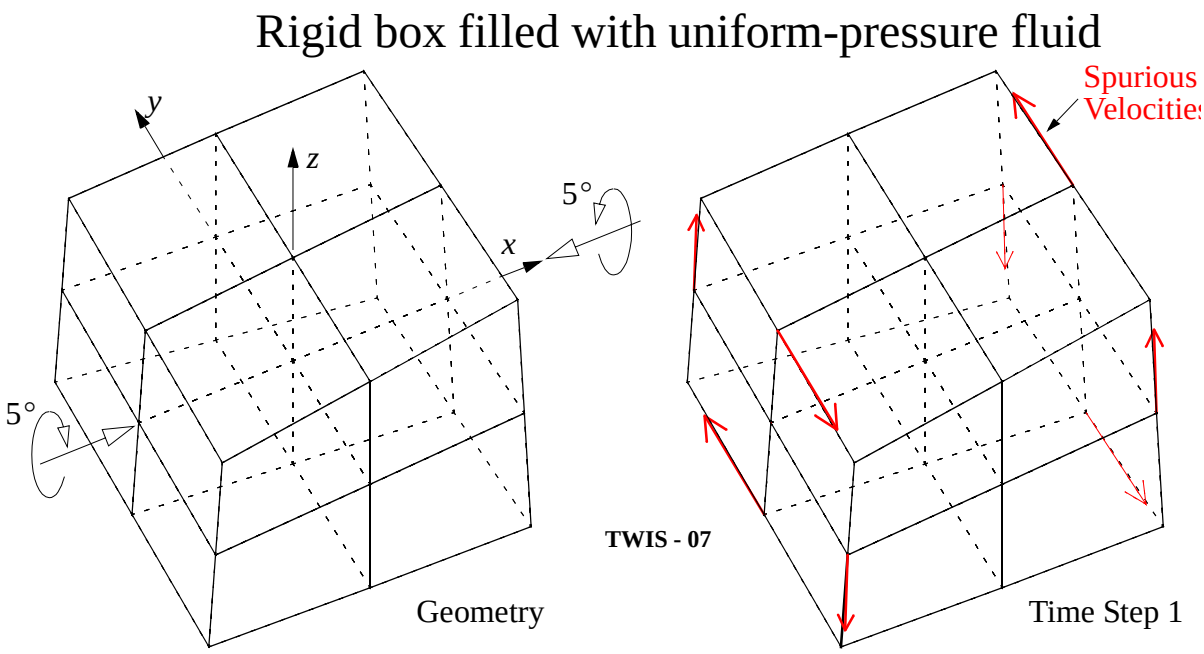

- The spurious velocities are due to a slight but non-negligible ***accuracy mismatch*** in the calculation of internal pressure forces, on one hand, and of reaction forces (i.e., the direction of the FSA normal) on the other hand.
- Purely geometric methods use no information about internal fluid element formulation.
- However, in such cases the UP method ensures perfect equilibrium.

The FSCR Method

For full generality, it is suggested to use the ***FSCR method***, which results from a ***combination of the UP and FSA algorithms***, exploiting the strengths of both.

The FSCR algorithm proceeds qualitatively as follows (see [19-20] for full details):

- The search for the normal direction (possibly, 2 directions in 3D) is first performed by the FSA algorithm. Let us indicate by $\underline{n}_1$ and $\underline{n}_2$ the resulting normals. Then, an independent evaluation of "the" normal (just one direction) is performed by the UP method. We indicate with $\underline{n}_P$ the result. The following cases must be distinguished:

- If the FSA calculation yields a nodal influence domain composed *only by couples of mutually opposite faces*, then we know that $\underline{n}_P$ is at best very imprecise, if not undetermined. Therefore $\underline{n}_1$ and, if relevant, $\underline{n}_2$ are retained.

- In all other cases, the nodal influence domain contains at least one 'single' (non-coupled) element face and the normal direction resulting from the UP method is more accurate in general than the FSA one(s). If the FSA calculation yields just one normal $\underline{n}_1$, this normal is simply rejected and $\underline{n}_P$ is retained instead. However, when the FSA method detects *two normals*, we may not simply drop both of them in favour of the (single) $\underline{n}_P$ normal. In such a case, $\underline{n}_1$ and $\underline{n}_2$ are corrected, see paper, so as to become "compatible" with $\underline{n}_P$, i.e. so that $\underline{n}_P$ is contained in the plane defined by $\underline{n}_1$' and $\underline{n}_2$' (the corrected $\underline{n}_1$ and $\underline{n}_2$).

JOINT RESEARCH CENTRE

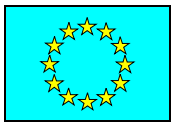

European Commission
Institute for the Protection and Security of the Citizen
European Laboratory for Structural Assessment

Scheme of the FSCR method

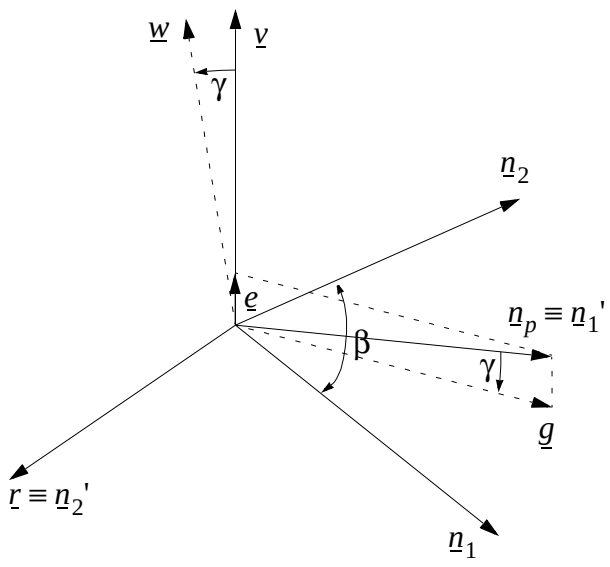

- $\underline{n}_1$, $\underline{n}_2$ and $\underline{n}_p$ are unit vectors
- In practical cases, the angle β is such that $60° \le \beta < 180°$
- $\underline{v} = (\underline{n}_1 \times \underline{n}_2) / \left\| \underline{n}_1 \times \underline{n}_2 \right\|$

  The $\underline{v}$ vector is unitary and normal to the plane defined by $\underline{n}_1$ and $\underline{n}_2$
- $\underline{e} = (\underline{n}_p \cdot \underline{v})\underline{v}$
- $\underline{g} = \underline{n}_p - \underline{e}$
- The $\underline{g}$ vector is the projection of $\underline{n}_p$ over the plane defined by $\underline{n}_1$ and $\underline{n}_2$
- $\underline{r} = (\underline{g} \times \underline{v}) / \left\| \underline{g} \times \underline{v} \right\|$
- $\begin{cases} \underline{n}_1' \equiv \underline{n}_p \\ \underline{n}_2' \equiv \underline{r} \end{cases}$
- Note that $\underline{n}_1' \perp \underline{n}_2'$ by construction.

The FSR Method (Rigid Structures)

A slightly modified version of the FSA model, called the FSR algorithm (Fluid-Structure-Rigid), deals with applications in which the ***structural displacements*** for the range of expected fluid pressures are ***negligible***. Usually in such cases the rigid structure is completely neglected for efficiency reasons and ***only the fluid*** is modelled.

The main differences with respect to FSA, see Table 3, are:

- The search for a structural node corresponding to each fluid node on the 'interface', step A1, is dropped;
- The search for the normal(s), step A2, is done exactly like in the FSA case, but these normals are held fixed, i.e. they ***do not change direction*** during the transient calculation;
- The compatibility conditions Eq. (77) now involve the degrees of freedom of the fluid node only:

$$\underline{v}_F \cdot \underline{n} = 0 \qquad (89)$$

This directive ***dramatically simplifies*** the prescription of fluid boundary conditions in geometrically complex cases.

Table 4 - The FSR algorithm

Algorithm R

For each fluid node F declared subjected to FSR conditions:

R2 Find the normal(s) $\underset{\sim}{n}$ to the interface: this corresponds to step A2 of the FSA algorithm;

R3 'Write down' the relation(s) $v_{Fn} = 0$ to be inserted in the system of linear relations between degrees of freedom; since the boundary is rigid, the coefficients in these relations are constant and have to be computed only once.

Once all such relations are written, solve the system to determine the Lagrange multipliers and the reactions.

Application to Finite Volumes

The FS algorithms illustrated above in a FE context have been applied with success also to the node-centred Finite Volume formulation.

- Minor adjustments are necessary because the time integration scheme used in the FV context is ***first-order*** accurate, not second-order.
- The two schemes may be reconciled by adding a ***corrective force term*** to the equilibrium equation (see [15] for details).

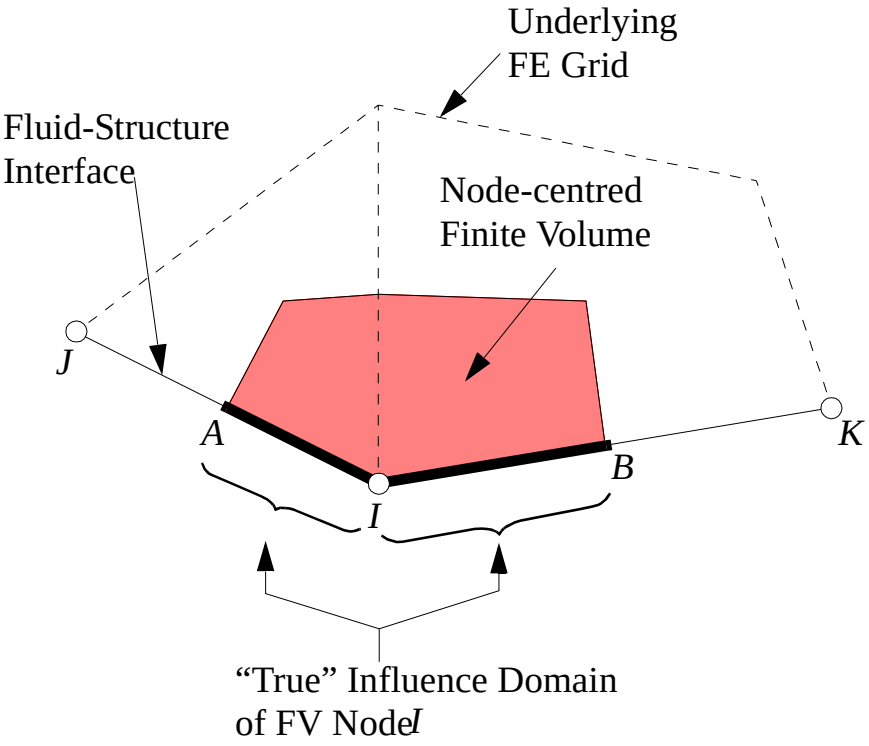

Influence domain to compute the geometric normal in a FV context

Prepared for the Course “Fluid-Structure Interaction in Fast Transient Dynamics”
Organised by UPC, Barcelona (E) 4-7 May 2004.

Course Notes

Part IV

Advanced Topics and Applications

Folco Casadei

Joint Research Centre - IPSC
European Laboratory for Structural Assessment, T.P. 480
21020 Ispra (Varese) - Italy
E-mail: folco.casadei@jrc.it
Web: http://europlexus.jrc.it

JOINT RESEARCH CENTRE

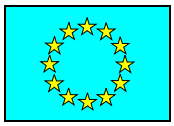

European Commission
Institute for the Protection and Security of the Citizen
European Laboratory for Structural Assessment

Some “simple” FSI test cases

Before showing industrial applications, let us consider some simple but realistic examples in order to illustrate how an input data set is set up.

Explosion in a tank

- If the tank walls are ***rigid***, there is no need to model the structure: use is made of the ***FSR*** directive.
- If the tank is ***deformable***, we model it and use the ***FSA*** directive.

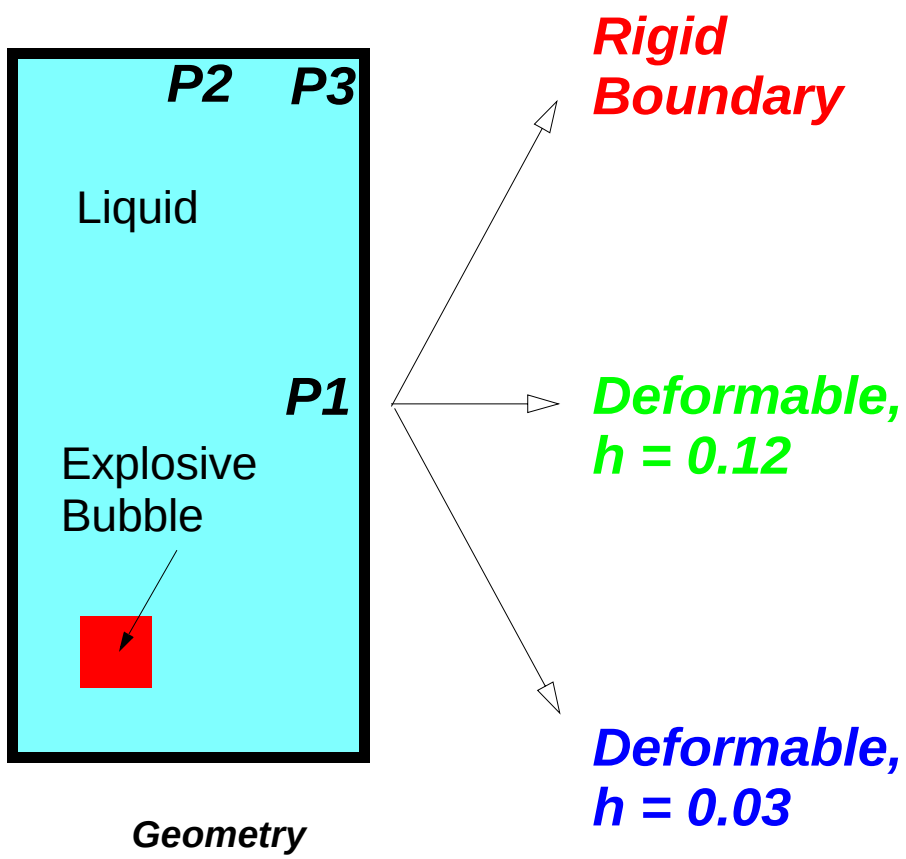

Input data for the rigid case

```
TANK - 02
$-----------------------------------------------------Problem type
CAST UNFO 'tank02.sauv' MESH
DPLA NONL ALE
$-------------------------------------------------Problem dimensions
DIME
 PT2L 250 FL24 200 MATE 3
 NALE 23 NBLE 250
 FSA  65 IFSA 224 TABL 1 10
TERM
$-----------------------------------------------------------Geometry
GEOM
 FL24 FLUI
TERM
$-----------------------------------------------------Grid motion
GRIL LAGR LECT LAG TERM
     EULE LECT FSRN TERM
     ALE LECT FLUI TERM
     AUTO GAM0 0.5 AUTR
$-----------------------------------------------------------Materials
MATE
$ WT0 liquid water
     FLUT RO 1000.0454482d0 EINT 0.0d0 GAMM 7.15d0
          PB 3.010d9 ITER 1 ALF0 1 RREF 1000.0d0
          CONV 0.1d0 BET0 1 KINT 0 AHGF 0 CL 0.5
          CQ 2.56 PMIN 0 NUM 8
          LECT LIQU TERM
$ high-pressure perfect gas (explosive bubble)
     FLUT RO 20. EINT 2.5E5 GAMM 1.4 PB 0
          ITER 1 ALF0 1 BET0 1 KINT 0 AHGF 0 CL 0.5
          CQ 2.56 PMIN 0 NUM 1 LECT EXPL TERM
$-----------------------------------------------Boundary conditions
LIAI FSR LECT FSRN TERM
$-----------------------------------------Printouts/Postprocessing
ECRI VITE TFRE 0.5E-3
     FICH K200 'tank02.k200' TFREQ 0.5E-3 POIN TOUS
          VARI DEPL VITE ECRO ECRC LECT 1 TERM
     FICH TPLO 'tank02.tplo' TFRE 6.E-6 DESC 'TANK02'
          POIN LECT TPLN TERM ELEM LECT TPLE TERM
$-------------------------------------------------------------Options
OPTI PAS AUTO NOTEST STEP IO CSTA 0.5
$-----------------------------------------------Transient calculation
CALCUL TINI 0 TEND 5.0E-3
FIN
```

Input data for the deformable case

```
TANK - 01
$-----------------------------------------------------Problem type
CAST UNFO 'tank01.sauv' MESH
DPLA NONL ALE
$-------------------------------------------------Problem dimensions
DIME
 PT3L 70 PT2L 250 ZONE 2
 FL24 200 ED01 60 MATE 3
 NALE 23 NBLE 250
 FSA  65 IFSA 224 TABL 1 10
TERM
$-----------------------------------------------------------Geometry
GEOM
 FL24 FLUI
 ED01 STRU
TERM
$-----------------------------------------------Geometric complements
EPAI 0.12 LECT STRU TERM
$-----------------------------------------------------Grid motion
GRIL LAGR LECT LAG TERM
     ALE LECT FLUI TERM
     AUTO GAM0 0.5 AUTR
$-----------------------------------------------------------Materials
MATE
$ steel
     VM23 RO 7800. YOUNG 1.6E11 NU 0.333 ELAS 1.05E8
          TRAC 2 1.05E8 .656256E-3 1.6105E10 1.00066
          LECT STRU TERM
$ WT0 liquid water
     FLUT RO 1000.0454482d0 EINT 0.0d0 GAMM 7.15d0
          PB 3.010d9 ITER 1 ALF0 1 RREF 1000.0d0
          CONV 0.1d0 BET0 1 KINT 0 AHGF 0 CL 0.5
          CQ 2.56 PMIN 0 NUM 8
          LECT LIQU TERM
$ high-pressure perfect gas (explosive bubble)
     FLUT RO 20. EINT 2.5E5 GAMM 1.4 PB 0
          ITER 1 ALF0 1 BET0 1 KINT 0 AHGF 0 CL 0.5
          CQ 2.56 PMIN 0 NUM 1 LECT EXPL TERM
$-------------------------------------------------Boundary conditions
LIAI FSA LECT FSAN TERM
$-----------------------------------------Printouts/Postprocessing
ECRI VITE TFRE 0.5E-3
     FICH K200 'tank01.k200' TFREQ 0.5E-3 POIN TOUS
          VARI DEPL VITE ECRO ECRC LECT 1 TERM
     FICH TPLO 'tank01.tplo' TFRE 6.E-6 DESC 'TANK01'
          POIN LECT TPLN TERM ELEM LECT TPLE TERM
$-------------------------------------------------------------Options
OPTI PAS AUTO NOTEST STEP IO CSTA 0.5
$-----------------------------------------------Transient calculation
CALCUL TINI 0 TEND 5.0E-3
FIN
```

Results

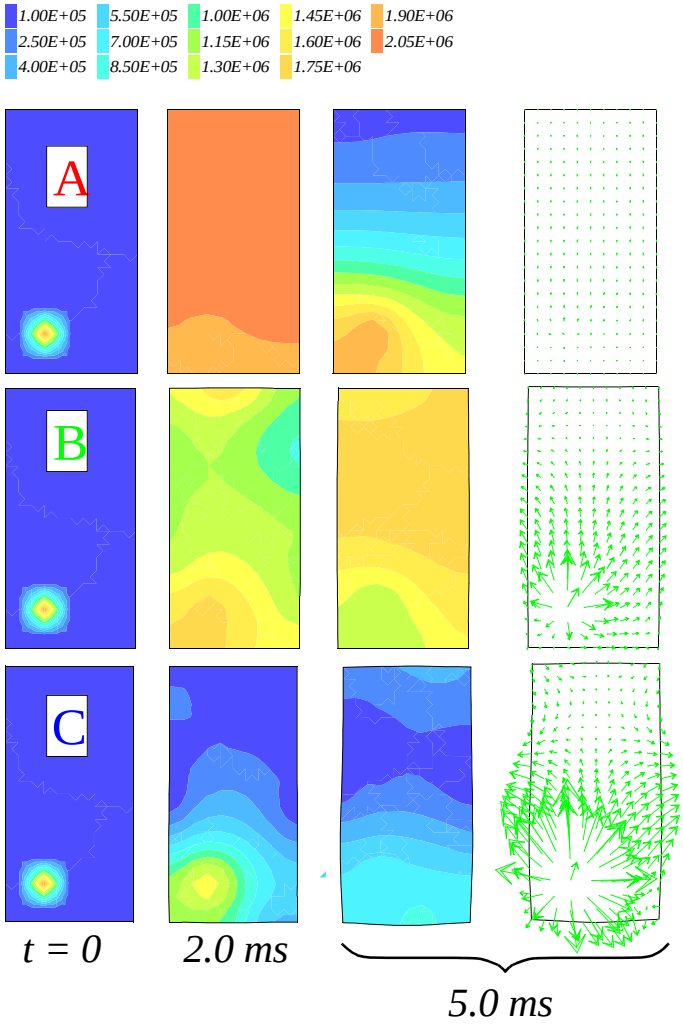

Note the dramatic change in pressures with relatively small deformations of the strucure

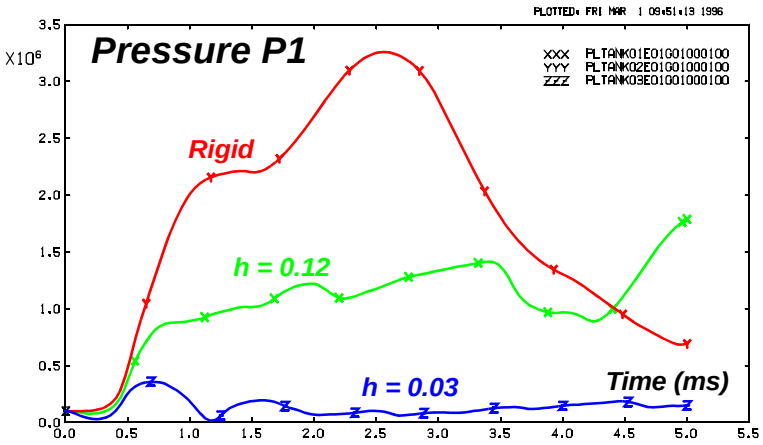

JOINT RESEARCH CENTRE

European Commission
Institute for the Protection and Security of the Citizen
European Laboratory for Structural Assessment

Explosion in a 3D helicoidal tube [19]

This example illustrates well the tremendous efficiency of the FSR directive in some ***geometrically complex*** 3D cases.

Description:

The model simulates the propagation of a pressure wave in a helicoidal tube. The structure (tube) surrounding the fluid is assumed to be rigid and not included in the model since, as shown in Lesson 8, the incorrect behaviour of the FSA algorithm in describing the conditions along the external surface of the fluid does not depend on the actual presence or not of a structure.

Most of the tube is initially filled up by a gas at uniform low pressure while a higher pressure zone, simulating an explosion, is generated near the larger-diameter extremity at the initial time. During the transient, a high-pressure wave is expected to propagate along the tube, interacting with the (rigid) walls, and eventually being reflected at the thinner extremity of the tube. In fact, both extremities are also supposed to be closed by rigid walls for simplicity.

When the FSA algorithm is used spurious, non-physical velocities rapidly appear in the numerical solution in the central and thinner parts of the tube, long before the pressure wave reaches these zones. Since the pressure is initially uniform in this part of the mesh, the fluid should clearly be in equilibrium and not move before the arrival of the pressure wave.

Problem definition

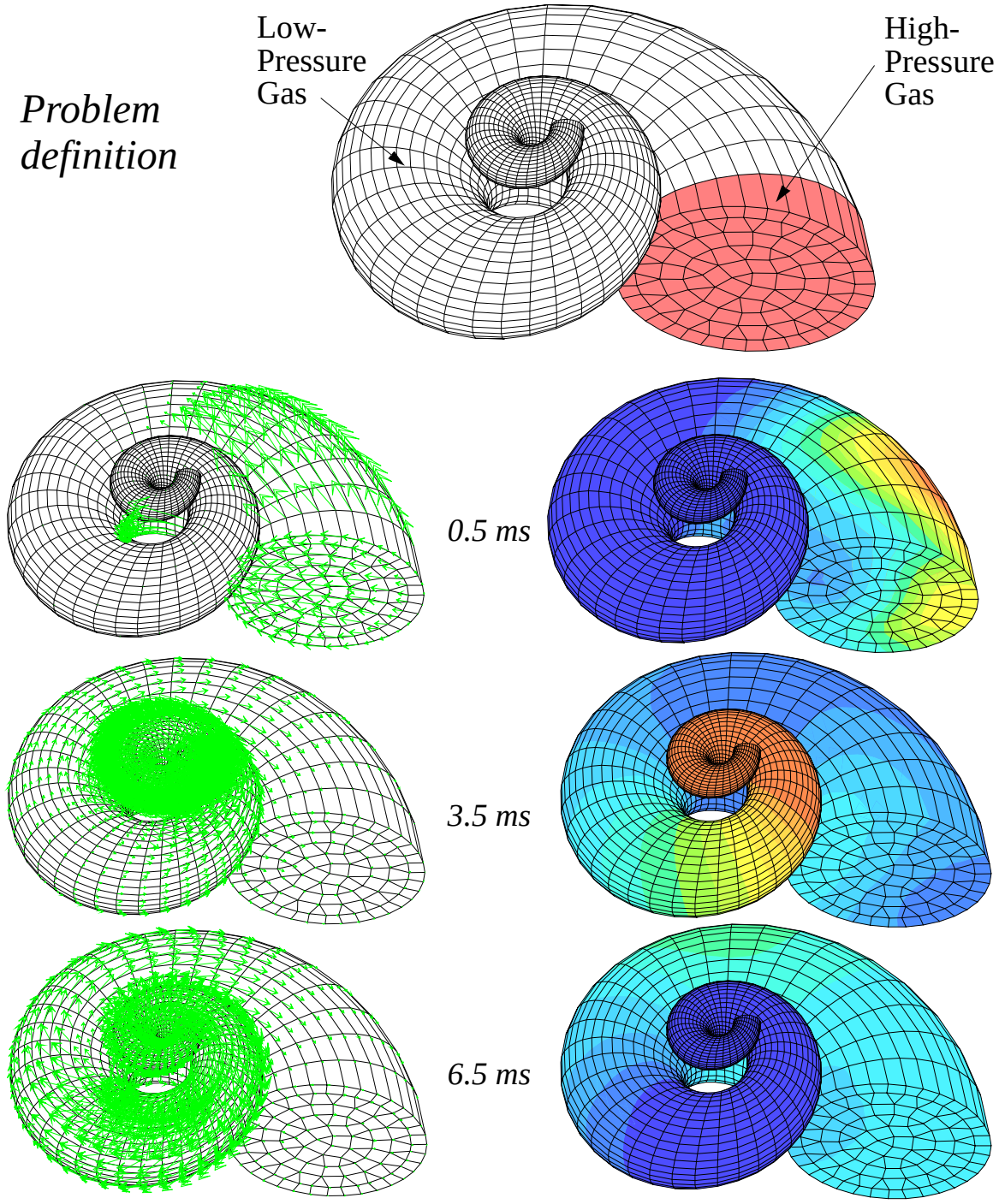

JOINT RESEARCH CENTRE

European Commission
Institute for the Protection and Security of the Citizen
European Laboratory for Structural Assessment

Input data for the helicoidal tube

```
SOLI - 05
$-----------------------------------------------------Problem type
CAST UNFO 'soli05.sauv' MESH
TRID NONL EULE
$-------------------------------------------------Problem dimensions
DIME
 PT3L 8760 FL38 6264 FL36 2016 ZONE 2
 MATE 2 TABL 1 5
 NALE 1 NBLE 1 BLOQ 9000 MTEL 115
TERM
$-----------------------------------------------------------Geometry
GEOM FL38 SUR8 FL36 SUR6 TERM
$-----------------------------------------------------------Materials
MATE
$ high-pressure perfect gas
    FLUT RO 1.22 EINT 3.046E6 GAMM 1.269 PB 0
         ITER 1 ALF0 1 BET0 1 KINT 0 AHGF 0 CL 0.5
         CQ 2.56 PMIN 0 NUM 1
         LECT SUR1 TERM
$ same gas at a lower pressure
    FLUT RO 0.1237 EINT 3.046E6 GAMM 1.269 PB 0
         ITER 1 ALF0 1 BET0 1 KINT 0 AHGF 0 CL 0.5
         CQ 2.56 PMIN 0 NUM 1
         LECT SUR2 TERM
$-------------------------------------------------Boundary conditions
LIAI FSR LECT FSRN TERM
$-----------------------------------------Printouts/Postprocessing
ECRI VITE ECRO TFRE 3.5E-3 ELEM LECT SUR1 TERM
    FICH K2000 'soli05.k200' TFRE 0.5E-3 POIN TOUS
               VARI DEPL VITE ECRO ECRC LECT 1 TERM
$-----------------------------------------------------------Options
OPTI PAS AUTO NOTEST STEP IO LOG 1
     FSCR
$-------------------------------------------Transient calculation
CALCUL TINI 0 TEND 7.0E-3
FIN
```

A 3D box with internal structures [18]

This example, while still relatively simple geometrically, illustrates the effectiveness of the FSA directive also in case of ***internal structures*** with ***submerged egdes***

Description:

A cubic rigid tank contains a steel shell, clamped along the bottom edge. The bottom front corner of the tank contains an ‘explosive’, simulated by a high-pressure perfect gas while the rest of the tank contains the same gas at a lower pressure. Since the material is the same, the two gases may freely intermix, therefore the interface between the two gases is treated as ALE, not as Lagrangian. Fluid-structure interaction takes place on both sides of the steel shell. An extra difficulty is represented by the presence of the various submerged structural edges, around which the fluid should be able to flow. The analysis is performed up to a final time of 5 ms.

Although the problem is three-dimensional and includes several singular points all along the submerged structural edges and at the structural junctions, the input specification is exactly the same as in the simpler 2D examples considered before. The sliding algorithm performs all calculations automatically. The boundary conditions now involve three symmetry planes normal to the three global axes, plus the usual one-line specification for the fluid-structure interaction nodes. The run for this case took 65 s of CPU on an HP 9000 720 workstation (1994).

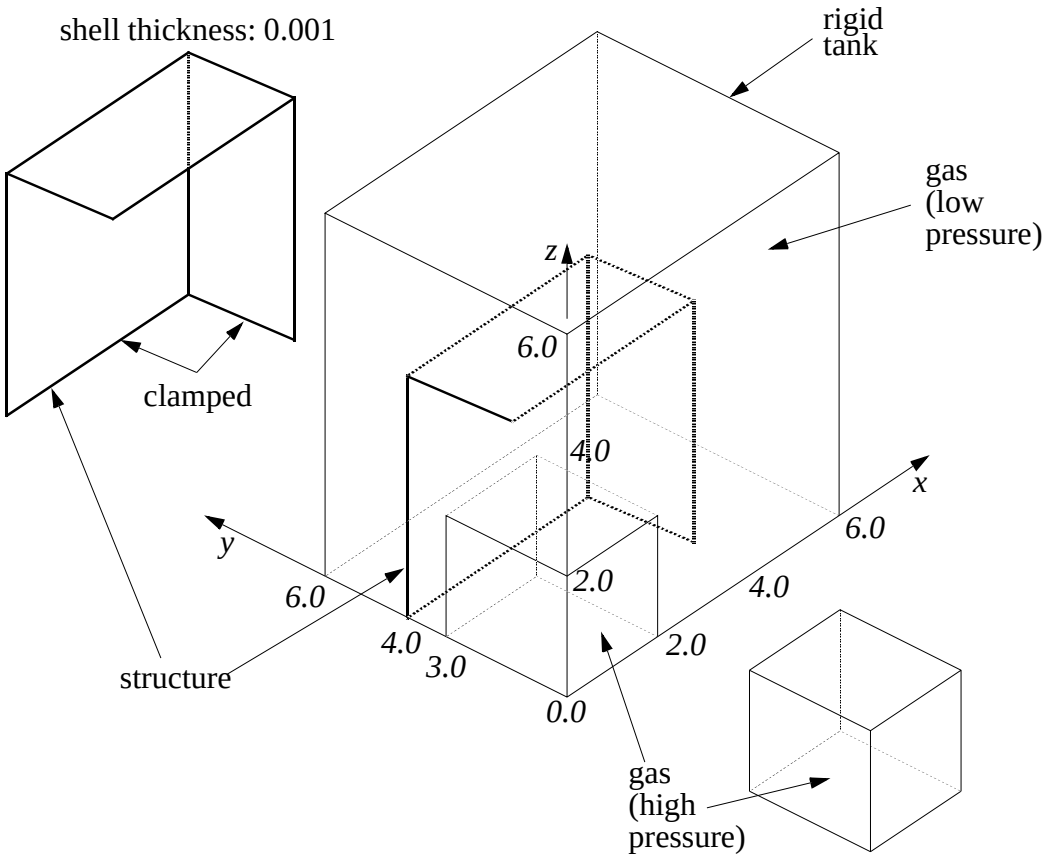
shell thickness: 0.001
rigid
tank
gas
(low
pressure)
z
6.0
4.0
clamped
x
y
6.0
4.0
2.0
6.0
4.0
3.0
2.0
0.0
structure
gas
(high
pressure)

Solution (velocities)

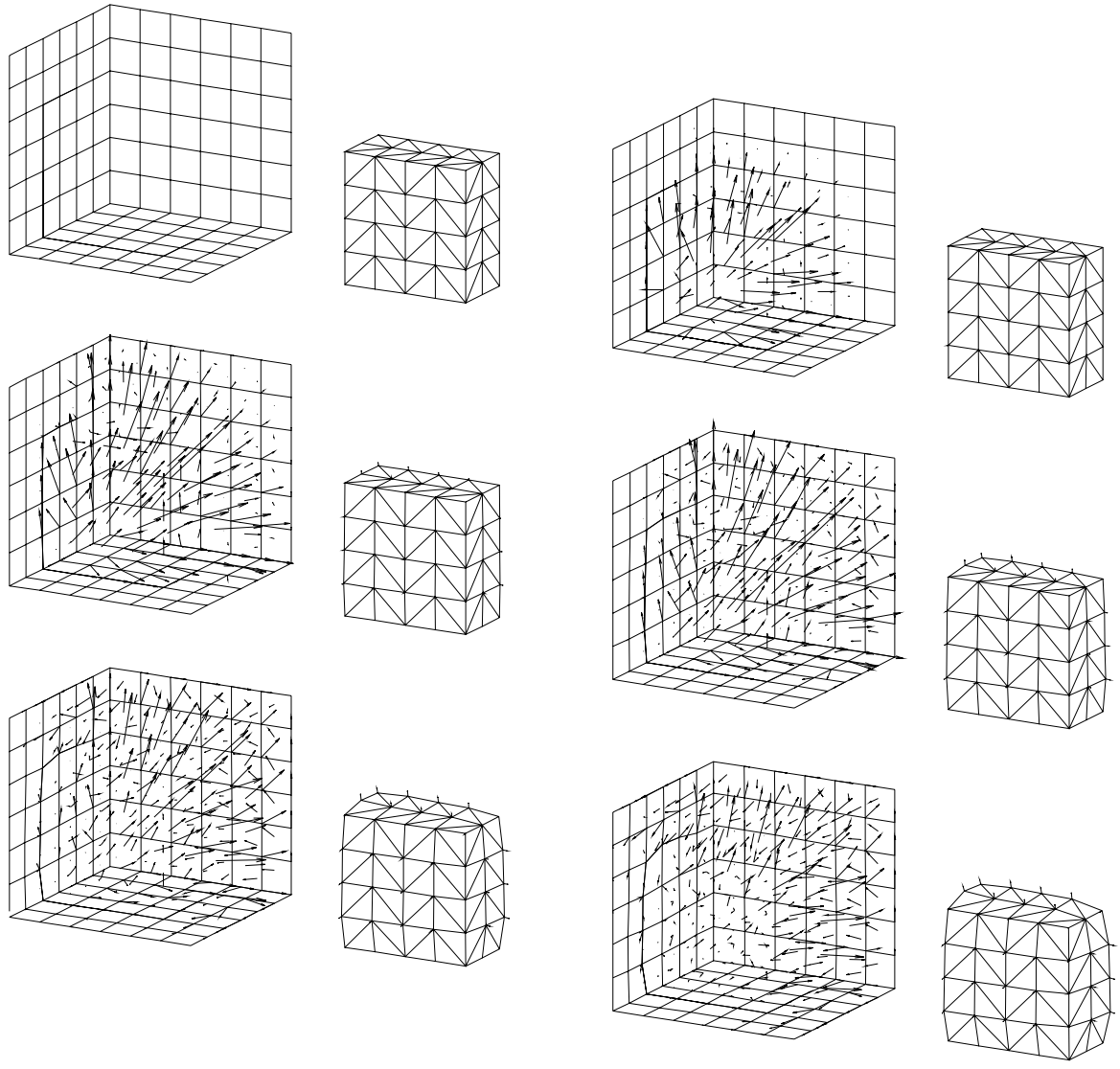

JOINT RESEARCH CENTRE

European Commission
Institute for the Protection and Security of the Citizen
European Laboratory for Structural Assessment

Solution (pressures)

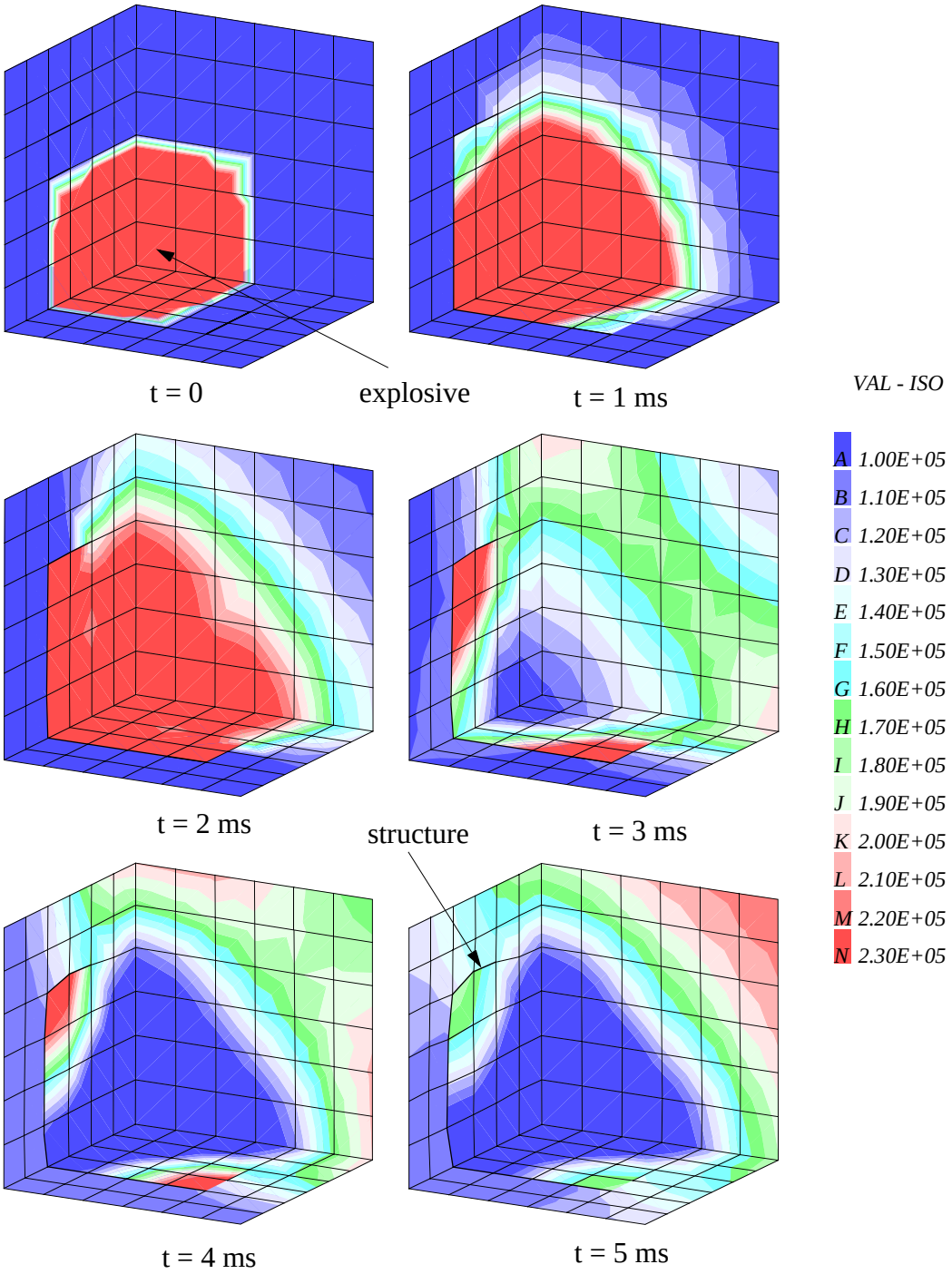

Input data for the 3D box

```
boxt - 11
$-----------------------------------------------------Problem type
CAST UNFO 'boxt11.sauv' MESH
TRID NONL ALE
$------------------------------------------------Problem dimensions
DIME
 PT6L 43 PT3L 377 FL38 216 COQI 64 ZONE 2
 MATE 3 TABL 1 5
 NALE 24 NBLE 369 BLOQ 359 FSA 77 IFSA 528 SYME 3
 LIAI 1655 35536 ECRO 12504 DMAT 55 MTPO 1 MTEL 216
TERM
$-------------------------------------------------------------Geometry
GEOM
  FL38 FLUI COQI STRU TERM
$-----------------------------------------Geometric complements
EPAI 0.001 LECT STRU TERM
$-----------------------------------------------------------Grid motion
GRIL LAGR LECT LAG TERM
     ALE  LECT FLUI TERM
     AUTO GAM0 0.5 AUTR
$-------------------------------------------------------------Materials
MATE
$ steel
     VM23 RO 7800. YOUNG 1.6E11 NU 0.333 ELAS 1.05E8
          TRAC 2 1.05E8 .656256E-3 1.6105E10 1.00066
          LECT STRU TERM
$ high-pressure perfect gas
     FLUT RO 1.22 EINT 3.046E6 GAMM 1.269 PB 0
          ITER 1 ALF0 1 BET0 1 KINT 0 AHGF 0 CL 0.5
          CQ 2.56 PMIN 0 NUM 1
          LECT BULL TERM
$ same gas at a lower pressure
     FLUT RO 0.1237 EINT 3.046E6 GAMM 1.269 PB 0
          ITER 1 ALF0 1 BET0 1 KINT 0 AHGF 0 CL 0.5
          CQ 2.56 PMIN 0 NUM 1
          LECT GAS TERM
$-----------------------------------------------Boundary conditions
LIAI BLOQ 123456 LECT BLOQALL TERM
     CONT SPLA NX 1 NY 0 NZ 0 LECT SYMMX TERM
     CONT SPLA NX 0 NY 1 NZ 0 LECT SYMMY TERM
     CONT SPLA NX 0 NY 0 NZ 1 LECT SYMMZ TERM
     FSA  LECT FSA TERM
$-------------------------------------------Printouts/Postprocessing
ECRI DEPL VITE CONT ECRO TFRE 5.0E-3
     ELEM LECT FLUI TERM
     FICH K2000 'boxt11.k200' TFRE 1.E-3 POIN TOUS
          VARI DEPL VITE ECRO ECRC LECT 1 TERM
$-------------------------------------------------------------------Options
OPTI PAS AUTO NOTEST STEP IO log 1
$-----------------------------------------------Transient calculation
CALCUL TINI 0 TEND 5.E-3 NMAX 1000
FIN
```

What if the structure is porous (perforated plate)?

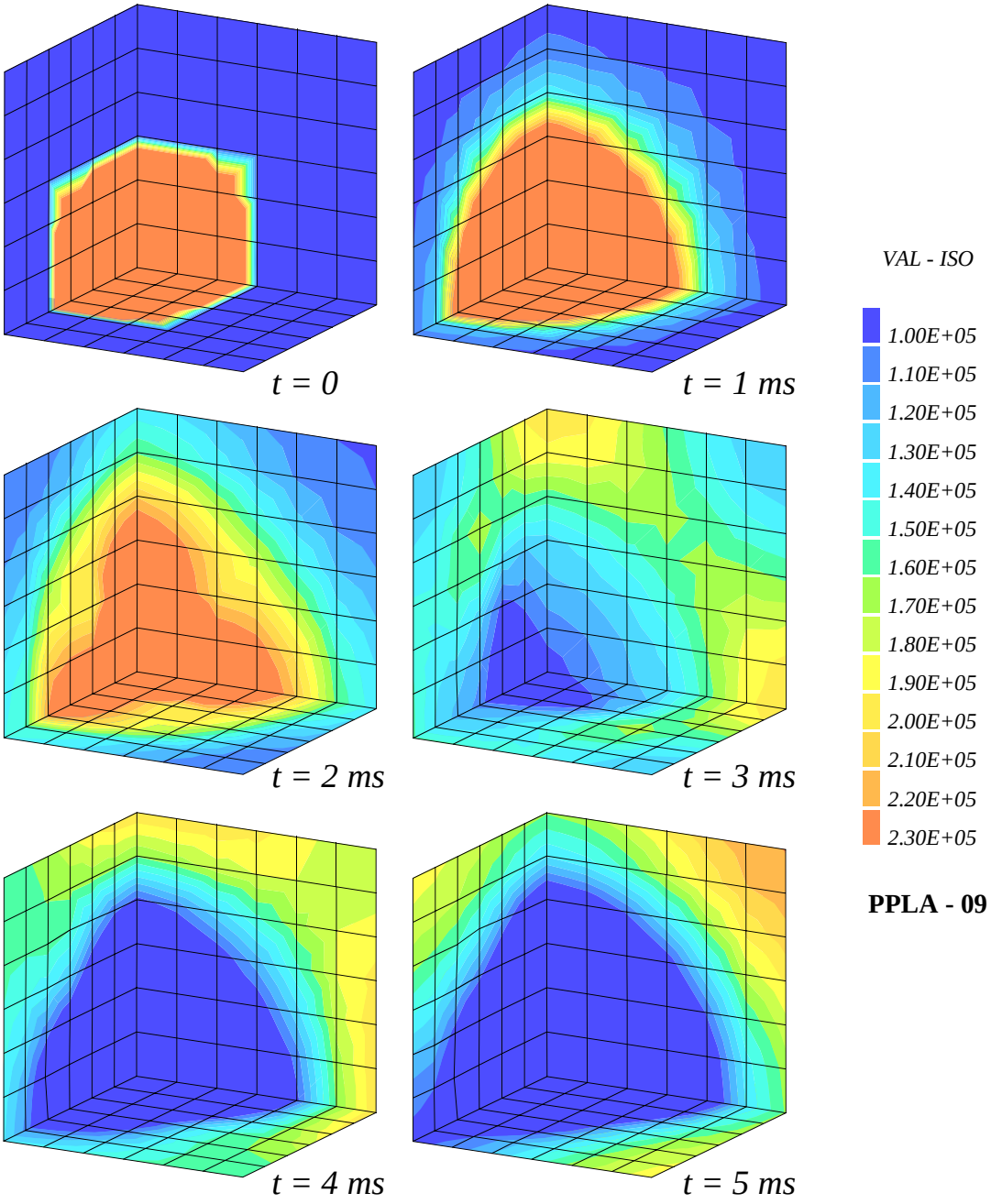

Resistance Coefficient ζ = 10

JOINT RESEARCH CENTRE
European Commission
Institute for the Protection and Security of the Citizen
European Laboratory for Structural Assessment

Input data for the perforated plate case

```
PPLA - 09
$-----------------------------------------------------Problem type
CAST 'ppla09.sauv' MESH
TRID NONL ALE
$-------------------------------------------------Problem dimensions
DIME
 PT6L 43 PT3L 377 FL38 216 COQI 64 CL3Q 32 ZONE 3
 MATE 4 TABL 1 5 NALE 24 NBLE 369 BLOQ 359 SYME 3
 LIAI 959 11223 ECRO 11168 DMAT 52
TERM
$-------------------------------------------------------------Geometry
GEOM
  FL38 FLUI COQI STRU CL3Q CLIM TERM
$-----------------------------------------Geometric complements
EPAI 0.001 LECT STRU TERM
$-----------------------------------------------------Grid motion
GRIL LAGR LECT LAG TERM
     ALE  LECT FLUI TERM
     AUTO GAM0 0.5 AUTR
$-------------------------------------------------------Materials
MATE
$ steel
     VM23 RO 7800. YOUNG 1.6E11 NU 0.333 ELAS 1.05E8
          TRAC 2 1.05E8 .656256E-3 1.6105E10 1.00066
          LECT STRU TERM
$ high-pressure perfect gas
     FLUT RO 1.22 EINT 3.046E6 GAMM 1.269 PB 0
          ITER 1 ALF0 1 BET0 1 KINT 0 AHGF 0 CL 0.5
          CQ 2.56 PMIN 0 NUM 1
          LECT BULL TERM
$ same gas at a lower pressure
     FLUT RO 0.1237 EINT 3.046E6 GAMM 1.269 PB 0
          ITER 1 ALF0 1 BET0 1 KINT 0 AHGF 0 CL 0.5
          CQ 2.56 PMIN 0 NUM 1
          LECT GAS TERM
$ impedance material for the perforated plate
     IMPE PPLT ZETA 10.0
          LECT CLIM TERM
$-------------------------------------------------Boundary conditions
LIAI BLOQ 123456 LECT BLOQALL TERM
     CONT SPLA NX 1 NY 0 NZ 0 LECT SYMMX TERM
     CONT SPLA NX 0 NY 1 NZ 0 LECT SYMMY TERM
     CONT SPLA NX 0 NY 0 NZ 1 LECT SYMMZ TERM
$-----------------------------------------Printouts/Postprocessing
ECRI DEPL VITE CONT ECRO FINT FEXT ACCE TFRE 2.5E-3
     FICH K2000 'ppla09.k200' TFRE 1.E-3 POIN TOUS CHAMELEM
     FICH TPLOT 'ppla09.tplo' FREQ 1 desc 'ppla09' POIN LECT TPLN TERM
$-----------------------------------------------------------------Options
OPTI PAS AUTO NOTEST STEP IO
$-------------------------------------------Transient calculation
CALCUL TINI 0 TEND 5.E-3 NMAX 1000
FIN
```

Industrial applications

Here are some examples of typical ***industrial*** applications:

- Safety of nuclear ***power plants*** (steam explosion, secondary containment);
- Safety of conventional power plants (accidents in electric transformers);
- Simulation of accidents in ***equipment*** (inner electric arc);

Most examples are ***courtesy of ENEL-PIS*** (ENEL Research - Hydraulics and Structures, Milano).

Steam explosion in a nuclear reactor [20]

Description:

The next test problem simulates the effects of a steam explosion in a nuclear power plant. The hypothetical accident scenario is the following: a severe malfunctioning in the reactor core causes melting of the fuel which falls to the bottom of the steel vessel and perforates it due to its extremely high temperature. The hot mixture drops into a water pool contained in the reinforced concrete cavity surrounding the reactor vessel, and causes a violent steam explosion. The huge pressure pushes the water up in the air-filled cavity and into a lateral room. The steel vessel is severely deformed plastically.

The precise material properties and other physical quantities such as heat transfer mechanisms and chemical reactions are very uncertain in this problem. However, a set of parametric numerical simulations may be set up to obtain a range of possible behaviours. Scope of the test was then to show that a numerical model of this problem is easily set up, thanks to the complete automation of FSI mechanisms.

Because of the presence of very heterogeneous fluids (air, liquid water, steam-corium mixture) and the relatively complex geometry, this problem was treated by a special FE model available in the code for multi-phase, multi-component flows. This eliminates the need for Lagrangian fluid-fluid interfaces in the model and largely simplifies the treatment of FSI.

The model uses 11474 nodes, 7664 fluid hexahedra and 3072 triangular shells for the structure. The first resukts figure shows the pressures in the fluid domain at various times and the next one the approximate position of the liquid water, in red in the mass fraction contour plot. The huge steam pressures in the lower cavity zone cause large deformations at the vessel bottom in the first 8 ms. Then the liquid is pushed up into the cavity and laterally into the room. At about 15 ms it reaches the cavity top and a water-hammer effect takes place (see the high pressure in the first figure) producing large plastic deformations in the upper part of the steel vessel. This calculation took 52531 steps for 50 ms and 60 hours CPU on a Pentium 200 PC.

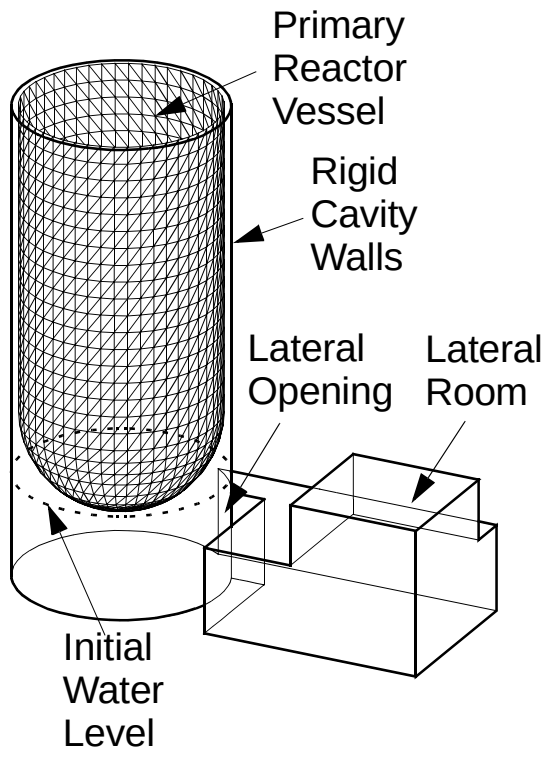

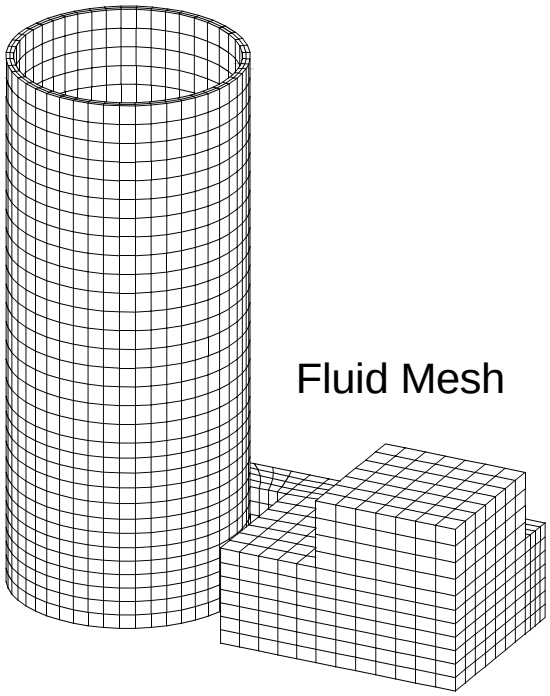

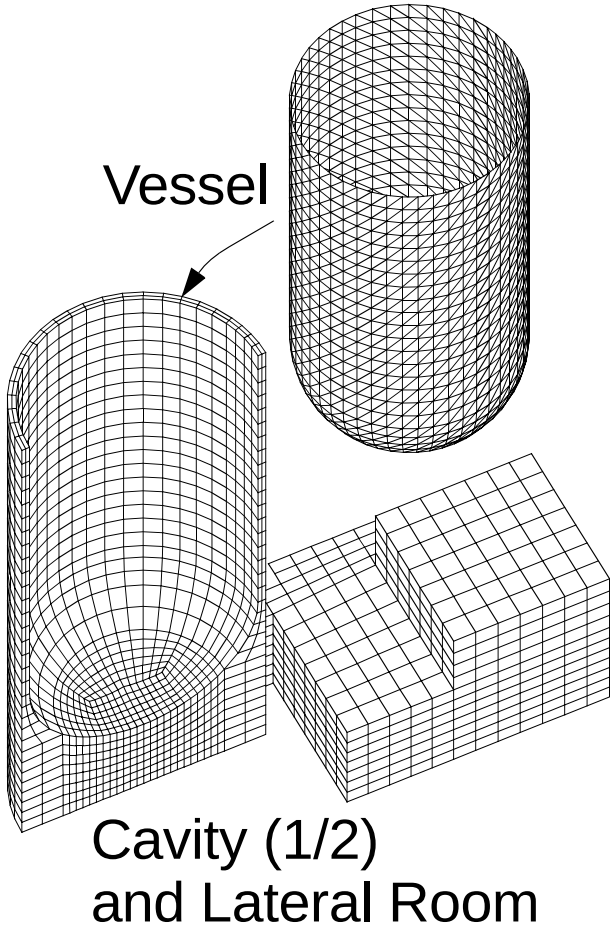

JOINT RESEARCH CENTRE

European Commission
Institute for the Protection and Security of the Citizen
European Laboratory for Structural Assessment

Solution

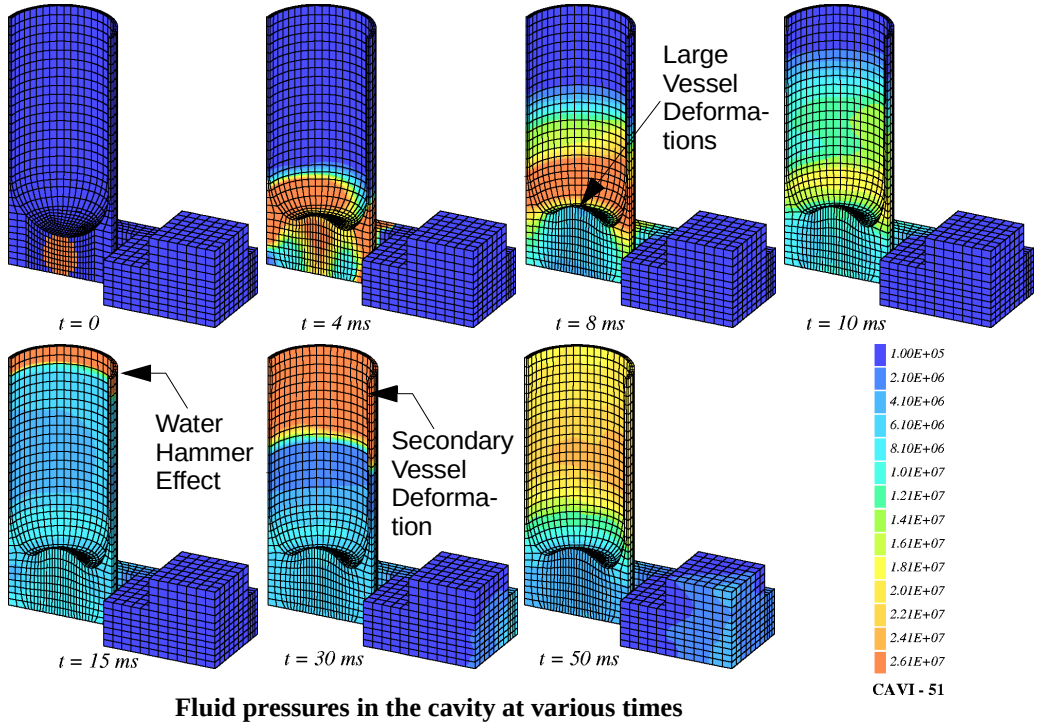

Fluid pressures in the cavity at various times

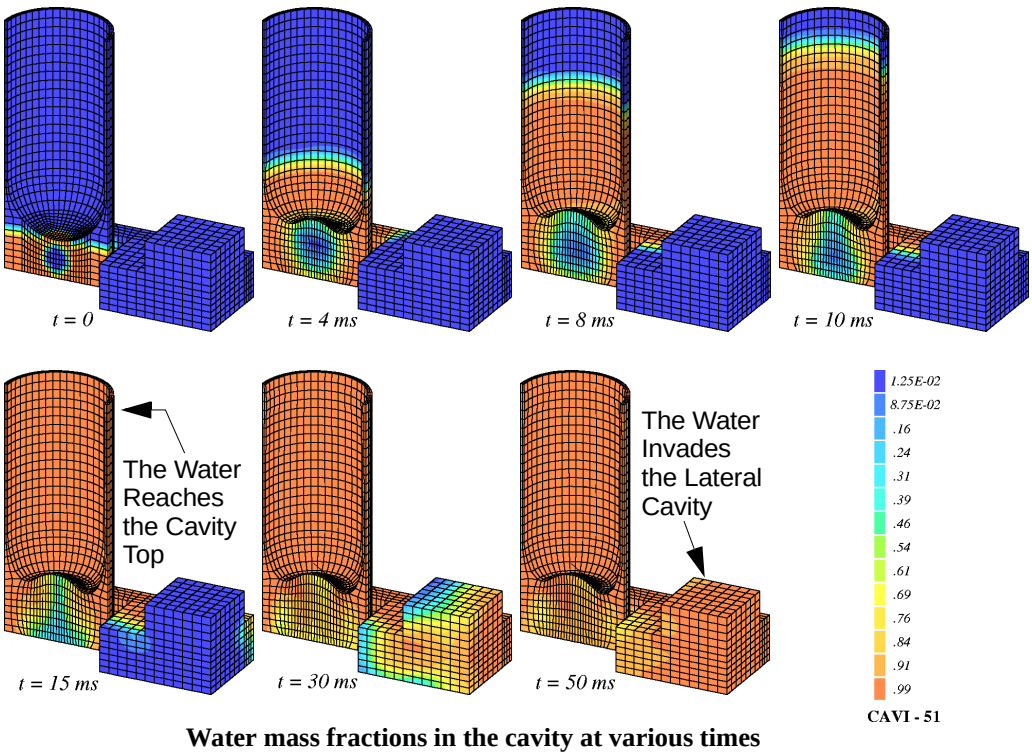

Water mass fractions in the cavity at various times

JOINT
RESEARCH
CENTRE

European Commission
Institute for the Protection and Security of the Citizen
European Laboratory for Structural Assessment

Pressure wave propagation in secondary containment [18]

Description:

A simulation of a hypothetical gas explosion in a reactor-like containment is considered. The complexity of this problem approaches that of real applications. Nevertheless, the effort for preparing a model, prescribing the sliding and other boundary conditions and performing the calculations is equivalent to those needed in the previous, academic-like examples. In particular, the actual input data file is again almost identical to those shown before, thanks to the use of mesh preprocessing. The problem geometry is assumed to be axisymmetric. The lower basement of the container is very thick, therefore it is simply modelled by a rigid boundary in the present analysis. On the other hand, the container walls are relatively thin and can be conveniently represented by shell elements without a topological thickness. This facilitates the treatment of structural branchings and of fluid-structure interactions.

The container is supposed to be initially filled up with air (represented by a perfect gas) at room temperature and atmospheric pressure. An explosion is assumed to take place in the lower part of the container at the initial time of the studied transient (t = 0). The explosion time is supposed to be very short compared with the time interval of interest—since what matters in the present analysis is the mechanical loading of the tank structures, not the explosion itself—therefore the explosive is represented by a perfect gas at high pressure, initially occupying the lower part of the tank. The nature of this perfect gas is assumed to be the same as that of the bulk air in the container, so that the two fluids may freely intermix. As a consequence, the interactions between fluids and structures in the present model are of the permanent type, because the whole container is filled up with fluid, and there is just one type of fluid, i.e. no Lagrangian interfaces are present in the model. Therefore, an interaction model of the ALE type may be used in the simulation.

The tank walls are made of prestressed reinforced concrete. For the scope of the present analysis, they may be supposed to remain in the elastic regime along the whole transient. Therefore, they are simply modelled by an homogeneous, isotropic, linear elastic material. For the finite element mesh, a relatively fine discretization is chosen, using 981 fluid elements and 88 shell elements. The transient response of the model was computed until a final time of 250 ms. The run took about 14000 time steps and used 1.5 hours of CPU on an HP 9000 715 personal workstation (1994).

Examples of the computed results are shown in the figures. In particular, the first results figure shows the structural deformations (displacements are magnified), the next one the structural velocities, ant the final one the fluid pressures.

Problem definition

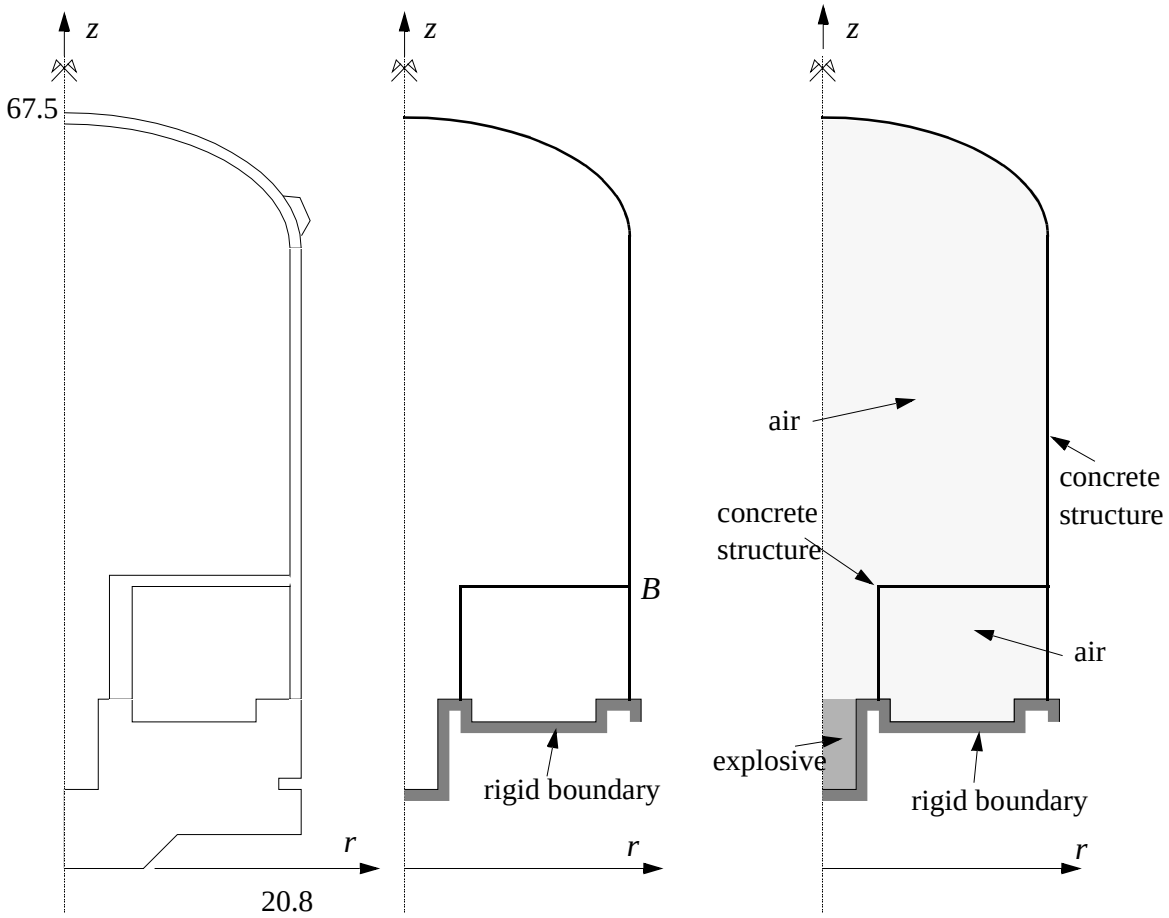

a) geometry b) geometrical model c) material distribution at t = 0

Solution (deformations, velocities)

Structural deformations (x 300)

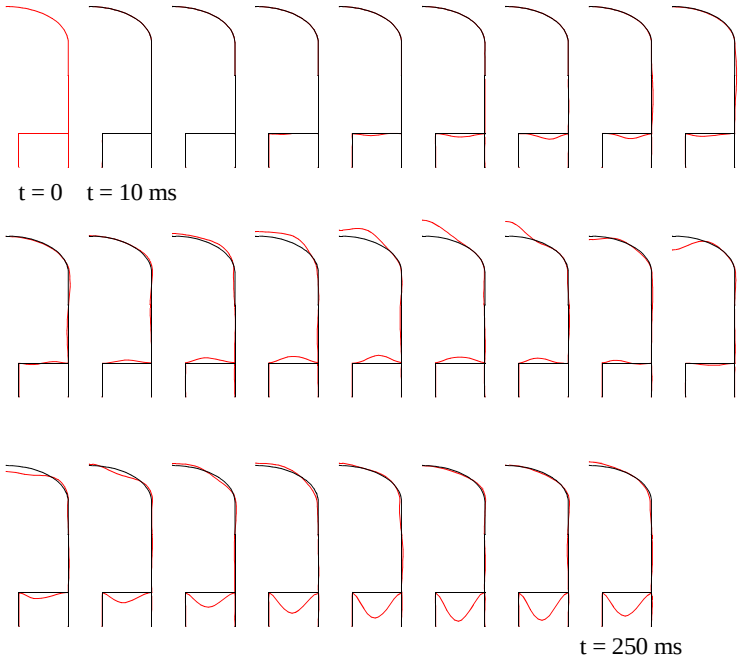

Structural velocities

JOINT RESEARCH CENTRE

European Commission
Institute for the Protection and Security of the Citizen
European Laboratory for Structural Assessment

Solution (pressures)

Pressure distributions during the transient

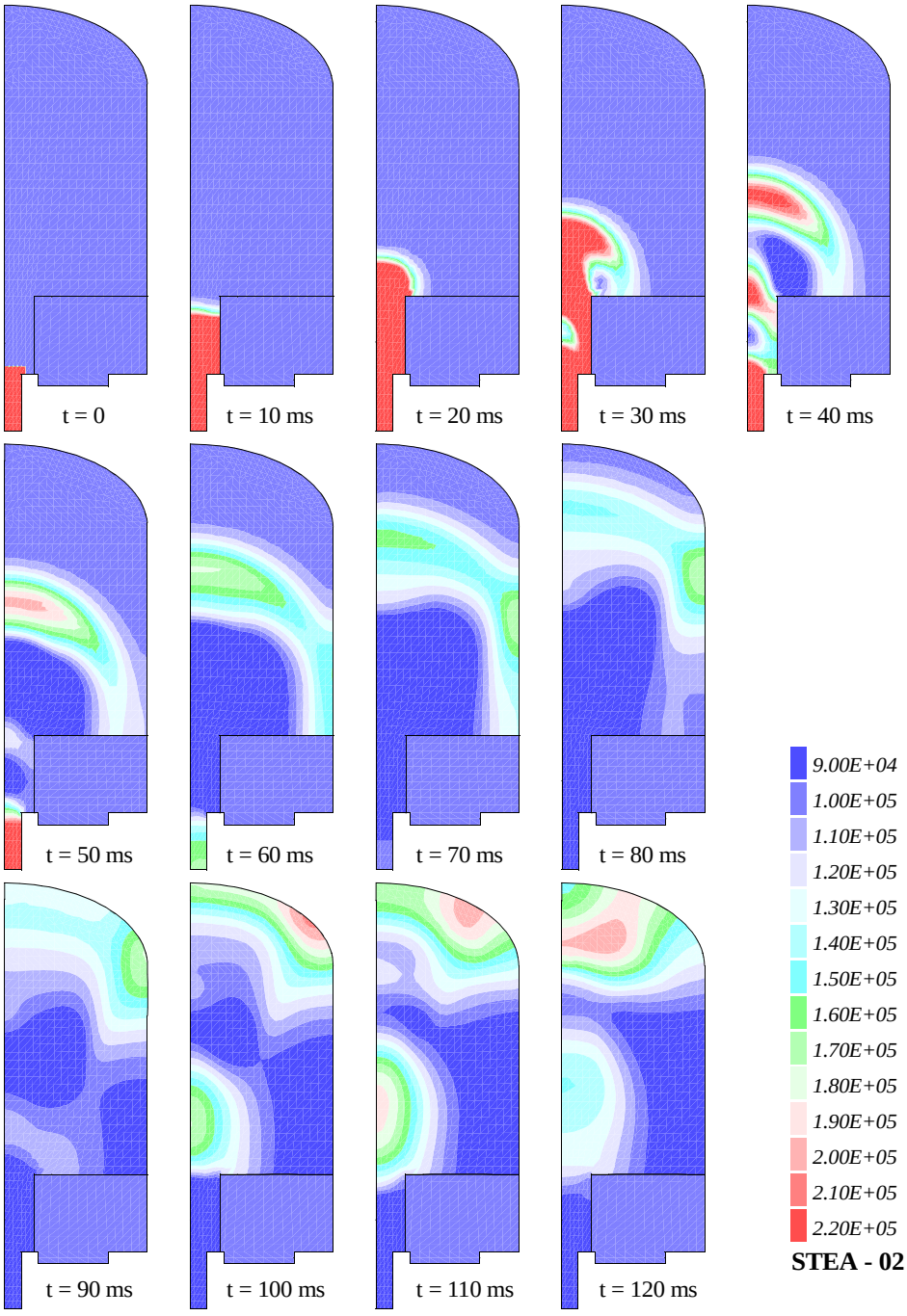

Explosion in an underground power plant [18]

Description:

We consider the simulation of an explosion in an underground cell. The problem is defined in the first figure. An underground cell of hexahedral shape is supposed to contain air at atmospheric pressure. Under hypothetical abnormal conditions, an explosion could take place in the center of the cell and an overpressure wave could be transmitted to the outside world through a triangle-shaped opening in the cell roof. The cell walls, including the closed part of the roof, are supposed to be very stiff and modelled by rigid boundaries in the present analysis. A cylindrical protection wall surrounds the cell top opening, but in an eccentric position with respect to the cell itself. For the sake of the present work, the wall is assumed to be made of an elastoplastic ductile material of very small thickness (0.001 units) so as to undergo significant deformations, in order to test the fluid-structure interaction algorithm. A domain of 80 x 80 x 40 units of the atmosphere surrounding the cell is modelled in the simulation. This allows to almost avoid pressure wave reflections along the external boundaries during the transient of interest (50 ms). An alternative approach would be discretizing a smaller domain and using absorbing boundary elements to mitigate wave reflections, as shown in other examples. The main goal of the calculation was to predict the maximum overpressures at the ground level in the region outside the wall during the transient, in order to estimate possible damage to the public.

The finite element mesh assumed in the model is shown in the figure. It uses 2048 fluid elements (mainly hexahedra) and 120 shell elements for the cylindrical wall. The run up to 50 ms simulated time took 300 time steps and used 0.5 hours of CPU on an HP 9000 715 personal workstation (1994). The input file for this case is completely analogous to the previous ones, showing the simplicity of the proposed method as far as the preparation of input data is concerned.

As an example of computed output results, the next figure shows fluid pressure distributions in the cell and inside the wall during the transient.

Problem definition

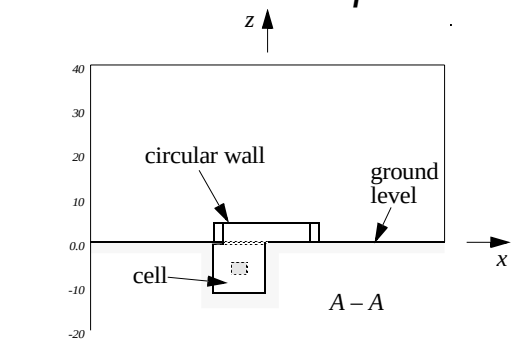

lateral view (general)

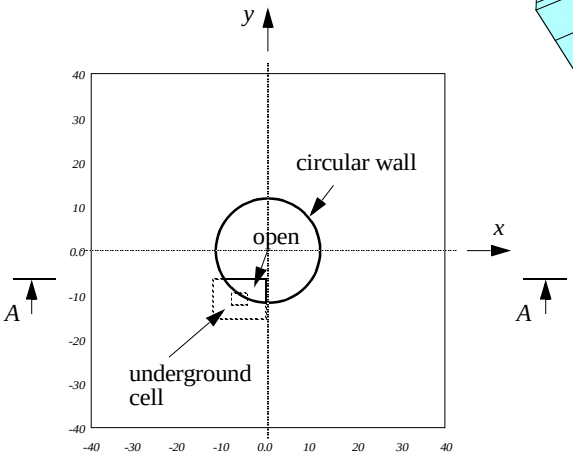

top view (general)

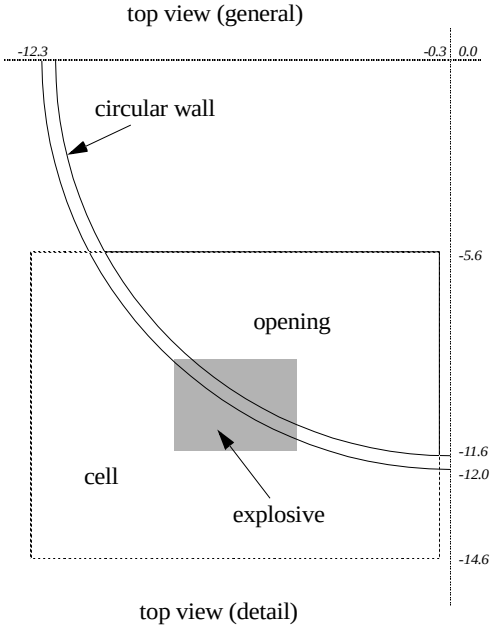

top view (detail)

Finite Element Model (seen from below)

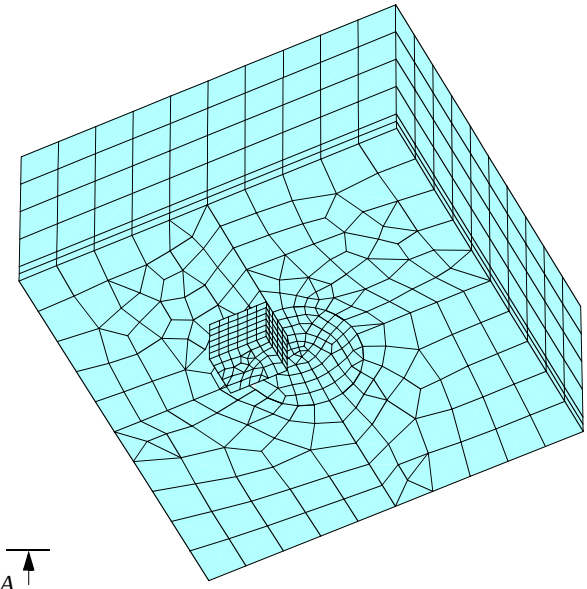

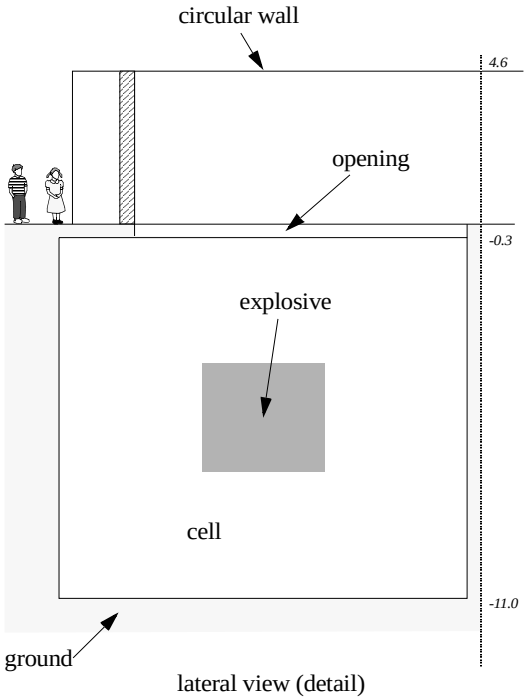

lateral view (detail)

JOINT RESEARCH CENTRE

European Commission
Institute for the Protection and Security of the Citizen
European Laboratory for Structural Assessment

Solution

Pressure distributions during the transient inside the cell and the wall

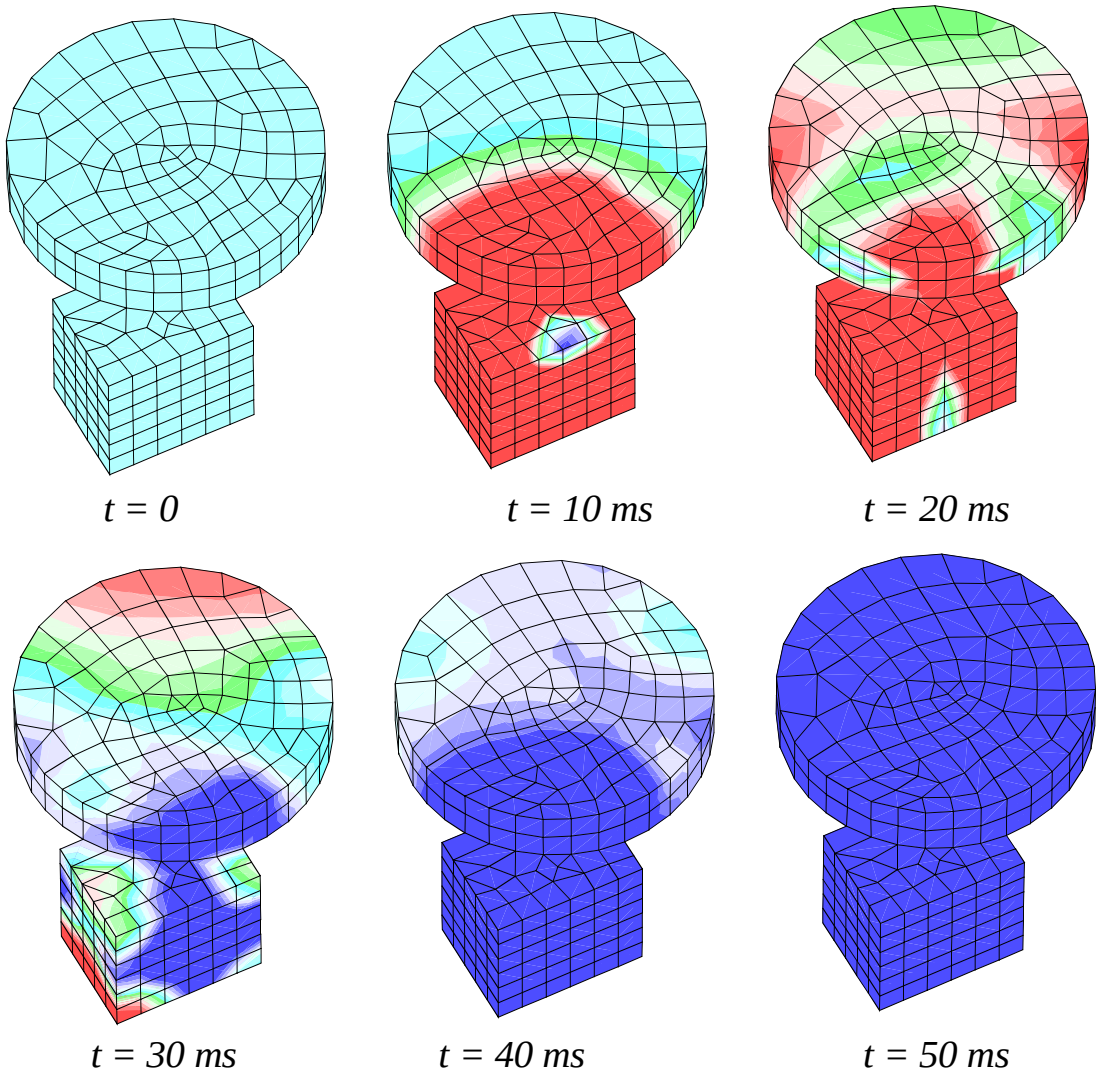

Accident due to electric arc in a transformer [15]

Description:

We consider a power transformer cell as part of an underground power plant. A full confinement (rigid walls) is assumed for the air surrounding the transformer. If an electrical fault occurs inside the oil-insulated equipment, an arc is likely to happen causing the pyrolisis of the mineral oil and the production of a huge quantity of gaseous hydrocarbons (over 70% hydrogen) which may ultimately break the transformer tank and propagate inside the cell.

Under critical circumstances, the air-hydrocarbons mixture may ignite giving rise to a strong blast. Aim of the case study is to assess the structural response, in case of explosion, of the aluminium tubes (1 m diameter) that contain and insulate, by means of SF6 gas, the high voltage bars outgoing from the power transformer. As the implemented model does not take into account gas diffusion and reactive flows, the following assumptions have to be made:

- the whole hydrocarbon mixture, that will be referred to as gas #1, is supposed to be initially located at the transformer top;
- the density of gas #1 is supposed to be the same as the one of the surrounding air, gas # 2;
- its combustion energy is stored inside the same zone and is instantaneously released at the start of the calculation.

These assumptions allow to determine the initial conditions of the high-pressure and temperature bubble, that initially contains the whole energy associated with the explosion. The procedure followed is detailed by Chillé et al. [15]. The explosive bubble is surrounded by air at normal conditions. Thanks to symmetry, just one half of the fluid domain is discretized by means of 63282 tetrahedra, and 686 prisms, while 3672 triangular shell elements are used to represent the structural part, i.e the aluminium tubes, to which an elastoplastic material is assigned. A second-order calculation was run up to 50 ms, requiring about 75350 CPU seconds and 7201 time steps on a Pentium 266 Mhz machine.

The central part of the figure shows the structural portion of the computational domain, composed of the aluminium tubes, which are treated as deformable and discretized by suitable shell elements, and the transformer and cell walls, which are treated as rigid and not discretized at all (the 'elements' appearing in the figure are just the surfaces of the fluid domain). The red spot marks the initially pressurised zone along the symmetry plane of the model. The upper right part of the figure shows a portion of the discretized fluid domain (continuum tetrahedral elements) and the embedded shell structural elements for the tubes.

The first results figure shows the computed mass fractions of air and hydrogen, respectively, at half-time and at the end of the transient. Color scales are so chosen that dark blue corresponds to 0.0 fraction and vivid red to 1.0 fraction of the concerned component. In this figure the bulk fluid has been removed and only the structural and rigid walls are represented.

The last results figure addresses the main purpose of the calculation, which was the prediction of blast pressure distributions and their effects on the deformable structures. A typical pressure contour plot is shown in the upper plot, at half-time of the transient, while the bottom plot represents the deformed shape of the tubes at 50 ms. Deformation is amplified 10 times and the colors correspond to the magnitude of displacement

Problem Definition

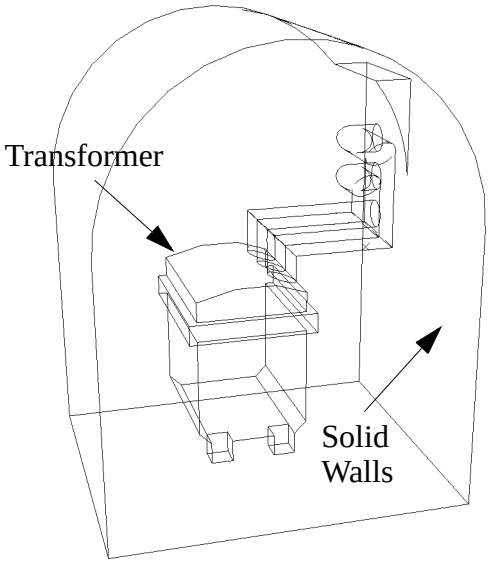

Fluid-Structure Mesh

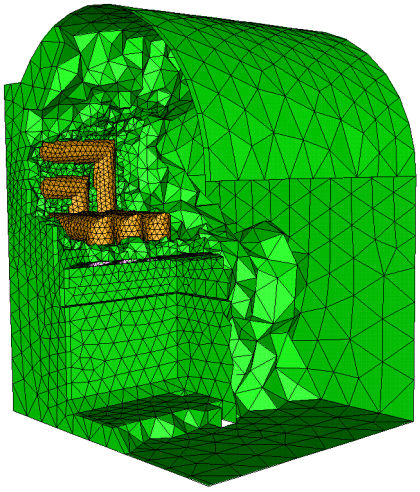

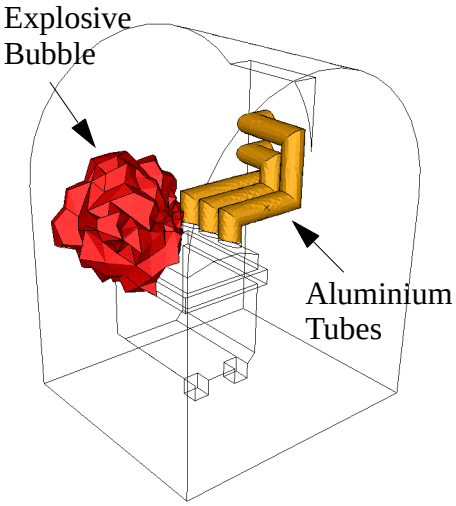

Initial Pressure

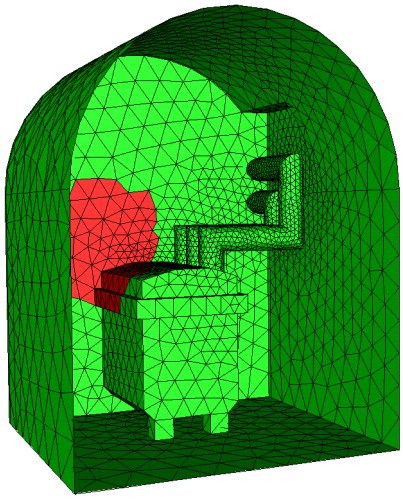

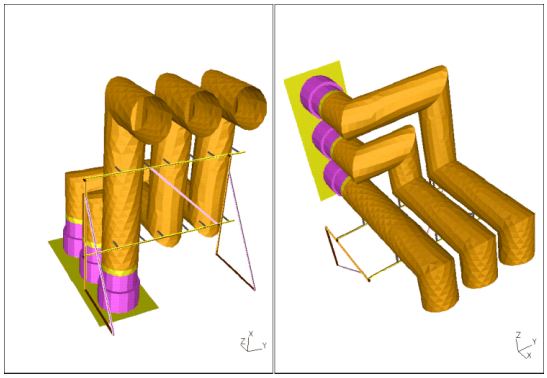

Initial tubes configu-ration

JOINT RESEARCH CENTRE

European Commission
Institute for the Protection and Security of the Citizen
European Laboratory for Structural Assessment

Solution (mass fractions)

Air Mass Fractions at 25 and 50 ms

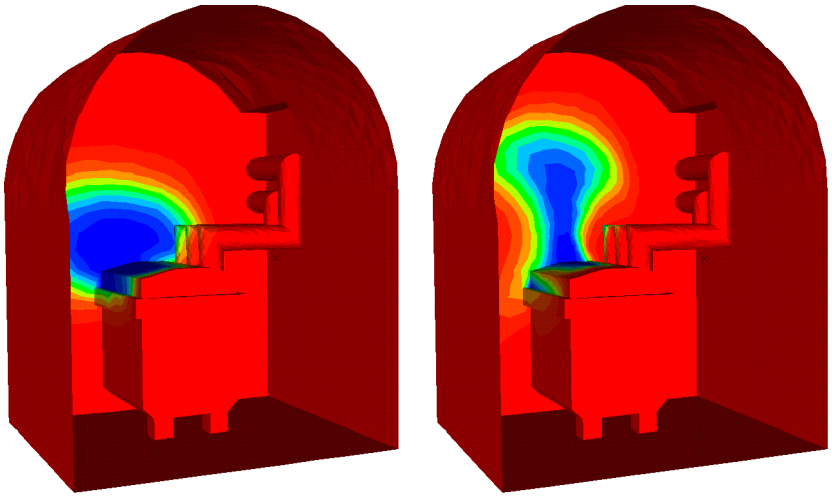

Hydrogen Mass Fractions at 25 and 50 ms

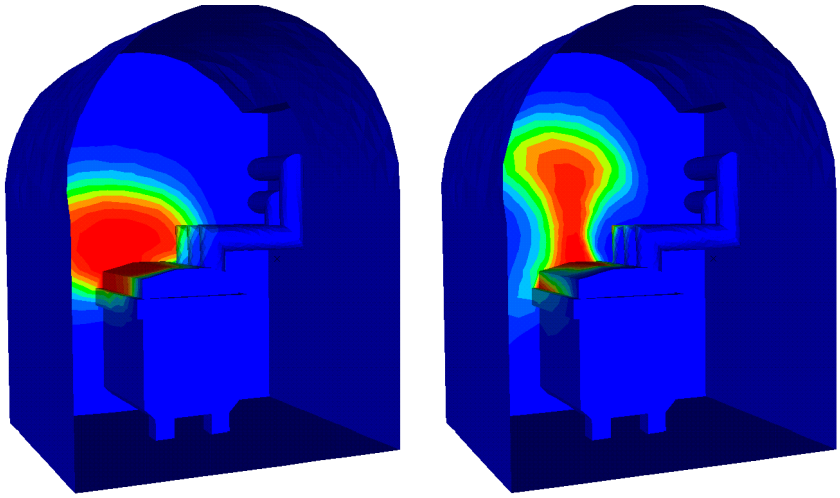

Solution (pressures, tube deformations)

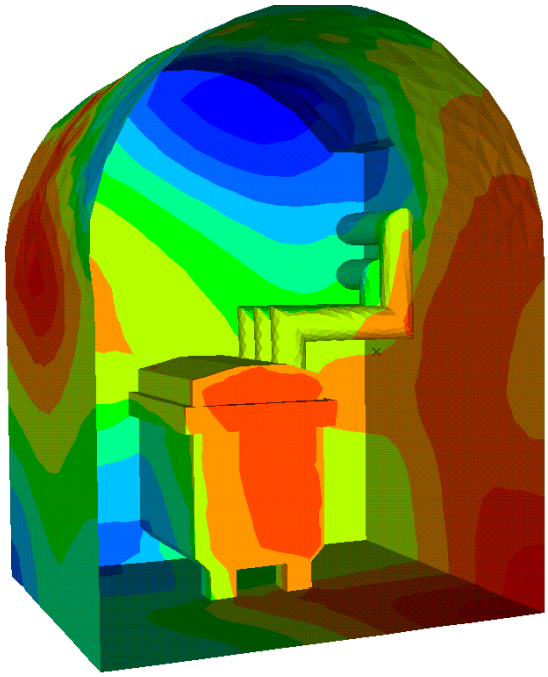

Resulting Fluid Pressures

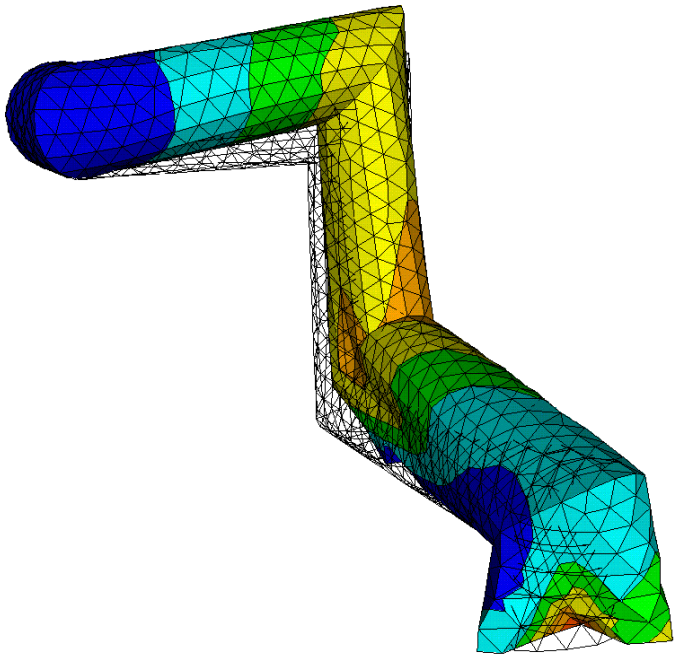

Structure Deformations (x 10)

Inner arc in electric equipment [20]

Description:

In the next and final test problem, an electric current transformer (CT) is considered. In this kind of device, the primary winding (a crossing rod) and the secondary one (wounded on a toroidal magnetic core) are located at the top of a tall structure (~1.5 m high), within a metallic cap. The toroidal magnetic core is supported by an iron tube bolted to a rigid base and coaxial with the external cylindrical ceramic structure. The base contains a large circular hole closed by a pressure relief device (rupture disk). The CT is filled with a dielectric gas and is connected to an external tank in correspondence of the aforementioned hole.

It has to be noted that the iron tube presents several bores at the bottom and at mid-height in order to allow gas flow towards the pressure relief device. In case of an accidental internal arc the gas pressure rapidly rises inside the transformer and, depending on arc current intensity and duration, it can bend the iron tube and open the relief device with subsequent ejection of gas towards the tank.

With purely demonstrative purposes, four Fluid-Structure calculations were performed by using an energy injection model for the electric arc and a rupture disk model to simulate the sudden gas discharge to the tank. The first run was carried out with the FV solver and the second one with the FE solver. Both runs used the calculation mesh shown in the lower part of the figure, consisting of 7676 fluid tethraedra and 3598 prisms for a total of 4990 nodes in the fluid domain, and of 1120 shell triangles for a total of 634 nodes in the structural domain. The containing structure was modelled as rigid, whilst the toroidal core and the metallic tube were considered as deformable elastoplastic bodies. Arc sparking was simulated by energy injection in a zone near the toroidal core (in red in the figure) for a total amount of 75 kJ released in 0.25 ms. Thanks to problem symmetry, just one half of the domain was discretized.

The results figure shows the pressures in the fluid domain at various times in the first run. After arc sparking initiation, the inner part of the iron tube is invaded by the pressure wave propagating through the bores. At about 3 ms, the rupture disk fails and pressure starts to rise also in the elbow connecting the CT with the tank. Towards the end of the transient, the metallic core moves towards the head as the inner tube bends.

Problem Definition

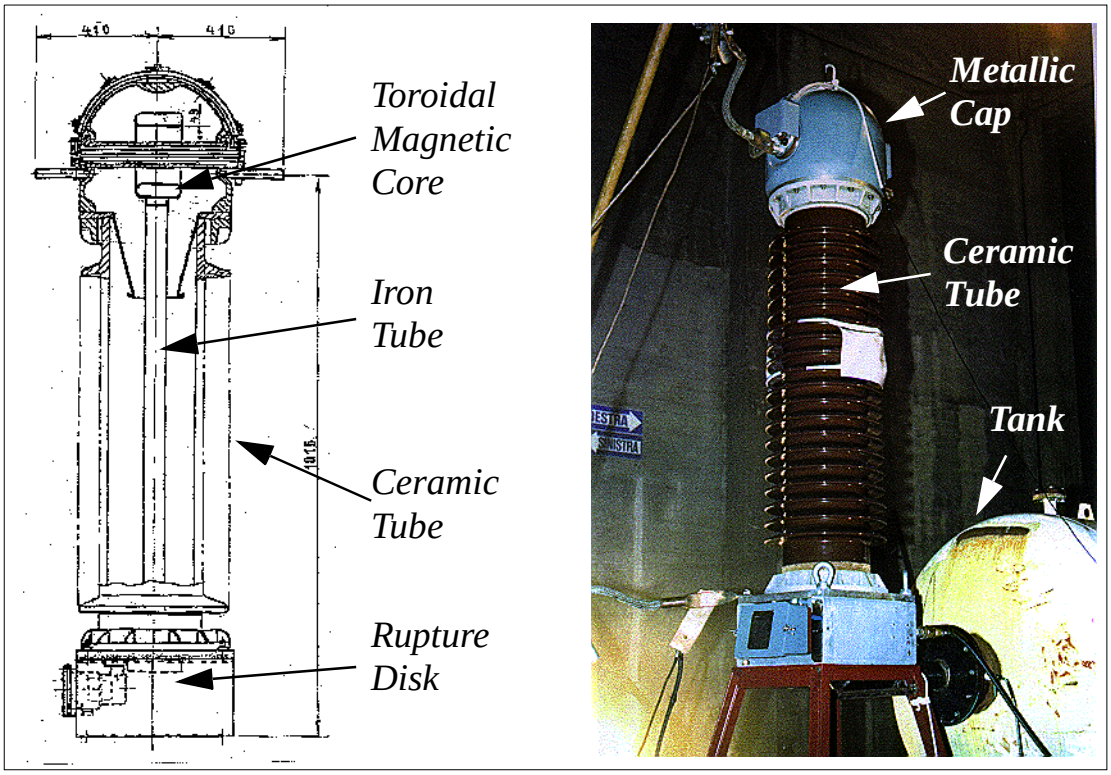

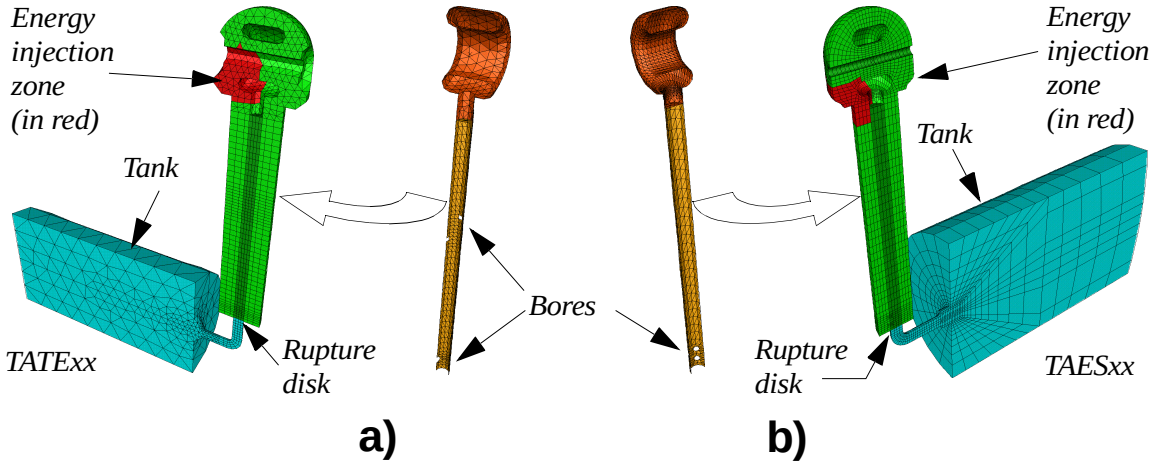

Calculation meshes for the CT: tetrahedra/prisms (a) and hexahedra (b)

JOINT RESEARCH CENTRE

European Commission
Institute for the Protection and Security of the Citizen
European Laboratory for Structural Assessment

Solution

a)

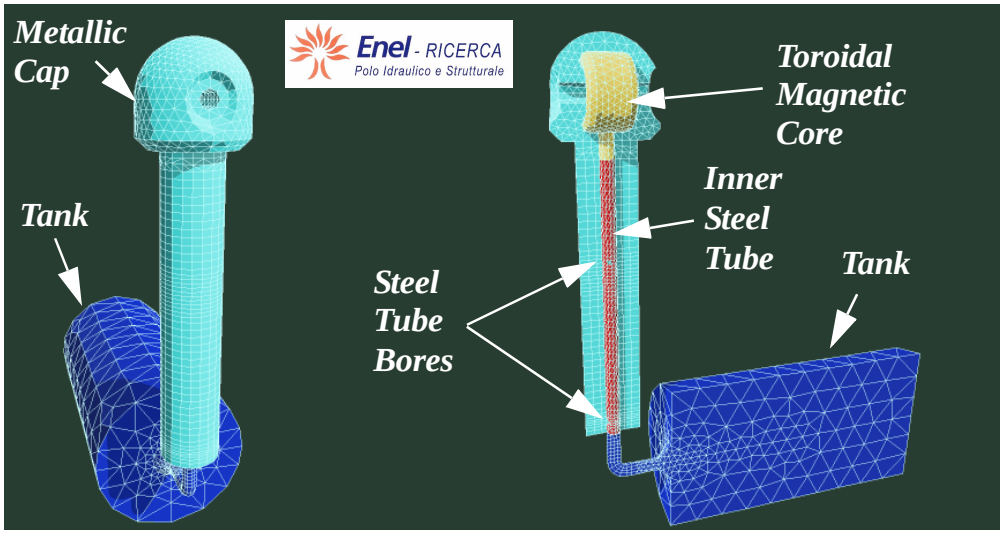

b)

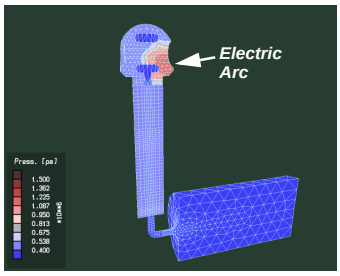

Arc Initiation (by Energy Injection)

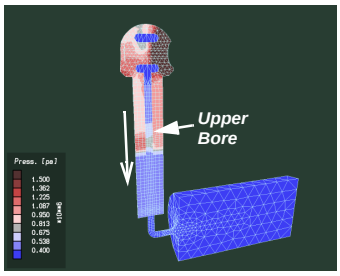

Gas Flows into Inner Tube through the Upper Bore

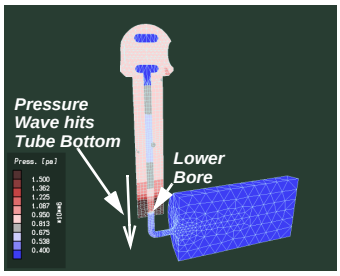

Gas Flows into Inner Tube also through the Lower Bore

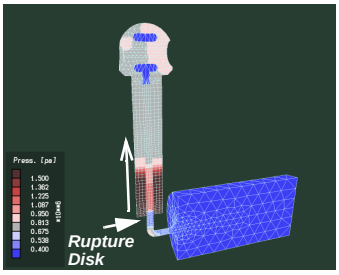

Rupture Disk at Inner Tube Breaks

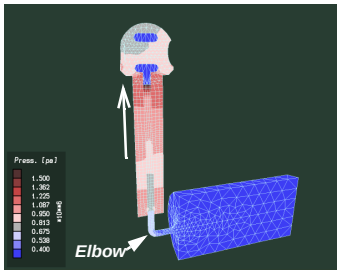

Gas Flows into the Tank through the Elbow

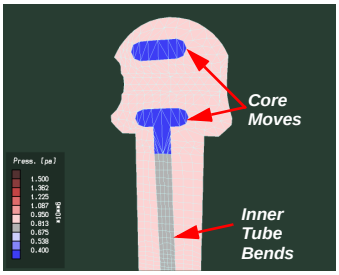

Inner Tube bends and Magnetic Core Moves Towards the Metallic Cap

a) Numerical model; b) Fluid pressures in the CT at various times, with FV tetrahedra/prisms

Other application areas

Some other possible application areas of fast transient dynamic analysis are presented, such as:

- ***Off-shore*** structures;
- Dynamic ***metal forming*** and technological processes;
- Simulation of ***earthquakes*** and wave propagation effects;
- etc. etc.

Attack on a submerged pipeline [18]

Description:

The present test case gives an example (now in full 3D) of fluid-structure interaction involving 'infinite' (non-reflecting) boundaries for the fluid and a completely submerged structure. The problem is defined in the first figure. The 3D nature of the problem is mainly caused by the fact that the explosive charge only extends for a length of 2.0 units along the z direction. The final time is assumed to be 45 ms because the explosive bubble becomes so large and distorted after this time that the calculation with a Lagrangian fluid-fluid interface would become impossible.

Thanks to symmetries (note that in the 3D model the plane z = 0 is also a symmetry plane, in addition to y = 0), only 1/8 of the domain shown in the first figure needs to be actually modelled by finite elements, provided suitable boundary conditions are specified. Also in this case use is made of boundary condition elements (now with 4 nodes) and absorbing material in order to avoid wave reflections at the fluid boundaries.

The initial finite element mesh is shown in the lower part of the figure. A series of CL3D-type elements (4-noded quadrilaterals) with absorbing material are placed along the absorbing boundary. The interface between the explosive and the liquid is Lagrangian, because the two materials should not intermix. The computation took 435 time steps and used 450 CPU seconds on an HP 9000 720 workstation (1993).

The results of this calculation are shown in the following figure. The deformed meshes at various times are represented in the upper part. Note that the external fluid boundary moves because it is declared Lagrangian. This allows to track its position in time. At the same time, the presence of absorbing elements along the boundary mitigates the pressure wave reflections thus approximating the behaviour of the real problem.

The fluid material velocities are shown in the lower part. The upper figure also shows the fluid pressure distributions at the same times. It appears from this figure that the wave reflections at the fluid boundaries are effectively mitigated by the presence of the absorbing elements.

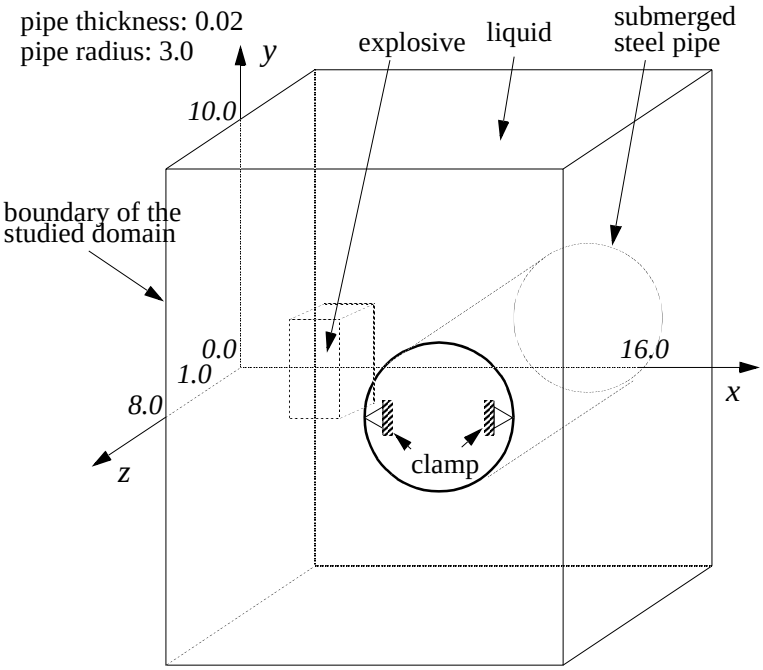

Problem definition

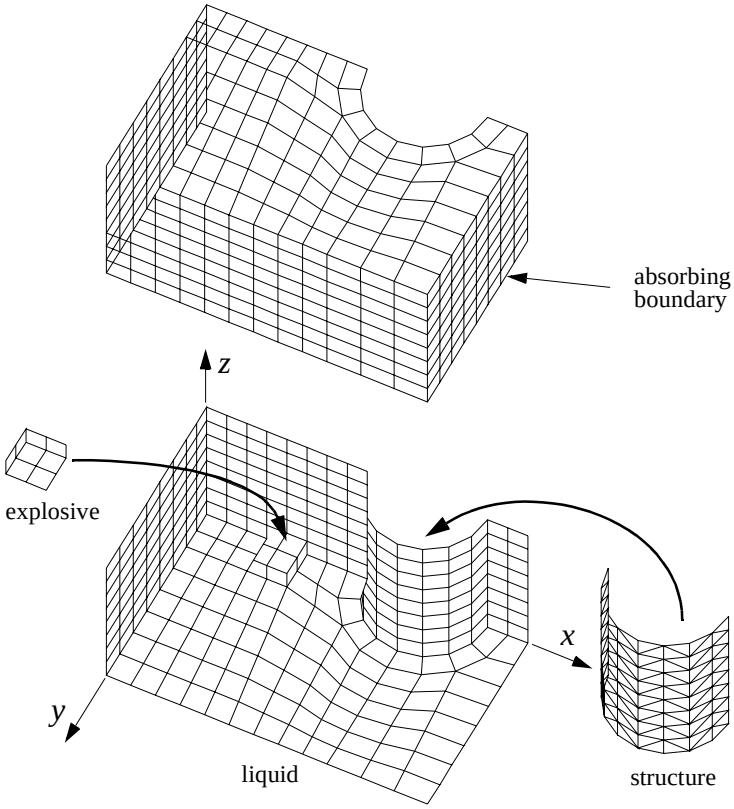

Finite Element Model (seen from below)

Results

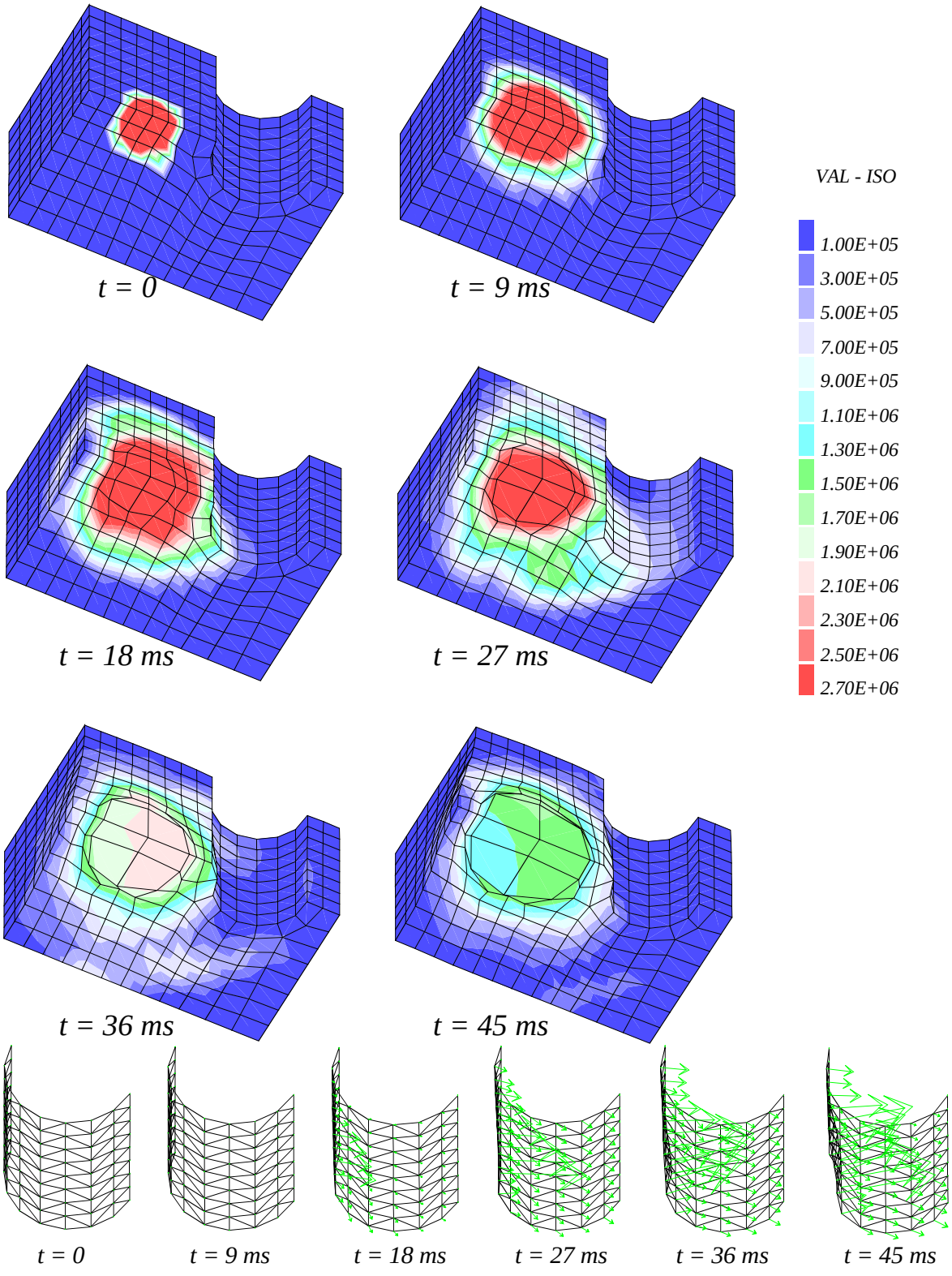

JOINT RESEARCH CENTRE
European Commission
Institute for the Protection and Security of the Citizen
European Laboratory for Structural Assessment

High-speed metal forming: punching

Description:

To illustrate the applicability of the ALE description in solids to real engineering or technological problems, an example of metal forming is presented. A similar case was solved by Ponthot (1988), but in a static analysis. The problem is the coining process, whereby a metallic slab or disk is deeply deformed by a punch. Two slightly different configurations were considered. In the first one (symmetric coining) two punches were used and a plane strain analysis was performed. In the second one (unsymmetric coining) only one punch was modelled, and an axisymmetric analysis was performed. The material was the same in both cases: an elasto-plastic material with E = 200 GPa, Poisson's ratio 0.3, yield stress 250 MPa, density 8930 Kg/m^3 and plastic modulus 1 GPa. Isotropic hardening was assumed. While the die (in the unsymmetric example) was considered rigid and without friction, all displacements of the material points in contact with the punches were inhibited along the horizontal direction (thus simulating complete adherence to the rigid tool) and a linear law in time was imposed along the vertical direction. The analyses were performed up to 60 % of reduction of the original piece height. The velocity of the punches was imposed and kept constant in time. All cases were modelled using 2 x 2 Gauss integration linear elements and the Lax-Wendroff algorithm. A schematic statement of the problems is presented in the first figure.

Note that the rigid-punch (frictionless) boundary conditions are rather difficult to implement in a Lagrangian case. Moreover, different meshes would be needed, depending on the height reduction required, because every reduction induces different deformations and, consequently, different element distortions. Finally, a Lagrangian description would require an ad-hoc mesh, particularly refined under the edge of the tool, where most of the deformation occurs.

The first figure shows the evolution of the yield stress (related to the equivalent plastic strain) during the deformation process for a punching velocity of 60 m/s. For the unsymmetric case, two different solutions were obtained, one using a rather coarse mesh (10 x 4 elements), the other with a finer mesh (20 x 8 elements). As appears from these figures, the ALE formulation allows to maintain element regularity and an accurate description of the boundary motion. The evolutions of the plastic areas are always leaded by the right corner of the tool. Note, however, that as expected a plastic band is clearly detected between the previously mentioned corner and the center of the specimen. This effect is more evident in the symmetric problem.

To compare the influence of the dynamic effects, different punch velocities were studied, in the range 0.15 to 300 m/s. The next figure shows the comparison between the final deformed shapes. Note that the differences in the solutions depend only on dynamic inertial effects. No

strain-rate dependency was introduced in the material description. In real cases, however, the variation of material properties with the rate of deformation is likely to play an important role in the overall behaviour of the forming process.

The influence of the dynamic effects is negligible for punching velocities under 3 m/s; but, as expected, the “fast” velocity cases induce a larger “back extrusion” while the quasi-static simulations allow a larger amount of material to flow outward. The external free surface shape is clearly dependent on the dynamic effects. Note that shear bands are present in every case; however, the faster the punching velocity, the larger is the plasticized area due to the inertia effects.

Although solutions can be obtained even at very slow punching velocities, they become very CPU-expensive. On the contrary, solutions at higher velocities are extremely cheap, thanks to the explicit time integration procedure adopted. Since deformation velocities in real technological processes often lie in the range where pronounced dynamic effects are foreseen, the method proposed here is expected to be competitive for the numerical simulation of this class of problems.

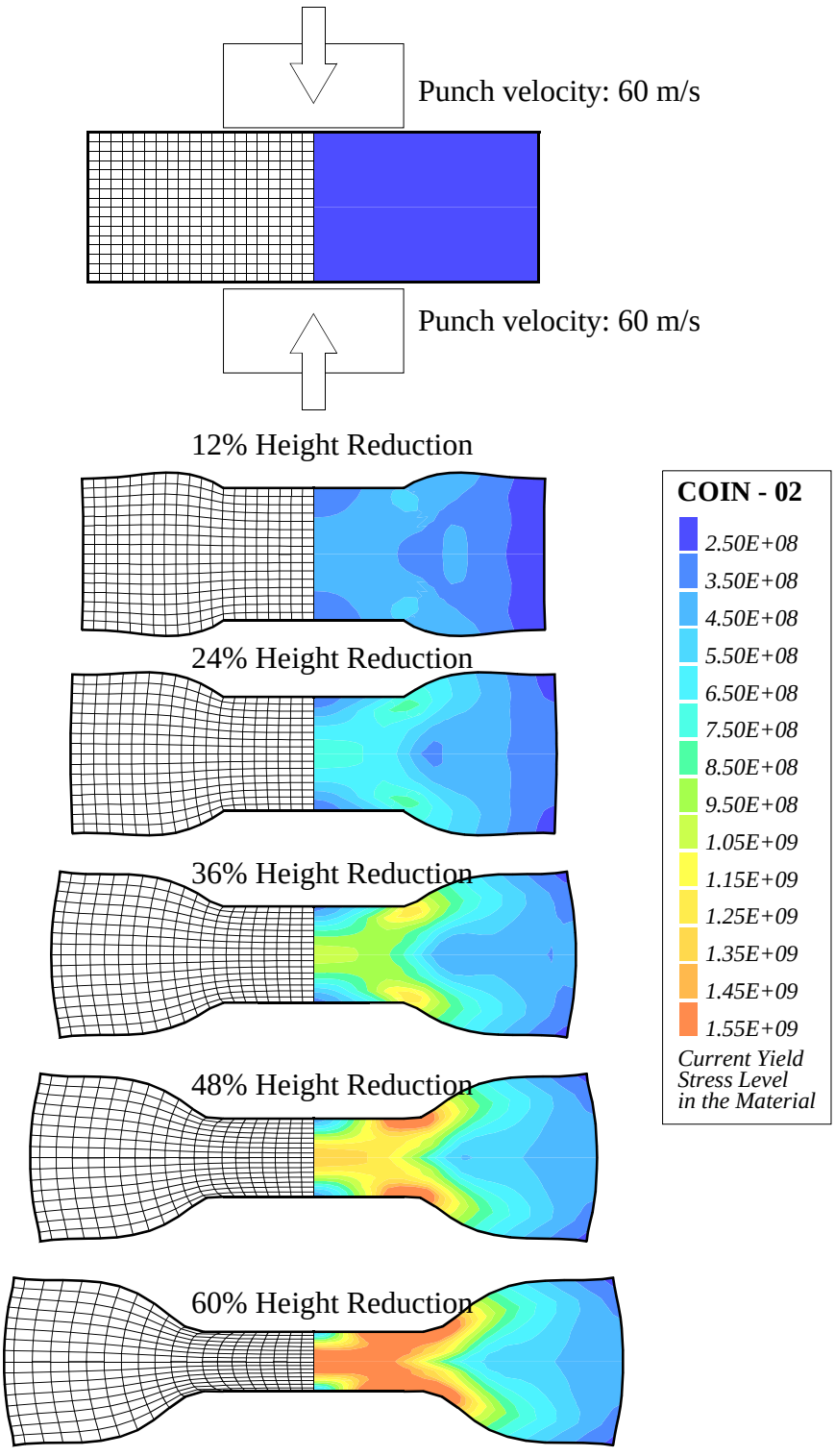

Calculation with Lax-Wendroff 2x2 element

Influence of the punch velocity

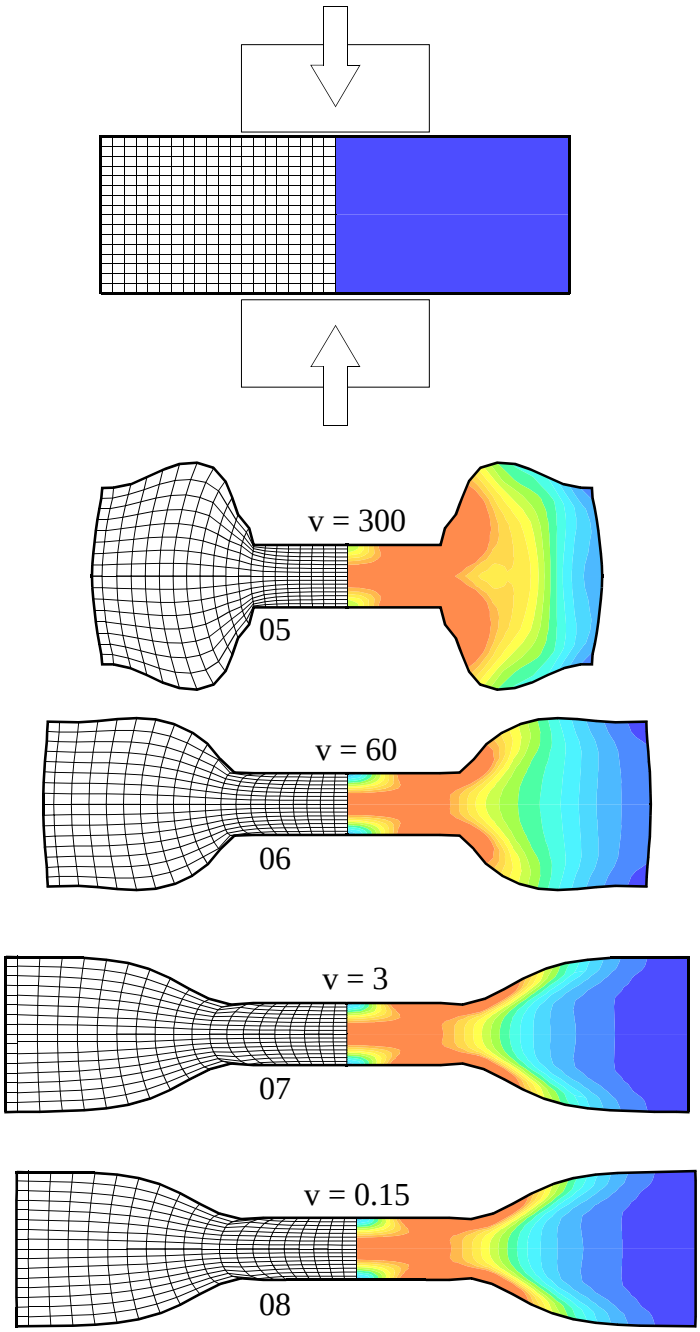

All calculations performed with Godunov (‘B’) model, 2x2

Coining

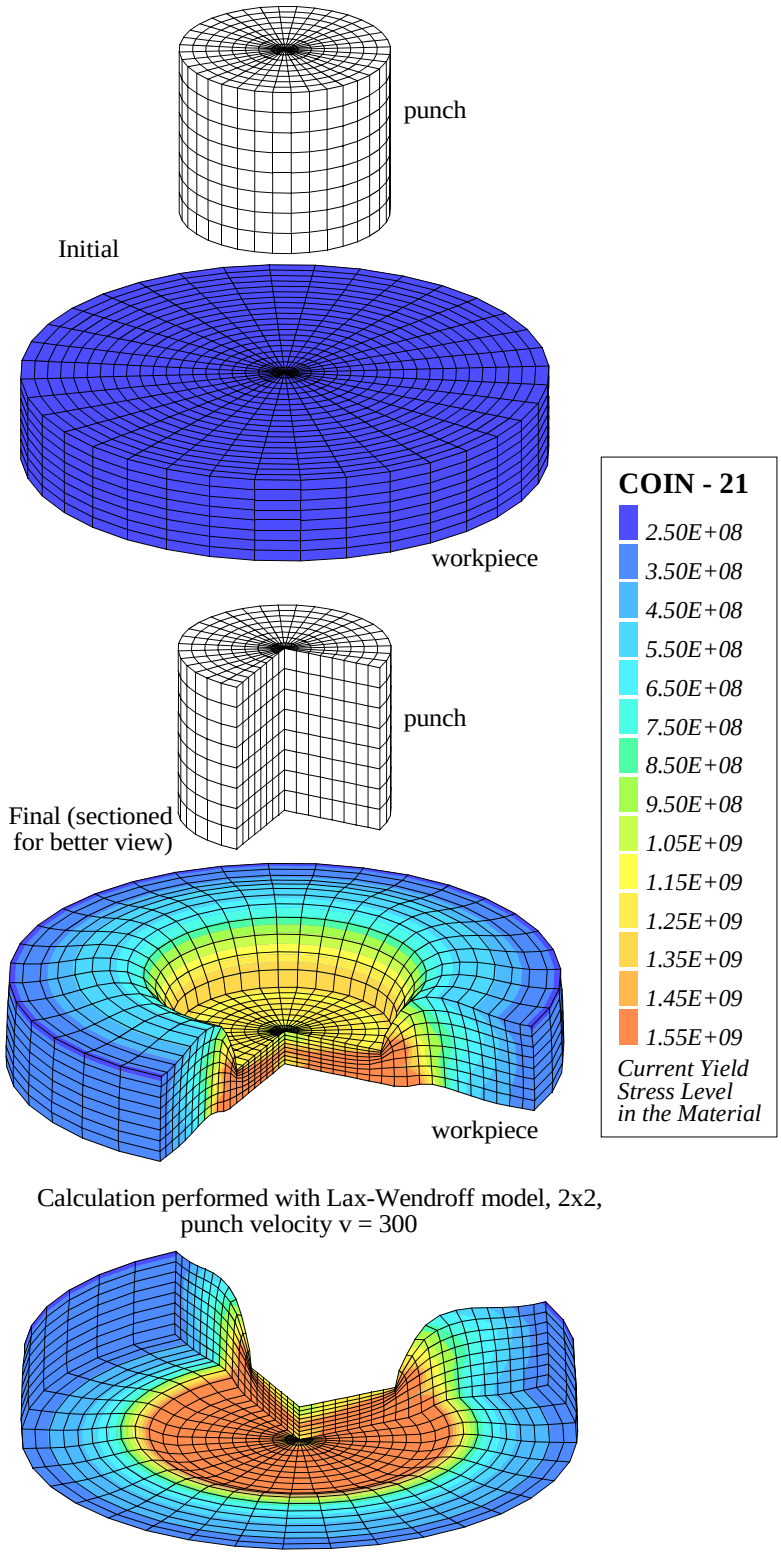

Calculation performed with Lax-Wendroff model, 2x2,
punch velocity v = 300

JOINT RESEARCH CENTRE

European Commission
Institute for the Protection and Security of the Citizen
European Laboratory for Structural Assessment

High-speed impact or traction

Description:

The impact of a cylindrical bar against a rigid wall has been considered by various authors in order to validate fast-transient dynamic computer codes, see e.g. Hallquist and Benson (1986), Halleux and Casadei (1987), Liu *et al.* (1988) and Predebon *et al.* (1991) and the references therein. G.I. Taylor (1948) was the first to recognize that the final length and shape of a cylinder impacting against a rigid surface (anvil) are quite sensitive to the constitutive behaviour of the material.

Although no analytical solution exists for such problems, and experimental results may be affected by complex phenomena such as friction between the cylinder and the anvil, an extremely accurate numerical solution can be obtained (at a high CPU cost, indeed) with the Lagrangian formulation, and then used to assess the quality of ALE solutions.

The data of the problem considered here are taken from Hallquist and Benson (1986): a cylindrical bar of radius 3.2 mm and length 32.4 mm impacts a rigid, frictionless wall, at an initial velocity of 227 m/s, see first figure. The material is assumed elastoplastic with isotropic hardening, with Young's modulus E = 117 GPa, Poisson's ratio 0.35, yield stress 400 MPa, density 8930 Kg/m^3 and plastic modulus 100 MPa. The final time of the simulation is 80 microseconds. In 1987, Halleux and Casadei presented a 2D axisymmetric solution of the problem, obtained by a 9-node parabolic element and the Lagrangian description with a mesh of 3 x 30 elements. The final height (H = 21.47) and radius (R= 7.113) of the projectile were in very good agreement with the values found by Hallquist and Benson (1986) using various 2D and 3D, finite-difference and finite-element codes.

More recently, the solution was repeated using the PLEXIS-3C code with the same quadratic element type, but a slightly more precise implementation of the constitutive law (an unnecessary approximation was present in the old implementation in the way the material stress curve was followed). This resulted in a slightly different final height (H = 21.41) and radius (R = 7.203). These values compare well with those found by Liu *et al.* (1988) in their Lagrangian solution.

In order to find an even more precise reference solution, the Lagrangian solution with the quadratic element was repeated by using finer meshes, until a satisfactory convergence (stabilization) of the results was obtained. A calculation with 6 x 60 elements yielded H = 21.41 and R = 7.218, while a model with an extremely fine mesh of 12 x 120 elements resulted in H =

21.41 and R = 7.230. The latter was considered an extremely precise solution and may be adopted as a reference.

The obtained ALE solution compares quite well to the reference Lagrangian solution. However, it may be noted that, although the ALE solution is quite accurate and can be obtained at a fraction of the CPU cost of a Lagrangian solution, this particular case is not very favorable in order to show the potential advantages of ALE techniques. In fact, while the ALE formulation allows to keep a much more regular mesh and avoids entangling, some accuracy is lost in the representation of the highly deformed “foot” of the projectile with only a few, large elements. There are cases, however, such as the next example (bar traction), where a Lagrangian description shows the opposite tendency: elements become too large and accuracy is lost. In these circumstances, an ALE description is favored by the possibility to keep elements regular, and shows its full potential.

The bar traction example is a simple extension of the previous one. The same geometry and material are taken, even the same initial velocity is prescribed but now the sign is opposite. Thus the present example simulates a sort of pulling test. It has been chosen because it presents another possible advantage of the ALE formulation. While the Lagrangian analysis suffers from excessive element distortion, precisely where the necking occurs, the ALE description allows a regular element size distribution everywhere.

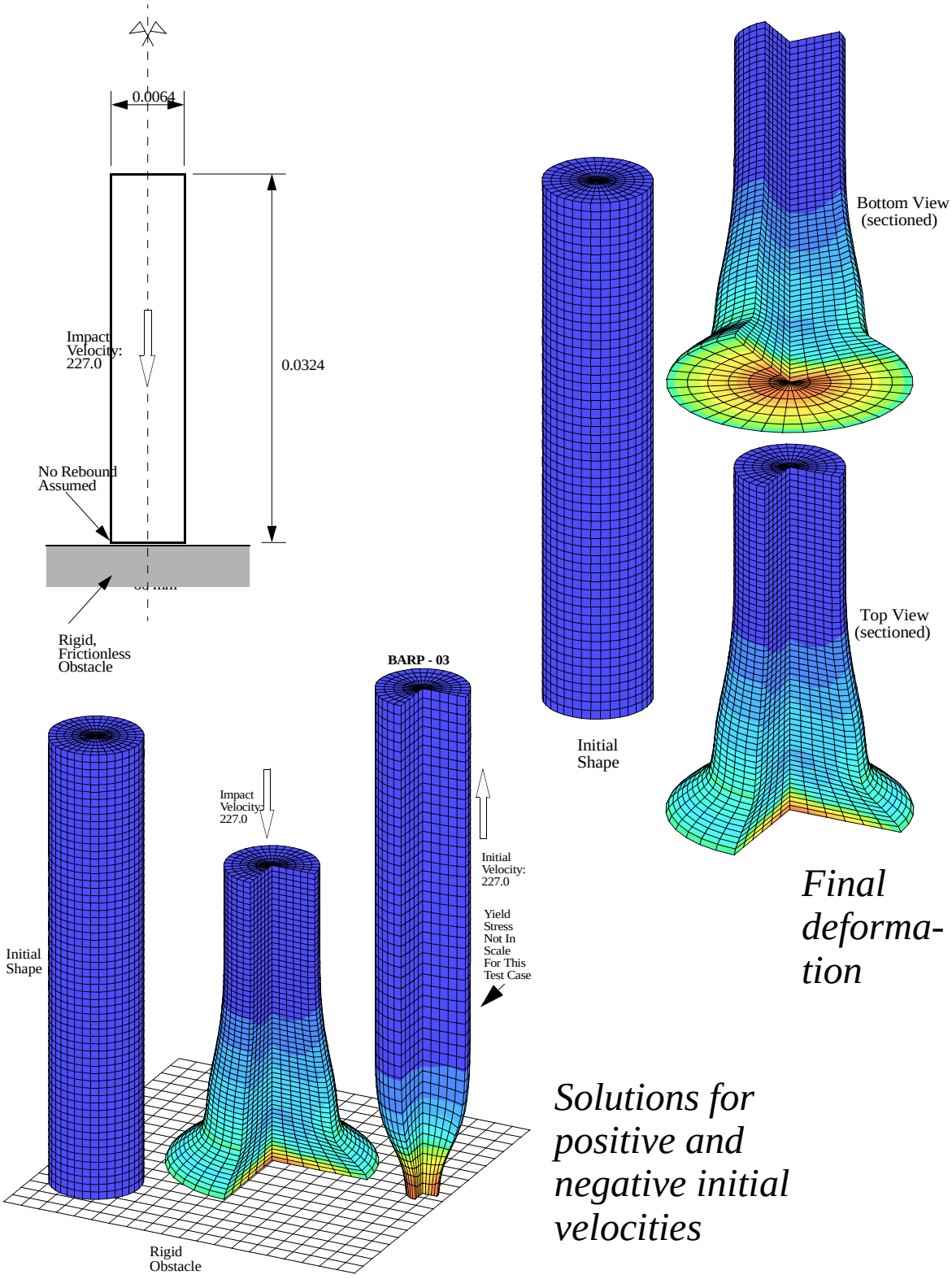

Final deformation

Solutions for positive and negative initial velocities

JOINT RESEARCH CENTRE

European Commission
Institute for the Protection and Security of the Citizen
European Laboratory for Structural Assessment

Earthquake simulation

- ***Spectral elements*** are used to model elastic wave propagation in the ***linear*** part of the model domain: these are more efficient than conventional finite elements for the same level of accuracy;
- Efficient ***absorbing boundary*** models and earthquake load generation models are available for the spectral part of the domain;
- The ***non-linear*** part of the domain (plasticity, damage, large deformations etc.), including foundations and ***buildings***, is modelled by fully non-linear ***finite elements***;
- The SE and FE sub-domains are ***interfaced*** by an accurate coupling condition (***mortar method***).

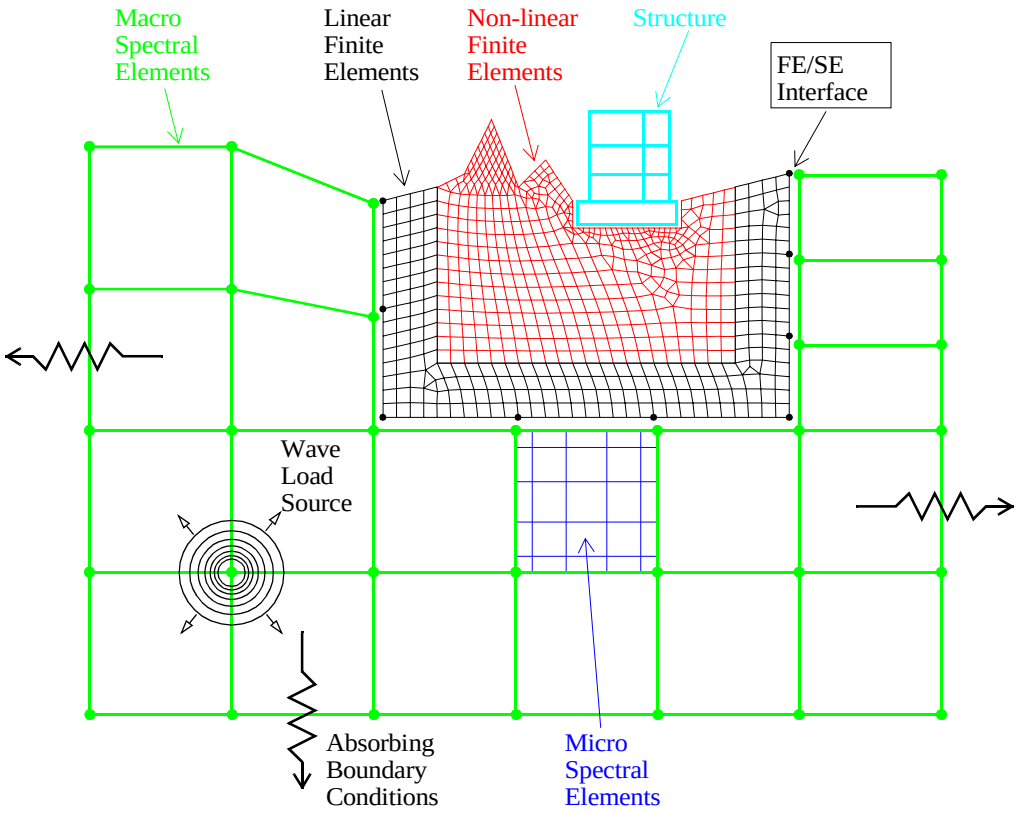

Earthquake in a cylindrical valley [22]

Description:

A model with an axisymmetric geometry has been set up, which may be used to validate 2D axisymmetric spectral elements in a comparison with the full 3D solution.

A cylindrical valley problem is taken as guideline to build the model, whose geometric characteristics are shown in the first figure.

The 3D model is discretised using MS38 spectral elements of order $N = 4$: only a quarter of the cylinder has been considered, thanks to the central symmetry with respect to the axis. Hence the lateral surfaces are constrained in order to allow symmetric displacements, the top surface is a free surface, the other two are absorbing boundaries. The plane wave load is a longitudinal Ricker's wave of type BETA, characterized by a frequency of 1 Hz.

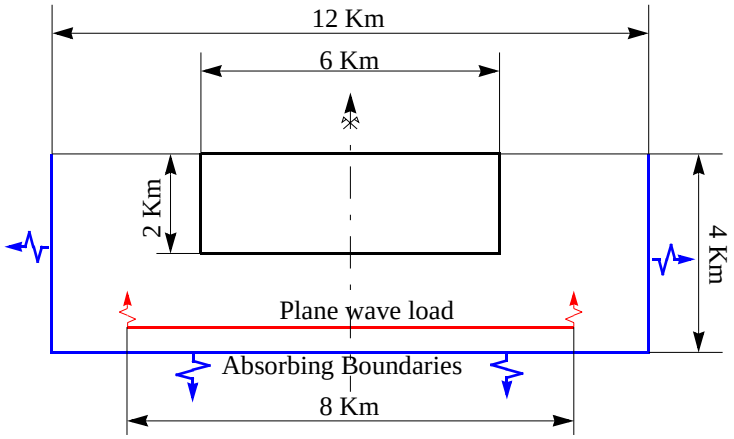

Problem Definition

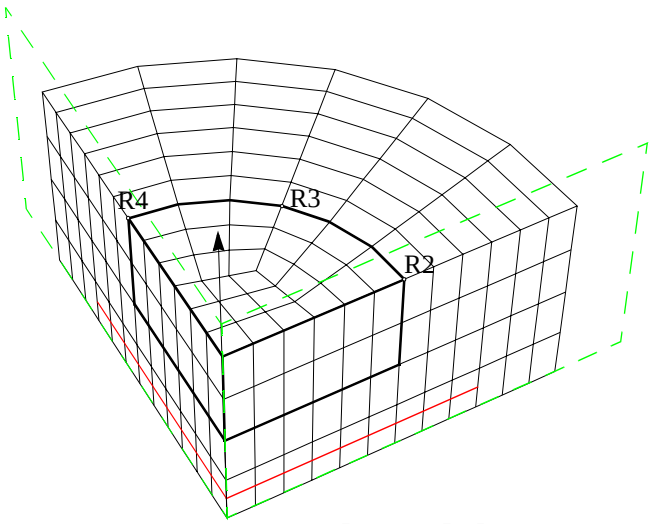

3D Numerical Model

Solution

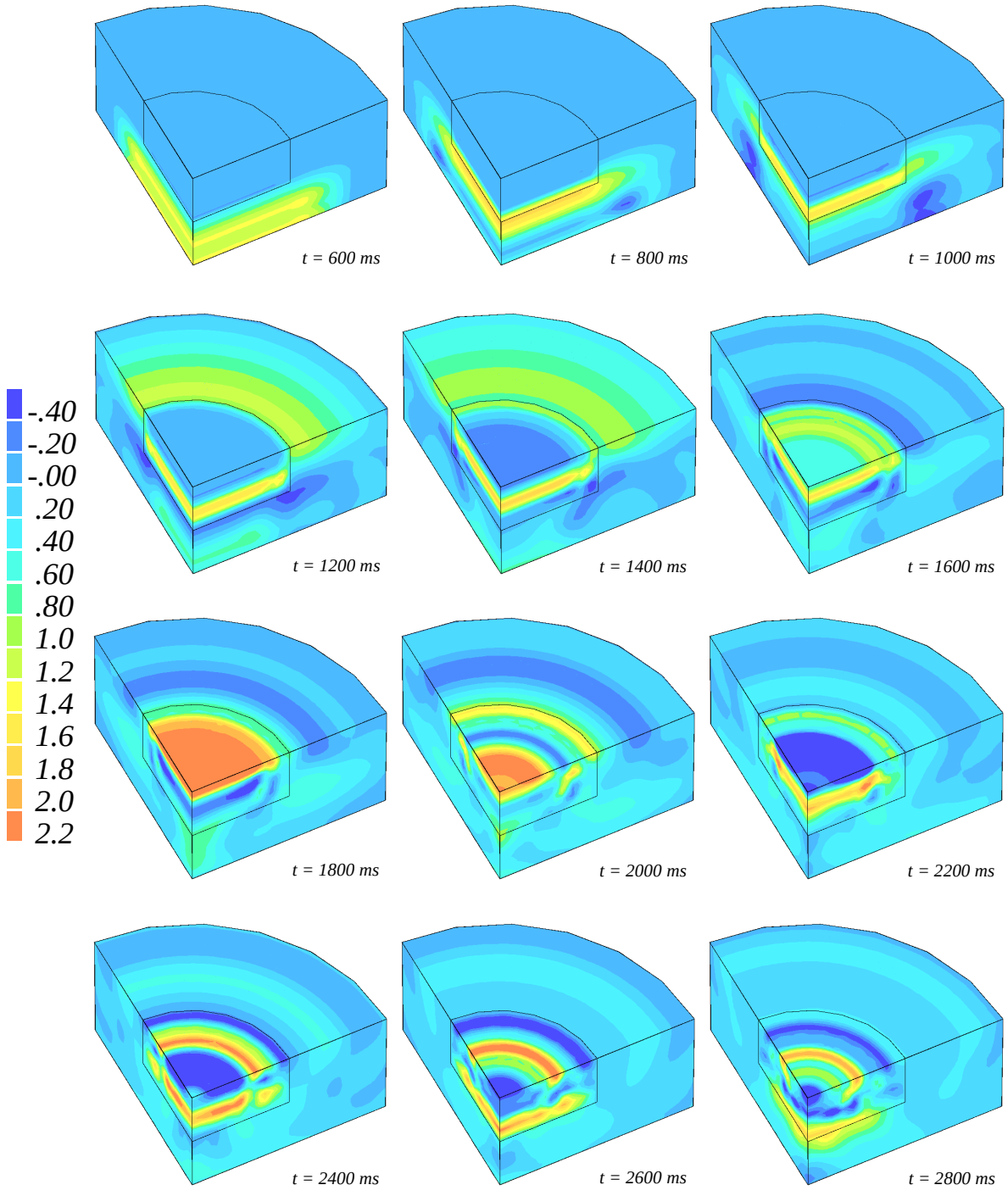

3D Numerical Solution (z-Displacement)

JOINT RESEARCH CENTRE

European Commission
Institute for the Protection and Security of the Citizen
European Laboratory for Structural Assessment

References

[1] J.P. HALLEUX: "*Computational Treatment of Transient Problems in Nonlinear STructural Mechanics*". Chapter 2 in Advances in Computational Nonlinear Mechanics, CISME Courses and Lectures N. 300, Ed. I. St. Doltsinis, Springer Verlag (1989).

[2] M. LEPAREUX, B. SCHWAB, A. HOFFMANN, P. JAMET, H. BUNG: "*Un programme général pour l'analyse dynamique rapide - Cas des tuyauteries*". Colloque: Tendances Actuelles en Calcul des Structures, Bastia, 6-8 November, (1985).

[3] T.J.R. HUGHES: "*Numerical Implementation of Constitutive Models: Rate-Independent Deviatoric Plasticity*". In Proc. of the Workshop on the Theoretical Foundation for Large-Scale Computations of Non-Linear Material Behaviour, Northwestern University, Evanston, Illinois, October 24-26, 1983 (eds. S. Nemat-Nasser, R.J. Aasro and G.A. Hegemier), Martinus Nijhoff Publishers, Dordrecht, 29-57, (1984).

[4] F. CASADEI, J. P. HALLEUX: "*Validation of the PLEXIS-3C computer code on academic and real test cases in structural dynamics*", 10th International Conference on Structural Mechanics in Reactor Technology, Anaheim, U.S.A., August 14-18, (1989).

[5] F. CASADEI, C. DELZANO, G. MAGONETTE, J. P. HALLEUX, G. VERZELETTI: "*Dynamic testing of large AISI-316 L steel specimens behaviour using L.D.T.F.*". 12th MPA-Seminar: Safety and Availability of Plant Technology, Staatliche Materialprüfungsanstalt, Stuttgart, Oct. 9-10, (1986). Also appeared in Nuclear Engineering and Design, Vol. 102, pp. 463-474, (1987).

[6] P. M. JONES, F. CASADEI, J. P. HALLEUX: "*Progress in numerical modelling of dynamic specimen behaviour in the L.D.T.F.*", 13th MPA-Seminar: The Contribution of Component and Large Specimen Testing to Structural Integrity Assessment, Staatliche Materialprüfungsanstalt, Stuttgart, Oct. 8-9, (1987). Also appeared in Nuclear Engineering and Design, Vol. 112, pp. 51-64, (1989).

[7] F. HARLOW, A.A. AMSDEN: "*Fluid Dynamics*", Los Alamos Scientific Laboratory of the University of California, Los Alamos, New Mexico, Report LA-4700, UC-34 (1971).

[8] J. DONEA, S. GIULIANI, J.P. HALLEUX: "*An Arbitrary Lagrangian Eulerian Finite Element Method for Transient Dynamic Fluid-Structure Interactions*". Computer Methods in Applied Mechanics and Engineering, 33, 689-723 (1982).

[9] J. DONEA: "*Arbitrary Lagrangian Eulerian Finite Element Methods. In Computational Methods for Transient Analysis*", T. Belytschko and T.J.R. Hughes, Eds., Chapter 10, North Holland, Amsterdam (1983).

[10] C.W. HIRT, A.A. AMSDEN, J.L. COOK: "*An Arbitrary Lagrangian-Eulerian Computing Method for all Flow Speeds*", Journal of Computational Physics, 14, 227 (1974).

[11] S. GIULIANI: "*An Algorithm for Continuous Rezoning of the Hydrodynamic Grid in Arbitrary Lagrangian Eulerian Computer Codes*", Nuclear Engineering and Design, 72, 205-212 (1982).

JOINT RESEARCH CENTRE

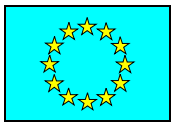

European Commission
Institute for the Protection and Security of the Citizen
European Laboratory for Structural Assessment

[12] J. DONEA, S. GIULIANI: "*An Explicit ALE Finite Element Formulation for 3D Transient Dynamic Fluid-Structure Interaction Problems*", EUR Report 11936 EN (1988).

[13] B. NKONGA, H. GUILLARD: "*Godunov-type method on non-structured meshes for three-dimensional moving boundary problems*", Computer Methods in Applied Mechanics and Engineering, 113, 183-204 (1994).

[14] A. SORIA, F. CASADEI: "*Arbitrary Lagrangian-Eulerian Multicomponent Compressible Flow with Fluid-Structure Interaction*". International Journal for Numerical Methods in Fluids, 25, 1263-1284, December (1997).

[15] A. SALA, F. CASADEI, A. SORIA: "*A 3-D Finite Volume Numerical Model of Compressible Multicomponent Flow for Fluid-Structure Interaction Applications*". IV Congreso de Mètodos Numèricos en Ingenierìa, Sevilla, Spain, 7-10 June (1999).

[16] F. CASADEI, A. DANERI, G. TOSELLI: "*Use of PLEXUS as a LMFBR primary containment code for the CONT benchmark problem*", 10th International Conference on Structural Mechanics in Reactor Technology, Anaheim, U.S.A., August 14-18, 1989.

[17] F. CASADEI, J. P. HALLEUX: "*On the treatment of fluid-structure interactions of the permanent type in PLEXIS-3C*". Second International Conference on Computational Structures Technology, Athens, Greece, 30 August-1 September (1994).

[18] F. CASADEI, J. P. HALLEUX: "*An Algorithm for Permanent Fluid-Structure Interaction in Explicit Transient Dynamics*". Computer Methods in Applied Mechanics and Engineering, 128, 3-4, 231-289, December (1995).

[19] F. CASADEI: "*Recent Advances in the Modeling of Fast Transient Fluid-Structures Interactions of the Permanent Type*". 14-th International Conference on Structural Mechanics in Reactor Technology, SMiRT-14, Lyon, France, August 17-22, (1997).

[20] F. CASADEI, A. SALA: "*Finite Element and Finite Volume Simulation of Industrial Fast Transient Fluid-Structure Interactions"*, 'European Conference on Computational Mechanics - Solids, Structures and Coupled Problems in Engineering - ECCM '99', Munich, Germany, August 31 - September 3, (1999).

[21] F. CASADEI, J.P. HALLEUX, A. SALA, F. CHILLÈ: "*Transient Fluid-Structure Interaction Algorithms for Large Industrial Applications"*, Computer Methods in Applied Mechanics and Engineering, Vol.190/24-25, pp. 3081-3110, March 2001.

[22] F. CASADEI, E. GABELLINI, G FOTÍA, F. MAGGIO, A. QUARTERONI: "*A Mortar Spectral/Finite Element Method for Complex 2D and 3D Elastodynamic Problems"*, Computer Methods in Applied Mechanics and Engineering, Vol. 191/45, pp. 5119-5148, November 2002.

[23] F. CASADEI, S. POTAPOV: "*Permanent Fluid-Structure Interaction with Nonconforming Interfaces in Fast Transient Dynamics*", submitted for publication in Computer Methods in Applied Mechanics and Engineering, 2003.